UNIVERSITY OF CALIFORNIA SAN DIEGO

Measuring and Investigating Periodic and Aperiodic Neural Activity

A dissertation submitted in partial satisfaction

of the requirements for the Doctor of Philosophy

in

Cognitive Science

by

Thomas Donoghue

Committee in Charge:

Professor Bradley Voytek, Chair
Professor Timothy Brown
Professor Virginia de Sa
Professor Lara Rangel
Professor John Serences

2020

The dissertation of Thomas Donoghue is approved, and it is acceptable in quality and form for publication on microfilm and electronically:

Chair

University of California San Diego

2020

TABLE OF CONTENTS

LIST OF FIGURES

LIST OF TABLES

LIST OF ABBREVIATIONS

EEG: electroencephalography

MEG: magnetoencephalography

ECoG: electrocorticography

LFP: local field potential

DSP: digital signal processing

PSD: power spectral density

ERP: event-related potential

ACKNOWLEDGEMENTS

Thank you to the original lab 'cohort' of grad students - Richard Gao, Tammy Tran, and Scott Cole - for being a truly tremendous group to embark on this adventure with. Thank you to Erik Peterson for getting the lab going with programming, and Roemer van der Meij for helping us develop our signal processing skills. Thank you also to Torben Noto, Sydney Smith, Ryan Hammonds, Eric Lybrand, Leo Waschke, and all the members of the VoytekLab past and present.

I would in particular like to thank my thesis advisor, Dr. Bradley Voytek. Thank you for your patience and guidance, through which you helped and allowed us to explore and set our own research paths, always helping us along the way. I would also like to thank my committee for guidance and feedback in preparing this thesis.

I would also like to thank the people who introduced me to research, including Dr. Kris Onishi, who showed me how to do structured and organized work, while answering interesting questions in creative ways, and Dr. Sylvain Baillet, Elizabeth Bock, and Francois Tadel, who introduced to the wondrous world of human electrophysiology research, and working with code.

I would like to thank the research assistants who helped me do all this work, including Will Fox, Aeri Kim, Priya Sebastian, Luyanda Mdanda, Julio Dominguez, Fenglin (Allen) Zhang, and Tyler Farnan. Thank for all of your help doing this research – working with you all has been a wonderful part of the grad school experience.

I would like to thank the programs and people that helped me move into a more programming oriented work, including the tireless work of those who put on the summer programs I attended, and everyone who has spent time developing software, advocating for best practices in scientific programming, and building materials and tutorials.

Chapter 1, in full, is a reprint of the material as it appears the following manuscript that has been submitted for publication: Donoghue T, Haller M, Peterson E, Varma P, Sebastian P, Gao R, Noto T, Lara A, Wallis J, Knight RT, Shestyuk A, & Voytek B. *Parameterizing Neural Power Spectra.* The dissertation author was the primary investigator and author of this paper.

Chapter 2, in full, is a reprint of the material as it appears the following manuscript that has been submitted for publication: Donoghue T, Dominguez J & Voytek B. *Electrophysiological Frequency Band Ratio Measures Conflate Periodic and Aperiodic Neural Activity.* The dissertation author was the primary investigator and author of this paper.

Chapter 3, in full is an adaption of materials that appear in the following manuscript that is currently being prepared for submission for publication: Donoghue T, Mdanda L, Sebastian P, & Voytek B. *Variability of Periodic and Aperiodic Electrophysiological Activity across the Cortex*. The dissertation author was the primary investigator and author of this paper.

VITA

2014	Bachelors of Arts & Science: Cognitive Science McGill University
2016	Masters of Cognitive Science University of California San Diego
2020	Doctor of Philosophy, Cognitive Science University of California San Diego

ABSTRACT OF THE DISSERTATION

On Measuring and Investigating Periodic and Aperiodic Neural Activity

by

Thomas Donoghue

Doctor of Philosophy in Cognitive Science

University of California San Diego, 2020

Professor Bradley Voytek, Chair

Understanding the functional organization of brain activity is a fundamental topic in neuroscience. Questions about how the brain coordinates information through space and time are often investigated with the use of neural field data – electrophysiological recordings of the aggregate electrical activity across groups of neurons. Such activity contains both periodic activity (neural oscillations), a common topic of investigation, and aperiodic activity, which has been less broadly studied, each of which have distinct interpretations. The overlap of these two components of activity is a source of difficulty for investigations which aim to measure and interpret the properties and dynamics of one or the other component, as methods that do not explicitly consider and measure both properties of the data are liable to conflate the two

components. Despite this, many commonly employed analysis methods do not attempt to explicitly measure and separate both periodic aperiodic activity.

In this work, we develop a new method for separating and measuring periodic and aperiodic activity, using frequency domain representations of neural field data. First, we propose a novel algorithm for parameterizing neural power spectra, and validate this approach on simulated data, and demonstrate how it can be applied to real datasets. Second, we systematically explore how power spectrum parameterization compares to canonical approaches, using the example of frequency band ratio measures. Here we show that such measures that analyze pre-defined frequency ranges without considering and separating aperiodic activity are liable to reflect confounded measures of aperiodic activity. Finally, we apply the novel method across a series of datasets, systematically exploring the properties and variability of periodic and aperiodic activity across the human cortex. In sum, this work motivates that both periodic and aperiodic activity are dynamic components, necessitating dedicated methods to appropriately measure and interpret changes in the data. In doing so, methods that do consider both aperiodic and periodic activity allow for better quantifications of brain activity that can be investigated for their putative relationships to demographics, cognition and disease states.

Introduction

1.1: Functional Organization of the Brain

With the development, around the turn of the 20th century, of what came to be called the 'Neuron Doctrine' (Ramón y Cajal, 1911), came the start of what we now recognize as modern neuroscience. Within this framework, 120 years of investigation have examined how networks of physically distinct cells, using a combination of electrical and chemical signaling, make up the nervous system, ultimately underlying everything we perceive, think, or do. Through many technological developments, much work has mapped detailed characterizations of many components of the nervous system, including, for example, physiological structures that make up neurons, morphological structure of single cells, patterns of gene expression across the brain, and mapping between cell activity and the external world.

What have been slower to emerge are integrative, functional descriptions of how this all works together. Of the many remaining mysteries of the nervous system, many open questions remain regarding the functional organization of brain activity. Given the approximately 80 billion neurons in the human brain (Azevedo et al., 2009), connected by relatively fixed anatomy (over short timescales, at least), how is it that the brain is able to parse, select, ignore, and combine information streams in all of the wonderfully flexibly ways that are the biological underpinnings of our rich cognitive lives. To function as it does, the mammalian brain must have powerful, flexible, and efficient mechanisms for coordinating information as it does, across multiple spatial and temporal scales.

There are clearly powerful organizational activities at play – processes that can be either reactive or directed, and that flexibly adapt to a broad range of sensory inputs and motor outputs. Understanding the functional organization of the nervous system is an important topic of investigation. This is true not only in terms of being a key question in basic science, but also due to its relevance to clinical work, as a multitude of disorders across psychiatry and neurology display seemingly disordered, or at least different, patterns and organizations of neural activity, though we generally do not yet understand why.

1.2: Electrophysiology

Prior to, and contemporaneously to anatomical work, which led to our understanding of the core structural properties of the brain, and the aforementioned Neuron Doctrine, other work probed the functional activity of the brain. By the late 19th century, experiments demonstrated the electrical excitability of the cerebral cortex, and the impact of electrical stimulation (Millett, 1998). Subsequent work by David Ferrier extended this line of inquiry, relating cortical stimulation to organized patterns of behavioral responses, offering some of the first functional mappings of electrical neural activity (Sandrone & Zanin, 2014).

Building on this work, Richard Caton continued systematic investigations of electrical signaling in the brain, and went on to record what are now thought to be the first demonstrations of systematic patterns of electrical activity – or brain waves (Ormerod, 2006). Adolf Beck continued this line of investigation, noting continuous electrical oscillations of brain activity, and noting that these patterns of neural activity reacted and related to sensory stimulation (Coenen & Zayachkivska, 2013). By the end of the 1800s, the brain was known to have structured and

functionally relevant patterns of electrical activity, starting a research program and line of investigation into the functional organization of the brain that has continued to this day.

The work up until this point had all been in model organisms. Subsequent work, including the development of better amplifiers, led to more generalized methods of recording, that could be applied to human subjects. This lead to the development of electroencephalography (EEG), allowing for recording electrical activity in human subjects, which again noted neural oscillations, that came to be termed as distinct bands, such as alpha and beta (Berger, 1929). By the early 20th century, systematic evoked responses to external events also began to be reported with human subjects – for example, the demonstration of 'on-effects' following the presentation of light or sound (Davis, 1939). Slightly later came the first descriptions of evoked-potentials related to cognitive concepts, such as expectation, including the contingent-negative variation (CNV) (Walter et al., 1964), and the P300 (Sutton et al., 1965).

These early investigations, and their success, have led to vibrant and expansive research programs investigating electrical neural activity, and how it relates to functional organization and cognitive performance. Recordings of electrical fields in the brain, such as measured by intra-cranial electrodes, such as in local field potential (LFP) or electrocorticography (ECoG), or extra-cranial recordings such as electroencephalography (EEG) or magnetoencephalography (MEG) are now common recordings in neuroscience.

Analyses of neural field data are now applied and developed across many different areas of research, in order to leverage and investigate functional activity of the brain. Such investigations focus on different aspects of interest from the data – for example, investigating rhythmic patterns of activity, now typically called neural oscillations, and/or distinct transient

events, that can be evoked, such as event-related potentials, or endogenous such as K-complexes during sleep. It was also noted early on that such data had aperiodic properties, meaning ongoing, non-periodic activity, such as 1/f-like activity (Motokawa, 1949). Altogether, there appear to be three *types* of activity in neural field data: periodic activity, ongoing aperiodic activity, and transient events.

1.3: Periodic Activity

Neural oscillations are a ubiquitous feature of brain activity and are thought to play a key role in neural functioning (Buzsáki & Draguhn, 2004), while their disruption is implicated in a broad group of psychiatric and neurological disorders (Voytek & Knight, 2015). Neural oscillations, as observed in the local field potential (LFP), are composed of aggregate activity across hundreds to thousands of individual neurons, reflecting primarily synaptic activity (Buzsáki et al., 2012), generated by interactions and patterns of excitation and inhibition across groups of neurons (Wang, 2010). Neural oscillations are typically investigated in particular bands of interest, for example as delta (0.5 - 4 Hz), theta (4 - 8 Hz), alpha (8 - 13 Hz), beta (13 - 30 Hz), and gamma (30 - 60 Hz) – though the specific frequency bands used can vary between experiments and species.

Neural oscillations are thought to relate the functional organization of neural activity. Theories of how they do so include that they aid in information flow within the brain by flexibly aligning and misaligning oscillations between brain regions (Fries, 2005; Varela et al., 2001). These kinds of phase alignments, as they are known, have been shown to organize information flow between different areas (Colgin et al., 2009), and help form dynamic brain communication

networks (van der Meij et al., 2012) which aid in cognition, perception, and behavior (Voytek, Kayser, et al., 2015).

There is a long history of findings that support that neural oscillations have functional impact of neural processing and behavioral outcomes. Early work demonstrated that evoked potentials could only be elicited in the occipital cortex at certain phases of the ongoing alpha wave (Bishop, 1932). Behavioral correlates were demonstrated soon after, as it was reported that alpha phase at the time of stimulus presentation relates to reaction time in a visual detection task (Lansing, 1957). Subsequent work, including using online systems to present stimuli at particular phases of ongoing signals, further demonstrated impacts of oscillatory phase on behavior and perception (Varela et al., 1981).

In the time since, extensive research programs have investigated patterns of oscillatory activity within and between subjects, and their relation to cognition and disease. There are multiple views on the role and of neural oscillations in neural function. One proposal is that low frequency oscillations create 'windows of excitability', in which there is rhythmic bursts of increased neuronal excitation (Dugué et al., 2011). This idea has been extended to suggest this implies that perception is actually a rhythmic process, with cortical oscillations acting as a discrete sampling mechanism (VanRullen et al., 2014), creating perceptual and attentional cycles (VanRullen, 2016). However, alternate views more in line with the longstanding view that alpha oscillations reflect inhibition (Klimesch et al., 2007) have suggested that oscillations reflect pulses of rhythmic inhibition (Jensen & Mazaheri, 2010). Despite these ongoing debates, neural field data, and in particular rhythmic components therein are clearly a salient topic of investigation across neuroscience and psychology.

1.4: Aperiodic Activity

Electrophysiological field data also displays prominent aperiodic – meaning irregular, or non-periodic – activity (B. J. He, 2014). In frequency representations, this is seen as the 1/f-like structure of neural power spectra. This activity, roughly following a power-law distribution, is sometimes described as being 'scale-free' or 'self-similar' activity. Despite the early observation of 1/f distributed activity in electrophysiological data (Motokawa, 1949), relatively little work has explored the properties and interpretations of aperiodic activity, as compared to, for example, the broad literature exploring periodic activity (neural oscillations). Where studies have investigated aperiodic activity, there is a large variability in the methods employed, and interpretations of results. Altogether, there is a currently a lack of consensus for methods, interpretations, and best practices guidelines for investigations of aperiodic activity in neural field data.

By 1/f, it is meant that there is a power-law relation between power and frequency, reflecting exponentially decreasing power across increasing frequencies. We will refer to this activity as the aperiodic 'component' of the data, which, in neural field data, reflects the majority of the power. In the simple case, this manifests as a linear relationship between frequency and power, when plotted in log-log spacing, which can be captured by a line. In this simple y = a * f^{χ} formulation, the `a` parameter, will be referred to as the aperiodic 'offset', and the 'χ' parameter will be referred to as the aperiodic 'exponent'. The aperiodic exponent is analogous to the slope of the line of the log-log power-spectrum, sometimes referred to as the spectral 'slope'. This kind of power-law distributed activity is seen in many other physical systems, and as such is a feature of inquiry across areas of physics and mathematics.

Some early investigations of aperiodic activity started by mapping 1/f properties across the cortex in the awake state (Freeman et al., 2003; Pritchard, 1992) and also comparing across species between rabbits and humans (Freeman & Zhai, 2009). The broadband offset of neural power spectra has been correlated with firing rate of the underlying neural population (Manning et al., 2009; Miller et al., 2009). More recent work has continued to demonstrate that aperiodic neural activity is a dynamic signal, and has been shown to correlate with age (W. He et al., 2019; Voytek, Kramer, et al., 2015), state, such as sleep (Lendner et al., 2020) or anesthesia (Colombo et al., 2019). Aperiodic activity has been investigated in task contexts, including in response inhibition (Pertermann et al., 2019), perceptual tasks (Waschke et al., 2017), visual tasks (El Boustani et al., 2009; Lin et al., 2016; Podvalny et al., 2015), and working memory (Sheehan et al., 2018; Voytek, Kramer, et al., 2015). Aperiodic neural activity has also been found to related to diseases such as ADHD (Robertson et al., 2019), Schizophrenia (Molina et al., 2020), Parkinson's (Martin et al., 2018), and stroke (Leemburg et al., 2018).

Aperiodic neural activity has been analyzed under multiple conceptual frameworks. Some approaches seek to explore and explain aperiodic activity in terms of physiological models of putative generators of field data (Freeman & Zhai 2009; Gao et al, 2017). Other investigations consider aperiodic activity in terms of the variability, and/or level of 'neural noise' in the system (Voytek et al, 2015a; Waschke, 2017). More functional frameworks also focus on aperiodic activity as a scale-free phenomenon (He, 2014), focusing on fractal properties and self-similarity (Eke et al, 2002; Schaefer et al, 2014) and/or long-term dependencies in time series and/or critical states in dynamical systems (Palva et al, 2013). Collectively, the dynamic nature and theoretical interest of aperiodic activity has propelled a key interest in measuring and interpreting such activity.

1.5: Methods of Analysis of Neural Field Data

Any given analysis of neural field data typically focuses on properties of interest of a particular component of the data. For example, when analyzing periodic activity, one might focus on a burst of alpha (~10 Hz) activity, and analyze its power, temporal extent, or waveform properties. Other investigations may seek to measure the amplitude and latency of transient events, such as an event-related potential of interest, or the color of noise or global field power of aperiodic activity.

The analysis of neural field data has therefore developed a rich ecosystem of approaches adopted and adapted from the field of digital signal processing (DSP), with the goal of identifying and measuring particular components of interest, such as neural oscillations, transient events, or aperiodic activity – which are all present and overlapping in the data. Such analyses typically employ approaches across both the time and frequency domain, employing transforms such as filters, to select frequency ranges of interest; time-frequency analyses, to examine signal dynamics through time; and analyses of patterns and statistical properties of the data, etc. Each of these analyses makes assumptions of the data, both in the ways they get applied and operate on the data, and in how they are typically interpreted.

Though recorded as fluctuations across time, analyses of neural field data often include representing and transforming the data in the frequency domain. Mathematically, via the Fourier theorem, *any* continuous time series can be perfectly represented by a Fourier Series – as a combination of sinusoidal waveforms. This mathematical convenience has led to the widespread use of frequency-domain representations and transformations. However, and importantly, frequency domain representations do not themselves imply or demonstrate any particular

property of the data. For example, computing a power spectrum of neural field data, as is commonly done, does not, by itself, demonstrate that the signal contains or is comprised of sinusoidal periodic activity. Since neural data is known to contain not only periodic, but also aperiodic activity (B. J. He, 2014), care must be taken to appropriately apply methods, and investigate and interpret the data appropriately.

1.5: Conclusions & Outline of the Dissertation

Altogether, the investigation of the functional organization of neural activity is an important domain of research, and commonly explored through the collection and analysis of neural field data. Such investigations often focus on periodic or evoked components of the data, with relatively little work seeking to measure and investigate concomitant aperiodic activity, that is also present in the signal, and is itself a dynamic and informative component of the data. Methods of investigation that are applied to such data embody particular assumptions and conceptualizations of the data, and should be applied and interpreted with care, as they may conflate changes in different components of the data if they are not appropriately applied and interpreted.

This dissertation examines and explores the methodological approaches for investigating neural field data, considering in particular the problem of appropriately measuring and interpreting the combination of aperiodic and periodic activity that is present in such signals. Chapter 1 investigates properties of neural field data, and proposes a method for separating and measuring aperiodic and periodic activity, addressing limitations of many commonly applied methods. This method is validated across simulated data, and in a series of empirical applications. Chapter 2 further investigates methods for analyzing neural field data, investigating

frequency band ratios, and comparing them to explicit parameterization of periodic and aperiodic features. Chapter 3 then adopts the method proposed for measuring periodic and aperiodic activity, applying it further to a series of datasets, investigating patterns and variability of periodic and aperiodic activity.

References

Azevedo, F. A. C., Carvalho, L. R. B., Grinberg, L. T., Farfel, J. M., Ferretti, R. E. L., Leite, R. E. P., Filho, W. J., Lent, R., & Herculano-Houzel, S. (2009). Equal numbers of neuronal and nonneuronal cells make the human brain an isometrically scaled-up primate brain. *The Journal of Comparative Neurology*, *513*(5), 532–541. https://doi.org/10.1002/cne.21974

Berger, H. (1929). *Über das Elektrenkephalogramm des Menschen*. https://doi.org/10.1007/BF01797193

Bishop, G. H. (1932). Cyclic changes in excitability of the optic pathway of the rabbit. *American Journal of Physiology*, *103*(1), 213–224. https://doi.org/10.1152/ajplegacy.1932.103.1.213

Buzsáki, G., Anastassiou, C. A., & Koch, C. (2012). The origin of extracellular fields and currents—EEG, ECoG, LFP and spikes. *Nature Reviews Neuroscience*, *13*(6), 407–420. https://doi.org/10.1038/nrn3241

Buzsáki, G., & Draguhn, A. (2004). Neural oscillations in cortical networks. *Science*, *304*(5679), 1926–1929. https://doi.org/10.1126/science.1099745

Coenen, A., & Zayachkivska, O. (2013). Adolf Beck: A pioneer in electroencephalography in between Richard Caton and Hans Berger. *Advances in Cognitive Psychology*, *9*(4), 216–221. https://doi.org/10.5709/acp-0148-3

Colgin, L. L., Denninger, T., Fyhn, M., Hafting, T., Bonnevie, T., Jensen, O., Moser, M.-B., & Moser, E. I. (2009). Frequency of gamma oscillations routes flow of information in the hippocampus. *Nature*, *462*(7271), 353–357. https://doi.org/10.1038/nature08573

Colombo, M. A., Napolitani, M., Boly, M., Gosseries, O., Casarotto, S., Rosanova, M., Brichant, J.-F., Boveroux, P., Rex, S., Laureys, S., Massimini, M., Chieregato, A., & Sarasso, S. (2019). The spectral exponent of the resting EEG indexes the presence of consciousness during unresponsiveness induced by propofol, xenon, and ketamine. *NeuroImage*, *189*, 631–644. https://doi.org/10.1016/j.neuroimage.2019.01.024

Davis, H. (1939). Electrical phenomena of the brain and spinal cord. *Annual Review of Physiology*, *1*(1), 345–362. https://doi.org/10.1146/annurev.ph.01.030139.002021

Dugué, L., Marque, P., & VanRullen, R. (2011). The Phase of Ongoing Oscillations Mediates the Causal Relation between Brain Excitation and Visual Perception. *Journal of Neuroscience*, *31*(33), 11889–11893. https://doi.org/10.1523/JNEUROSCI.1161-11.2011

El Boustani, S., Marre, O., Béhuret, S., Baudot, P., Yger, P., Bal, T., Destexhe, A., & Frégnac, Y. (2009). Network-State Modulation of Power-Law Frequency-Scaling in Visual Cortical Neurons. *PLoS Computational Biology*, *5*(9), e1000519. https://doi.org/10.1371/journal.pcbi.1000519

Freeman, W. J., Holmes, M. D., Burke, B. C., & Vanhatalo, S. (2003). Spatial spectra of scalp EEG and EMG from awake humans. *Clinical Neurophysiology*, *114*(6), 1053–1068. https://doi.org/10.1016/S1388-2457(03)00045-2

Freeman, W. J., & Zhai, J. (2009). Simulated power spectral density (PSD) of background electrocorticogram (ECoG). *Cognitive Neurodynamics*, *3*(1), 97–103. https://doi.org/10.1007/s11571-008-9064-y

Fries, P. (2005). A mechanism for cognitive dynamics: Neuronal communication through neuronal coherence. *Trends in Cognitive Sciences*, *9*(10), 474–480. https://doi.org/10.1016/j.tics.2005.08.011

He, B. J. (2014). Scale-free brain activity: Past, present, and future. *Trends in Cognitive Sciences*, *18*(9), 480–487. https://doi.org/10.1016/j.tics.2014.04.003

He, W., Donoghue, T., Sowman, P. F., Seymour, R. A., Brock, J., Crain, S., Voytek, B., & Hillebrand, A. (2019). Co-Increasing Neuronal Noise and Beta Power in the Developing Brain. *BioRxiv*, 49. https://doi.org/10.1101/839258

Jensen, O., & Mazaheri, A. (2010). Shaping Functional Architecture by Oscillatory Alpha Activity: Gating by Inhibition. *Frontiers in Human Neuroscience*, *4*. https://doi.org/10.3389/fnhum.2010.00186

Klimesch, W., Sauseng, P., & Hanslmayr, S. (2007). EEG alpha oscillations: The inhibition-timing hypothesis. *Brain Research Reviews*, *53*(1), 63–88. https://doi.org/10.1016/j.brainresrev.2006.06.003

Lansing, R. W. (1957). Relation of brain and tremor rhythms to visual reaction time. *Electroencephalography and Clinical Neurophysiology*, *9*(3), 497–504. https://doi.org/10.1016/0013-4694(57)90037-8

Leemburg, S., Gao, B., Cam, E., Sarnthein, J., & Bassetti, C. L. (2018). Power spectrum slope is related to motor function after focal cerebral ischemia in the rat. *Sleep*, *41*(10). https://doi.org/10.1093/sleep/zsy132

Lendner, J. D., Helfrich, R. F., Mander, B. A., Romundstad, L., Lin, J. J., Walker, M. P., Larsson, P. G., & Knight, R. T. (2020). An electrophysiological marker of arousal level in humans. *ELife*, *9*, e55092. https://doi.org/10.7554/eLife.55092

Lin, A., Maniscalco, B., & He, B. J. (2016). Scale-Free Neural and Physiological Dynamics in Naturalistic Stimuli Processing. *ENeuro*, *3*(5). https://doi.org/10.1523/ENEURO.0191-16.2016

Manning, J. R., Jacobs, J., Fried, I., & Kahana, M. J. (2009). Broadband Shifts in Local Field Potential Power Spectra Are Correlated with Single-Neuron Spiking in Humans. *Journal of Neuroscience*, *29*(43), 13613–13620. https://doi.org/10.1523/JNEUROSCI.2041-09.2009

Martin, S., Iturrate, I., Chavarriaga, R., Leeb, R., Sobolewski, A., Li, A. M., Zaldivar, J., Peciu-Florianu, I., Pralong, E., Castro-Jiménez, M., Benninger, D., Vingerhoets, F., Knight, R. T., Bloch, J., & Millán, J. del R. (2018). Differential contributions of subthalamic beta rhythms and 1/f broadband activity to motor symptoms in Parkinson's disease. *Npj Parkinson's Disease*, *4*(1). https://doi.org/10.1038/s41531-018-0068-y

Miller, K. J., Sorensen, L. B., Ojemann, J. G., & den Nijs, M. (2009). Power-Law Scaling in the Brain Surface Electric Potential. *PLoS Computational Biology*, *5*(12), e1000609. https://doi.org/10.1371/journal.pcbi.1000609

Millett, D. (1998). Illustrating a revolution: An unrecognized contribution to the 'golden era' of cerebral localization. *Notes and Records of the Royal Society of London*, *52*(2), 283–305. https://doi.org/10.1098/rsnr.1998.0051

Molina, J. L., Voytek, B., Thomas, M. L., Joshi, Y. B., Bhakta, S. G., Talledo, J. A., Swerdlow, N. R., & Light, G. A. (2020). Memantine effects on EEG measures of putative excitatory/inhibitory balance in schizophrenia. *Biological Psychiatry: Cognitive Neuroscience and Neuroimaging*, S2451902220300471. https://doi.org/10.1016/j.bpsc.2020.02.004

Motokawa, K. (1949). Energy of Brain Waves and Energetics of the Brain. *The Tohoku Journal of Experimental Medicine*, *51*(1–2), 119–129. https://doi.org/10.1620/tjem.51.119

Ormerod, W. (2006). Richard Caton (1842–1926): Pioneer electrophysiologist and cardiologist. *Journal of Medical Biography*, *14*(1), 30–35. https://doi.org/10.1258/j.jmb.2006.04-22

Pertermann, M., Mückschel, M., Adelhöfer, N., Ziemssen, T., & Beste, C. (2019). On the interrelation of 1/f neural noise and norepinephrine system activity during motor response inhibition. *Journal of Neurophysiology*, *121*(5), 1633–1643. https://doi.org/10.1152/jn.00701.2018

Podvalny, E., Noy, N., Harel, M., Bickel, S., Chechik, G., Schroeder, C. E., Mehta, A. D., Tsodyks, M., & Malach, R. (2015). A unifying principle underlying the extracellular field potential spectral responses in the human cortex. *Journal of Neurophysiology*, *114*(1), 505–519. https://doi.org/10.1152/jn.00943.2014

Pritchard, W. S. (1992). The Brain in Fractal Time: 1/F-Like Power Spectrum Scaling of the Human Electroencephalogram. *International Journal of Neuroscience*, *66*(1–2), 119–129. https://doi.org/10.3109/00207459208999796

Ramón y Cajal, S. (1911). *Histologie du système nerveux de l'homme et des vertébrés*.

Robertson, M. M., Furlong, S., Voytek, B., Donoghue, T., Boettiger, C. A., & Sheridan, M. A. (2019). EEG Power Spectral Slope differs by ADHD status and stimulant medication exposure in early childhood. *Journal of Neurophysiology*. https://doi.org/10.1152/jn.00388.2019

Sandrone, S., & Zanin, E. (2014). David Ferrier (1843–1928). *Journal of Neurology*, *261*(6), 1247–1248. https://doi.org/10.1007/s00415-013-7023-y

Sheehan, T. C., Sreekumar, V., Inati, S. K., & Zaghloul, K. A. (2018). Signal Complexity of Human Intracranial EEG Tracks Successful Associative-Memory Formation across Individuals. *The Journal of Neuroscience*, *38*(7), 1744–1755. https://doi.org/10.1523/JNEUROSCI.2389-17.2017

Sutton, S., Braren, M., Zubin, J., & John, E. R. (1965). Evoked-potential correlates of stimulus uncertainty. *Science*, *150*(3700), 1187–1188. https://doi.org/10.1126/science.150.3700.1187

van der Meij, R., Kahana, M., & Maris, E. (2012). Phase-Amplitude Coupling in Human Electrocorticography Is Spatially Distributed and Phase Diverse. *Journal of Neuroscience*, *32*(1), 111–123. https://doi.org/10.1523/JNEUROSCI.4816-11.2012

VanRullen, R. (2016). Perceptual Cycles. *Trends in Cognitive Sciences*, *20*(10), 723–735. https://doi.org/10.1016/j.tics.2016.07.006

VanRullen, R., Zoefel, B., & Ilhan, B. (2014). On the cyclic nature of perception in vision versus audition. *Philosophical Transactions of the Royal Society B: Biological Sciences*, *369*(1641), 20130214–20130214. https://doi.org/10.1098/rstb.2013.0214

Varela, F. J., Lachaux, J.-P., Rodriguez, E., & Martinerie, J. (2001). The brainweb: Phase synchronization and large-scale integration. *Nature Reviews Neuroscience*, *2*(4), 229–239. https://doi.org/10.1038/35067550

Varela, F. J., Toro, A., John, E. R., & Schwartz, E. L. (1981). Perceptual framing and cortical alpha rhythm. *Neuropsychologia*, *19*(5), 675–686. https://doi.org/10.1016/0028-3932(81)90005-1

Voytek, B., Kayser, A. S., Badre, D., Fegen, D., Chang, E. F., Crone, N. E., Parvizi, J., Knight, R. T., & D'Esposito, M. (2015). Oscillatory dynamics coordinating human frontal networks in support of goal maintenance. *Nature Neuroscience*, *18*(9), 1318–1324. https://doi.org/10.1038/nn.4071

Voytek, B., Kramer, M. A., Case, J., Lepage, K. Q., Tempesta, Z. R., Knight, R. T., & Gazzaley, A. (2015). Age-Related Changes in 1/f Neural Electrophysiological Noise. *Journal of Neuroscience*, *35*(38), 13257–13265. https://doi.org/10.1523/JNEUROSCI.2332-14.2015

Walter, W. G., Cooper, R., Aldridge, V. J., McCallum, W. C., & Winter, A. L. (1964). Contingent negative variation: An electric sign of sensorimotor association and expectancy in the human brain. *Nature*. https://doi.org/10.1038/203380a0

Wang, X.-J. (2010). Neurophysiological and Computational Principles of Cortical Rhythms in Cognition. *Physiological Reviews*, *90*(3), 1195–1268. https://doi.org/10.1152/physrev.00035.2008

Waschke, L., Wöstmann, M., & Obleser, J. (2017). States and traits of neural irregularity in the age-varying human brain. *Scientific Reports*, *7*(1). https://doi.org/10.1038/s41598-017-17766-4

Chapter 1

Parameterizing Neural Power Spectra

Abstract

Electrophysiological signals across species exhibit both periodic and aperiodic properties. Periodic oscillations are widely studied, having been linked to numerous physiological, cognitive, behavioral, and disease states. Most analyses of oscillations are conducted on canonically-defined frequency bands. This is done without consideration of the aperiodic (1/f-like) component, which compromises the accurate detection and measurement of periodic oscillations. The aperiodic component of neural power spectra has received less attention than oscillations, but emerging evidence shows that it is dynamic and changes with age, task demands, and cognitive states. The aperiodic broadband offset may reflect population spiking while its exponent may reflect relative excitation/inhibition. Problematically, standard analytic approaches conflate periodic parameters (center frequency, power, bandwidth) with aperiodic ones (offset, exponent), compromising physiological interpretations. To overcome the limitations of traditional narrowband analyses and to reduce inferential errors caused by conflating periodic and aperiodic features, we introduce a novel algorithm for semi-automated parameterization of neural power spectra. Spectra are parameterized as a combination of the aperiodic component and putative periodic oscillatory peaks. This parameterization algorithm performs as well as expert human labelers for periodic oscillations and reliably captures ground

truth parameters in simulation. Notably, this algorithm requires no *a priori* specification of bands; it extracts as many oscillations as are found in the data, after controlling for the aperiodic component. Finally, we demonstrate how this approach can be used to analyze age-related changes in working memory and we demonstrate its utility for large-scale data exploration and analysis.

Introduction

Neural oscillations are widely studied, with tens-of-thousands of publications to date. Nearly a century of research has shown that oscillations reflect a variety of cognitive, perceptual, and behavioral states (Buzsaki & Draguhn, 2004; Engel et al., 2001), with recent work showing that oscillations aid in coordinating interregional information transfer (Fries, 2005; Voytek et al., 2015). Notably, oscillatory dysfunction has been implicated in nearly every major neurological and psychiatric disorder (Kopell et al., 2014; Voytek & Knight, 2015). Following historical traditions, the vast majority of the studies examining oscillations rely on canonical frequency bands, which are approximately defined as: infraslow (< 0.1 Hz), delta (1-4 Hz), theta (4-8 Hz), alpha (8-12 Hz), beta (12-30 Hz), low gamma (30-60 Hz), high frequency activity (60-250 Hz), and fast ripples (200-400 Hz). Although most of these bands are often described as oscillations, standard approaches fail to assess whether an oscillation—meaning rhythmic activity within a narrowband frequency range—is truly present (**Fig. 1A,B**).

In the frequency domain, oscillations manifest as narrowband peaks of power above the aperiodic component (**Fig. 1A**) (Buzsáki et al., 2013; B. J. He, 2014). Examining predefined frequency regions in the power spectrum, or applying narrowband filtering (*e.g.*, 8-12 Hz for alpha) without parameterization, can lead to a misrepresentation and misinterpretation of physiological phenomena, because apparent changes in narrowband power can reflect several different physiological processes (**Fig. 1C,D**).

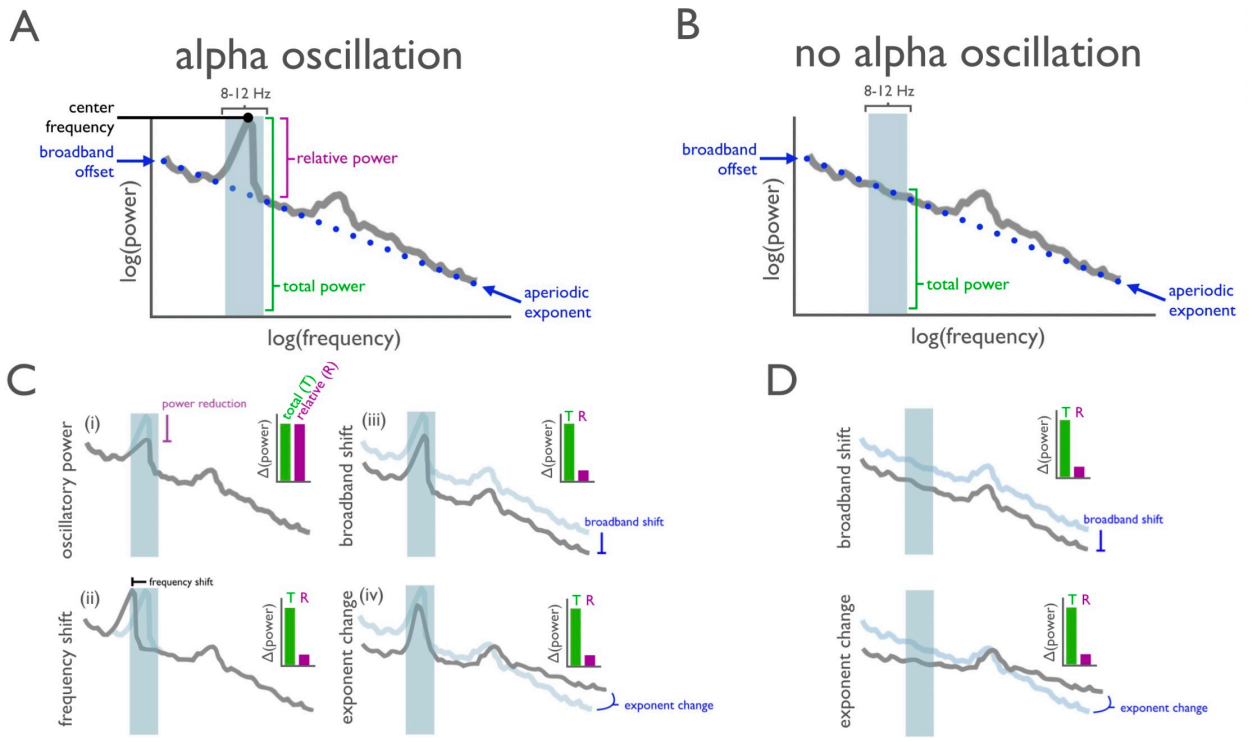

Figure 1.1 | Overlapping nature of periodic and aperiodic spectral features. (**A**) Example neural power spectrum with a strong alpha peak in the canonical frequency range (8-12 Hz, blue shaded region) and secondary beta peak (not marked). (**B**) Same as **A**, but with the alpha peak removed. (**C-D**) Apparent changes in a narrowband range (blue shaded region) can reflect several different physiological processes. Total power (green bars in the inset) reflects the total power in the range, and relative power (purple bars in the insets) reflect relative power of the peak, over and above the aperiodic component. (**C**) Measured changes, with a peak present, including: (i) oscillatory power reduction; (ii) oscillation center frequency shift; (iii) broadband power shift, or; (iv) aperiodic exponent change. In each simulated case, *total* measured narrowband power is similarly changed (inset, green bar), while only in the true power reduction case (i) has the 8-12 Hz oscillatory power *relative to* the aperiodic component actually changed (inset, purple bar). (**D**) Measured changes, with no peak present. This demonstrates how changes in the aperiodic component can be erroneously interpreted as changes in oscillation power when only focusing on a narrow band of interest.

These apparent changes include: (i) reductions in true oscillatory power (Crone, 1998; Jasper & Penfield, 1949); (ii) shifts in oscillation center frequency (Bullock, 1981; Haegens et al., 2014; Klimesch, 1999; Mierau et al., 2017; Obrist, 1954; Samaha & Postle, 2015); (iii) reductions in broadband power (Manning et al., 2009; Miller et al., 2012; Winawer et al., 2013), or; (iv) changes in aperiodic exponent (Freeman & Zhai, 2009; Gao, 2016; Gao et al., 2017; B. J. He, 2014; Podvalny et al., 2015; Voytek et al., 2015). When narrowband power changes are observed, the implicit assumption is typically a frequency-specific power change (**Fig. 1C.i**), however, each of the alternative cases can also manifest as apparent oscillatory power changes, even when there is no oscillation present (**Fig. 1D**). That is, changes in any of these parameters can give rise to identical changes in total narrowband power (**Fig. 1C,D**).

Even if an oscillation is present, careful adjudication between different oscillatory features—such as center frequency and power—is required. Variability in oscillation features is ignored by many approaches examining predefined bands and, without careful parameterization, these differences can easily be misinterpreted as narrowband power differences (Cole & Voytek, 2019) (**Fig. 1C**). For example, there is clear variability in oscillation center frequency across species (Bullock, 1981), age (Dustman et al., 1993; Obrist, 1954), and cognitive/behavioral states (Haegens et al., 2014; Mierau et al., 2017; Samaha & Postle, 2015). Oscillation bandwidth may also change, but this parameter is underreported in the literature. Thus, what is thought to be a difference in band-limited oscillatory power could, instead, reflect center frequency differences between groups or conditions of interest (Cole & Voytek, 2019; Lansbergen et al., 2011) (**Fig. 1C.ii**).

Interpreting band-limited power differences is further confounded by the fact that oscillations are embedded within aperiodic activity (represented by the dotted blue line in Fig 1A). This component of the signal stands in contrast to oscillations in that it need not arise from any regular, rhythmic process (Bullock et al., 2003). For example, signals such as white noise, or even a single impulse function, have power at all frequencies despite there being, by definition, no periodic aspect to the signal (**Fig. S1B**). Due to this aperiodic activity, pre-defined frequency bands or narrowband filters will always estimate non-zero power, even when there is no detectable oscillation present (**Fig. 1B, S1**).

In neural data, this aperiodic activity has a 1/f-like distribution, with exponentially decreasing power across increasing frequencies. This component can be characterized by a $1/f^{\chi}$ function, whereby the χ parameter, hereafter referred to as the aperiodic exponent, reflects the pattern of aperiodic power across frequencies, and is equivalent to the negative slope of the power spectrum when measured in log-log space (Miller et al., 2009). The aperiodic component is additionally parameterized with an 'offset' parameter, which reflects the uniform shift of power across frequencies. This aperiodic component has traditionally been ignored, however even when it is acknowledged it is treated as noise or as a nuisance variable to be corrected for, such as is done in spectral whitening (Groppe et al., 2013), rather than a feature to be explicitly parameterized.

Ignoring or correcting for the aperiodic component is problematic, as this component also reflects physiological information. The aperiodic offset, for example, is correlated with both neuronal population spiking (Manning et al., 2009; Miller et al., 2012) and the fMRI BOLD signal (Winawer et al., 2013). The aperiodic exponent, in contrast, has been related to the integration

of the underlying synaptic currents (Buzsáki et al., 2012), which have a stereotyped double-exponential shape in the time-domain that naturally gives rise to the 1/f-like nature of the power spectral density (PSD) (Gao et al., 2017). Currents with faster time constants, such as excitatory (E) AMPA, have relatively constant power at lower frequencies before power quickly decays whereas for inhibitory (I) GABA currents power decays more slowly as a function of frequency. This means that the exponent will be lower (flatter PSD) when E>>I, and larger when E<<I (Gao et al., 2017). Thus, treating the aperiodic component as "noise" ignores its physiological correlates, which in turn relate to cognitive and perceptual (Podvalny et al., 2015) states, while trait-like differences in aperiodic activity have been shown to be potential biological markers in development (W. He et al., 2019) and aging (Voytek et al., 2015) as well as disease, such as depression (Veerakumar et al., 2019), ADHD (Robertson et al., 2019), or schizophrenia (Molina et al., 2020).

To summarize, periodic parameters such as frequency (Bullock, 1981; Haegens et al., 2014; Klimesch, 1999; Mierau et al., 2017; Obrist, 1954; Samaha & Postle, 2015), power (Crone, 1998; Jasper & Penfield, 1949), and potentially bandwidth, as well as the aperiodic parameters of broadband offset (Manning et al., 2009; Miller et al., 2012; Winawer et al., 2013) and exponent (Freeman & Zhai, 2009; Gao, 2016; Gao et al., 2017; B. J. He, 2014; Podvalny et al., 2015; Voytek et al., 2015), can and do change in behaviorally and physiologically meaningful ways, with some emerging evidence suggesting they interact with one another (Becker et al., 2018). Reliance on *a priori* frequency bands for oscillatory analyses can result in the inclusion of aperiodic activity from outside the true physiological oscillatory band (**Fig. 1C.ii**). Failing to consider aperiodic activity confounds oscillatory measures, and masks crucial behaviorally and physiologically

relevant information. Therefore, it is imperative that spectral features are carefully parametrized to minimize conflating them with one another and to avoid confusing the physiological basis of "oscillatory" activity with aperiodic activity that is, by definition, arrhythmic.

To better characterize the signals of interest, and overcome the limitations of traditional narrowband analyses, we introduce an efficient algorithm for semi-automatically parameterizing neural PSDs into periodic and aperiodic components. This algorithm extracts putative periodic oscillatory parameters characterized by their center frequency, power, and bandwidth; it also extracts the offset and exponent parameters of the aperiodic component (Fig. 2). Importantly, this algorithm requires no specification of narrowband oscillation frequencies; rather, it identifies oscillations based on their power above the aperiodic component.

We test the accuracy of this algorithm against simulated power spectra where all the parameters of the periodic and aperiodic components are known, providing a ground truth against which to compare the algorithm's ability to recover those parameters. The algorithm successfully captures both periodic and aperiodic parameters, even in the presence of significant simulated noise (Fig. 3). Additionally, we show that algorithm performs comparably to expert human raters who manually identified peak frequencies in both human EEG and non-human local field potential (LFP) spectra (Fig. 4). Finally, we demonstrate the utility of algorithmic parameterization. First we replicate and extend previous results demonstrating spectral parameter differences between younger and older adults at rest (Fig. 5). Finally, we find a novel link between the aperiodic component and behavioral performance in a working memory task (Fig. 6).

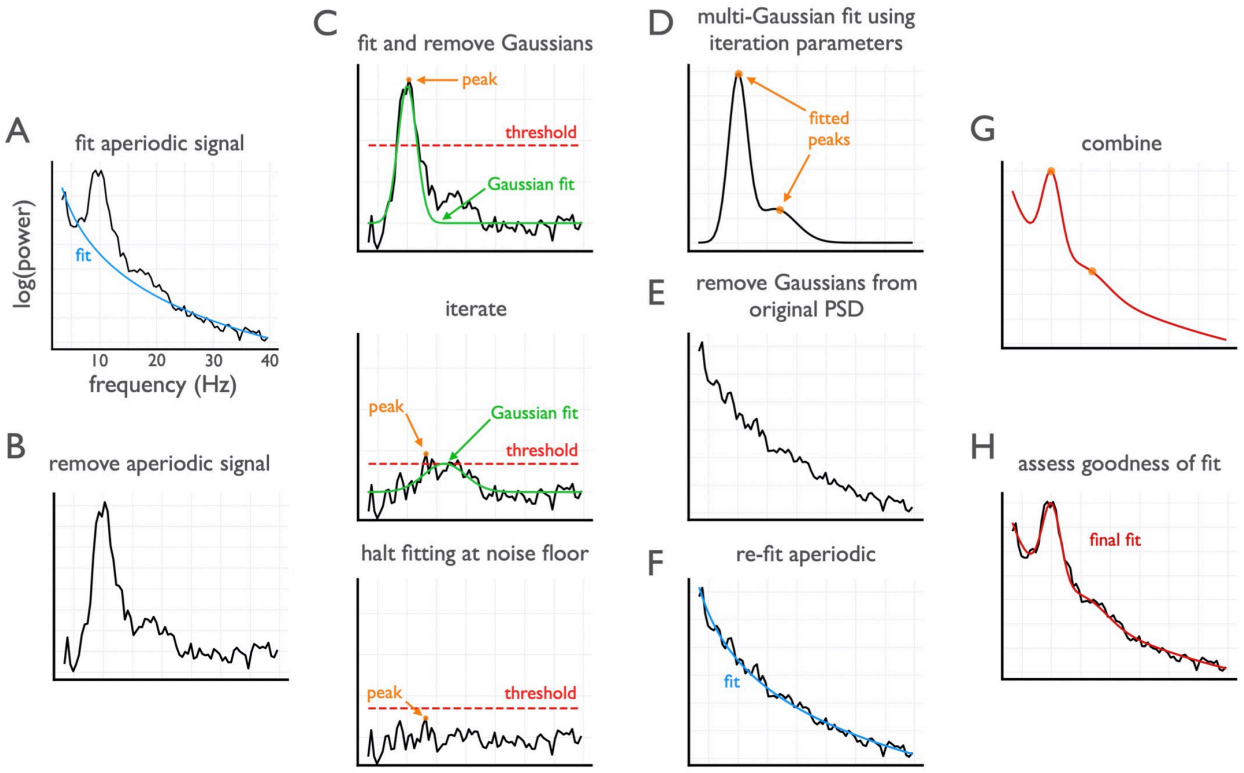

Figure 1.2 | Algorithm schematic on real data. (**A**) The power spectral density (PSD) is first fit with an estimated aperiodic component (blue). (**B**) The estimated aperiodic portion of the signal is subtracted from the raw PSD, the residuals of which are assumed to be a mix of periodic oscillatory peaks and noise. (**C**) The maximum (peak) of the residuals is found (orange). If this peak is above the noise threshold (red dashed line), calculated from the standard deviation of the residuals, then a Gaussian (green) is fit around this peak based on the peak's frequency, power, and estimated bandwidth (see **Methods**). The fitted Gaussian is then subtracted, and the process is iterated until the next identified point falls below a noise threshold or the maximum number of peaks is reached. The peak-finding at this step is only used for seeding the multi-Gaussian in **D**, and, as such, the output in **D** can be different from the peaks detected at this step. (**D**) Having identified the number of putative oscillations, based on the number of peaks above the noise threshold, multi-Gaussian fitting is then performed on the aperiodic-adjusted signal from **B** to account for the joint power contributed by all the putative oscillations, together. In this example, two Gaussians are fit with slightly shifted peaks (orange dots) from the peaks identified in **C**. (**E**) This multi-Gaussian model is then subtracted from the original PSD from **A**. (**F**) A new fit for the aperiodic component is estimated—one that is less corrupted by the large oscillations present in the original PSD (blue). (**G**) This re-fit aperiodic component is combined with the multi-Gaussian model to give the final fit. (**H**) The final fit (red)—here parameterized as an aperiodic component and two Gaussians (putative oscillations)—captures >99% of the variance of the original PSD. In this example, the extracted parameters for the aperiodic component are: broadband offset = -21.4 au; exponent = 1.12 au/Hz. Two Gaussians were found, with the parameters: (1) frequency = 10.0 Hz, power = 0.69 au, bandwidth = 3.18 Hz; (2) frequency = 16.3 Hz, power = 0.14 au, bandwidth = 7.03 Hz.

Methods

Algorithm development and analyses for this manuscript were done with the Python programming language. The code for the algorithm[i] and for the analyses[ii] presented in this paper are openly available.

Algorithmic parameterization

The parameterization method presented herein quantifies characteristics of electro- or magneto-physiological data, in the frequency domain. While many methods can be used to calculate the power spectra for algorithmic parametrization, throughout this investigation we use Welch's method (Welch, 1967). The algorithm conceptualizes the PSD as a combination of an aperiodic component, with overlying periodic components, or oscillations. These putative oscillatory components of the PSD are characterized as frequency regions of power over and above the aperiodic component, and are referred to here as "peaks". The algorithm operates on PSDs in *semilog*-power space, which is linearly spaced frequencies, and log-spaced power values, which is the representation of the data for all of the following, unless noted. The aperiodic component is fit as a function across entire fitted range of the spectrum, and each oscillatory peak is individually modeled with a Gaussian. Each Gaussian is taken to represent an oscillation, whereby the three parameters that define a Gaussian are used to characterize the oscillation (**Fig. 2**).

[i] https://github.com/fooof-tools/fooof

[ii] https://github.com/fooof-tools/Paper

This formulation models the power spectrum as:

$$P = L + \sum_{n=0}^{N} G_n \qquad (1)$$

where power, *P*, representing the PSD, is a combination of the aperiodic component, *L*, and *N* total Gaussians, *G*. Each G_n is a Gaussian fit to a peak, for *N* total peaks extracted from the power spectrum, modeled as:

$$G_n = a * exp\left(\frac{-(F-c)^2}{2w^2}\right) \qquad (2)$$

where *a* is the power of the peak, in log_{10}(power) values, *c* is the center frequency, in Hz, *w* is the standard deviation of the Gaussian, also in Hz, and *F* is the vector of input frequencies.

The aperiodic component, *L*, is modeled using a Lorentzian function, written as:

$$L = b - \log(k + F^{\chi}) \qquad (3)$$

where *b* is the broadband offset, χ is the exponent, and *k* is the "knee" parameter, controlling for the bend in the aperiodic component (Miller et al., 2009), with *F* as the vector of input frequencies. Note that when *k=0*, this formulation is equivalent to fitting a line in *log-log* space, which we refer to as the fixed mode. Note that there is a direct relationship between the slope, *a*, of the line in *log-log* spacing, and the exponent, χ, which is χ = -*a* (when there is no knee). Fitting with *k* allows for parameterizing bends, or knees, in the aperiodic component that are present in broad frequency ranges, especially in intracranial recordings (Miller et al., 2009).

The final outputs of the algorithm are the parameters defining the best fit for the aperiodic component and the *N* Gaussians. In addition to the Gaussian parameters, the algorithm computes transformed 'peak' parameters. For these peak parameters, we define: (1)

center frequency as the mean of the Gaussian; (2) aperiodic-adjusted power—the distance between the peak of the Gaussian and the aperiodic fit (this is different from the power in the case of overlapping Gaussians that might share overlapping power), and; (3) bandwidth as 2*std* of the fitted Gaussian. Notably, this algorithm extracts all these parameters together in a manner that accounts for potentially overlapping oscillations; it also minimizes the degree to which they are confounded and requires no specification of canonical oscillation frequency bands.

To accomplish this, the algorithm first finds an initial fit of the aperiodic component (**Fig. 2A**). This first fitting step is crucial and not trivial, as any traditional fitting method, such as linear regression, or even robust regression methods designed to account for the effects of outliers on linear fitting, can still be significantly pulled away from the true aperiodic component due to the overwhelming effect of the high power oscillation peaks. To account for this, we introduce a procedure that attempts to fit the aperiodic aspects of the spectrum only. To do so, initial seed values for offset and exponent are set to the power of the first frequency in the PSD and an estimated slope, calculated between the first and last points of the spectrum (calculated in *log-log* spacing, and converted to a positive value, since $\chi = -a$). These seed values are used to estimate a first-pass fit.

This first-pass aperiodic fit is then subtracted from the original PSD, creating a flattened spectrum, from which a power threshold (set at the 2.5 percentile) is used to find the lowest power points among the residuals, such that this excludes any portion of the PSD with peaks that have high power values in the flattened spectrum. This approach identifies only the data points along the frequency axis that are most likely to not be part of an oscillatory peak, thus isolating the parts of the spectrum that most likely to represent the aperiodic component (**Fig. 2A**). A

second fit of the original PSD is then performed only on these frequency points, giving a better estimate of the aperiodic component. This is, in effect, similar to approaches that have attempted to isolate the aperiodic component from oscillations by fitting only to spectral frequencies outside of an *a priori* oscillation (Voytek et al., 2015), but does so in a more unbiased fashion. The percentile threshold value can be adjusted if needed, but in practice rarely needs to be.

After the estimated aperiodic component is isolated, it is regressed out, leaving the non-aperiodic activity (putative oscillations) and noise (**Fig. 2B**). From this aperiodic-adjusted (*i.e.*, flattened) PSD, an iterative process searches for peaks that are each individually fit with a Gaussian (**Fig. 2C**). Each iteration first finds the highest power peak in the aperiodic-adjusted (flattened) PSD. The location of this peak along the frequency axis is extracted, along with the peak power. These stored values are used to fit a Gaussian around the central frequency of the peak. The standard deviation is estimated from the full-width, half-maximum (FWHM) around the peak by finding the distance between the half-maximum powers on the left- and right flanks of the putative oscillation. In the case where there are two overlapping oscillations, this estimate can be very wide, so the FWHM is estimated as twice the shorter of the two sides. From FWHM, the standard deviation of the Gaussian can be estimated via the equivalence:

$$std = \frac{FWHM}{2\sqrt{2ln2}} \qquad (4)$$

This estimated Gaussian is then subtracted from the flattened PSD, the next peak is found, and the process is repeated. This peak-search step halts when it reaches the noise floor, based on a parameter defined in units of the standard deviation of the flattened spectrum, re-calculated for each iteration (default = 2*std*). Optionally, this step can also be controlled by

setting an absolute power, and/or a maximum number of Gaussians to fit. The power thresholds (relative or absolute) determine the minimum power beyond the noise floor that a peak must extend in order to be considered a putative oscillation. Once the iterative Gaussian fitting process halts, in order to handle edge cases, Gaussian parameters that heavily overlap (whose means are within 0.75*std* of the other), and/or are too close to the edge (<= 1.0*std*) of the spectrum, are then dropped. The remaining collected parameters for the *N* putative oscillations (center frequency, power, and bandwidth) are used as seeds in a multi-Gaussian fitting method (Python: scipy.optimize.curve_fit). Each fitted Gaussian is constrained to be close to (within 1.5*std*) of its original guessed Gaussian. This process attempts to minimize the square error between the flattened spectrum and *N* Gaussians simultaneously (**Fig. 2D**).

This multi-Gaussian fit is then subtracted from the *original* PSD, in order to isolate an aperiodic component from the parameterized oscillatory peaks (**Fig. 2E**). This peak-removed PSD is then re-fit, allowing for a more precise estimation of the aperiodic component (**Fig. 2F**). When combined with the equation for the *N*-Gaussian model (**Fig. 2G**), this procedure gives a highly accurate parameterization of the original PSD (**Fig. 2H;** in this example, >99% of the variance in the original PSD is accounted for by the combined aperiodic + periodic components). Goodness-of-fit is estimated by comparing each fit to the original power spectrum in terms of the median absolute error (MAE) of the fit as well as the R^2 of the fit.

The fitting algorithm has some settings, that can be provided by the user, one of which defines the aperiodic mode, with options of 'fixed' or 'knee', which dictates whether to fit the aperiodic component with a knee. This parameter should be chosen to match the properties of the data, over the range to be fit. The algorithm also requires a setting for the relative threshold

for detecting peaks, which defaults to 2, in units of standard deviation. In addition, there are optional settings, which can be used to define: (1) the maximum number of peaks; (2) limits on the possible bandwidth of extracted peaks, and; (3) absolute, rather than relative, power thresholds. The algorithm can often be used without needing to change these settings. Some tuning may be useful for tuning algorithmic performance to different datasets with potentially different properties, for example, data from different modalities, data with different amounts of noise, and/or for fitting across different frequency ranges. Detailed description and guidance on these settings and if and how to change them can be found in the tool's documentation. All parameter names, as well as their descriptions, units, default values, and accessibility to the API are also presented in Supplementary Table 1.

Code for this algorithm is available as a Python package, licensed under an open source compliant Apache-2.0 license. The module supports Python >= 3.5, with minimal dependencies of *numpy* and *scipy* (>= version 0.19), and is available to download from the Python Package Index[iii]. The package is openly developed and maintained on GitHub[iv]. The project's repository includes the codebase, a test-suite, instructions for installing and contributing to the package, and the documentation materials. The documentation is also hosted on the documentation website[v], which includes tutorials, examples, frequently asked questions, a section on motivations for parameterizing neural power spectra, and a list of all the functionality available. On contemporary hardware (3.5 GHz Intel i7 MacBook Pro), a single PSD is fit in approximately

[iii] https://pypi.python.org/pypi/fooof/

[iv] https://github.com/fooof-tools/fooof/

[v] https://fooof-tools.github.io/fooof/

10-20 ms. Because each PSD is fit independently, this package has support for running in parallel across PSDs to allow for high-throughput parameterization.

Simulated PSD creation and algorithm performance analysis

Power spectra were simulated following the same underlying assumption of the fitting algorithm, that PSDs can be reasonably approximated as a combination of an aperiodic component and overlying peaks, that reflect putative periodic components of the signal. The equations used in the algorithm and described in the methods for the fitting procedure were used to simulate power spectra, such that for each simulated spectrum, the underlying parameters used to generate it are known. On top of the simulated aperiodic component with overlying peaks, white noise was added, with the level of noise controlled by a scaling factor. The power spectra were therefore simulated as an adapted version of equation (1):

$$P = L + \sum_{n=0}^{N} G_n + m\varepsilon \qquad (5)$$

Where P is a simulated power spectrum, L and G_n are the same as described in equations (2) and (3) respectively, ε is white noise, applied independently across frequencies, m is a multiplicative scaling factor of that noise.

For all simulations, the parameterization algorithm was used with settings of {peak_width_limits = [1,8], max_n_peaks = 6, min_peak_height = 0.1, peak_threshold = 2.0, aperiodic_mode = 'fixed'}, except where noted. For each set of simulations, 1000 power spectra were simulated for each condition. The algorithm was fit to each simulated spectrum, and estimated values for each parameter were compared to ground truth values of the simulated data. Deviation of the parameter values was calculated as the absolute deviation for the fit value

from the ground truth value. We also collected the goodness-of-fit metrics (error and R^2) and the number of fit peaks from the spectral parameterizations.

For the first set of simulations, power spectra were generated across the frequency range of 2-40 Hz, with a frequency resolution of 0.25 Hz (Fig 3A-F). The aperiodic component was generated with *y*-intercept (offset) parameter of 0, and without a knee (k=0). Exponent values were sampled uniformly from possibilities {0.5, 1, 1.5, 2}. Oscillation center frequencies came from the range of 3-34 Hz (1 Hz steps), with each center frequency sampled as the observed probability of center frequencies at that frequency in real data. For simulations in which there were multiple peaks within a single spectrum (Fig 3D-F), center frequencies were similarly sampled at random, with the extra constraint that a candidate center frequency was rejected if it was within 2 Hz on either side of another center frequency already selected for the simulated spectrum, such that individual spectra could not have superimposed peaks. Peak powers and bandwidths were sampled uniformly from {0.15, 0.20, 0.25, 0.4} and {1, 2, 3} respectively, independent of their center frequency.

A set of power spectra were generated with one peak per spectrum across five noise levels {0.0, 0.025, 0.05, 0.10, 0.15} (Fig 3A-C). In these simulations, the center frequency, power, and bandwidth of the fit peak, as well the aperiodic exponent, were compared to the ground truth parameters. In order to compare ground truth parameters to the spectral reconstructions, which potentially included more than one peak, the highest power peak was extracted from the spectral fit to use for comparison. In another set of simulations, PSDs were created with a varying number of peaks – between 0 and 4 – with a fixed noise value of 0.01 (Fig 3D-F). For these simulations, the performance of the algorithm was examined in terms of the fit error across the

number of peaks, as well by comparing the number of simulated peaks to the number of peaks in the spectral fit.

Simulated power spectra to test across a broader frequency range were generated across the frequency range of 1-100 Hz, with a frequency resolution of 0.5 Hz (Fig S2 A-C). These spectra were created with knees, using knee values of {0, 10, 25, 100, 150}, sampled with equal probability, with offset and exponent values sampled as done previously. For these spectra two peaks were added, one in the low frequency range, sampled as previously described, with an additional peak sampled with a center frequency sampled, with even probability, from between 50 and 90 Hz (in 1 Hz) steps, with the same sampled power and bandwidth values as used previously. These spectra were generated across different noise levels, as before. Spectra were fit using the same algorithm settings as before, except for aperiodic mode being set to 'knee'. Parameter reconstruction was evaluated, with the addition of calculating the accuracy of the reconstructed knee parameter.

Additional simulations were created to evaluate the model performance with respect to violations of model assumptions (Fig S3 A-I). To examine violations of the aperiodic model assumptions, a set of spectra were also simulated with knees (Fig 3A-C) but were fit in the 'fixed' aperiodic mode, using the same settings as before. Simulations were created as described above for simulations including knees, except that in order to evaluate the influence of knee parameters, spectra were simulated and grouped by knee values, for values of {0, 10, 50, 100, 150}, using a fixed noise level of 0.01. For these simulations, performance was primarily evaluated in terms of reconstruction accuracy of the aperiodic exponent, and in the number of fit peaks.

To examine model violations of the periodic component, power spectra were also simulated using asymmetric peaks in the frequency domain (Fig S3 D-F). For these simulations, peaks were simulated as skewed gaussians, in which an additional parameter is used that controls the skewness of the peaks (simulated in code with `scipy.stats.skewnorm`). These simulations were created across the frequency range of 2-40 Hz, with a fixed noise value of 0.01. Each spectrum contained a single peak, with peak parameters sampled as in the prior simulations for this range. A skew value was added to the peak, across conditions with skew values of {0, 5, 10, 25, 50}. For these simulations, performance was primarily evaluated in terms of reconstruction accuracy of the peak center frequency, and in the number of fit peaks.

In addition, time series simulations were created with non-sinusoidal oscillations (Fig 3G-I), to investigate how the algorithm performs with asymmetric cycles and the resulting power spectra. Simulations were created as time series signals of oscillations of asymmetric cycles combined with aperiodic activity, using the simulation tools in the NeuroDSP Python toolbox (Cole et al., 2019). Time series were simulated as 10 second segments at a sampling rate of 500 Hz. The aperiodic component of the signal was simulated as a 1/f signal, with exponent values sampled from the same values as above. The periodic component of the data was an asymmetric oscillation, with a peak frequency sampled as above. These oscillations were created with varying across rise-decay symmetry values (Cole & Voytek, 2017) of {0.5, 0.625, 0.75, 0.875, 1.0}. Note that a value of 0.5, with a symmetric rise and decay is a sinusoid, whereas values approaching 1 are increasingly sawtooth-like. The full signal was a combination of the two components, from which power spectra were calculated, using Welch's method (2 second segments, 50% overlap, Hanning window). The power spectrum models were then fit across the frequency range of [2,

40], using the same settings as above. For these simulations, performance was primarily evaluated in terms of reconstruction accuracy of the peak center frequency, and in the number of fit peaks.

Human labelers versus algorithm

In addition to simulated power spectra, randomly selected EEG (n = 64) and LFP (n = 42) PSDs were labeled by the algorithm and by expert human raters (n = 9). PSDs were calculated using Welch's method (Welch, 1967) (1 second segments, 50% overlap, Hanning window). These PSDs were then fit and labeled from 2 to 40 Hz. Note that human labeling was done only for the center frequencies of putative oscillations on the PSDs that had the aperiodic component still present, as this is the most common human PSD parameterization approach. This misses all other features that the algorithm can also parameterize (power, bandwidth, offset, and exponent). Raters gave a high/low confidence rating to their labels, to provide a human analog for overfitting, and all plots and analyses use only results from the high-confidence ratings (including low-confidence ratings significantly impairs human label performance). Comparisons of the number of average numbers of peaks fit to each spectrum were done using independent-samples t-tests, where for each spectrum we counted the number of peaks identified by the algorithm, and compared that number across all spectra to the average number of peaks the human raters found per spectrum.

In order to estimate a putative "truth" for real physiological data where ground truth is unknown, we used a majority rule approach wherein a "consensus truth" criterion was calculated for each PSD separately by estimating the majority consensus for each identified peak. Specifically, for each PSD, all peaks identified by every human labeler were pooled, and the

frequency of identification was established for each peak. Those peaks that were identified by the majority of labelers ($n > 4$) within 1.0 Hz of one another were set as the putative truth for that PSD. All human labelers, and the algorithm, were then scored against this putative truth. Precision, recall, and F_1 scores for human raters and the algorithm were calculated for each rater across all PSDs.

Accuracy measures were then averaged across human labelers and compared the those of the algorithm. Normally, precision is calculated as the number of true positives divided by the total of true positives and false positives. However, because ground truth is unknown, "true positive" and "false positive" here are defined relative to the consensus truth. Similarly, recall is calculated as the number of true positives divided by the total of true positives and false negatives.

The F_1 score is a weighted measure of accuracy that combines precision and recall. This metric is used because precision can be artificially very high while recall is very low; for example, it is possible to inflate precision by simply identifying a peak at every point along the frequency axis, thus no peaks would ever be missed, but recall would be severely impacted. If no peaks were found, precision and recall were all set to 0. Correct rejections were not included in performance estimates; had they been included, every non-peak that was correctly identified as such (most of the power spectra) would be marked as a correct rejection, skewing performance results.

For those instances when a human labeler or the algorithm identified no peaks in the PSD, precision and recall values were set to 0 if the putative truth contained any peaks, and to 1 if there was no consensus among human labelers on any of the peaks (i.e., the putative truth

criterion was 0 peaks). Thus, the majority rule scoring system did not penalize either human labelers or the algorithm for correctly rejecting false positives. All reported *p* values are Bonferroni corrected for the three correlated comparisons (precision, recall, and F_1) performed for each modality (EEG and LFP). Comparisons of these measures across PSDs were assessed using the z-score, where the algorithm's precision, recall, and F1 scores were compared to the distribution of the raters' scores. For the Spearman correlation, rater precision and recall on both EEG and LFP data were included.

Algorithmic analysis of EEG and LFP

Scalp EEG data. Electroencephalography (EEG) data from a previously described study (Tran et al., 2016) were re-analyzed here. Briefly, we collected 64-channel scalp EEG from 17 younger (20-30 years old) and 14 older (60-70 years old) participants while they performed a visual working memory task as well as a resting state period. All participants gave informed consent approved by the University of California, Berkeley Committee on Human Research. Participants were tested in a sound-attenuated EEG recording room using a 64+8 channel BioSemi ActiveTwo system. EEG data were amplified (-3dB at ~819 Hz analog low-pass, DC coupled), digitized (1024 Hz), and stored for offline analysis. Horizontal eye movements (HEOG) were recorded at both external canthi; vertical eye movements (VEOG) were monitored with a left inferior eye electrode and superior eye or fronto-polar electrode. All data were referenced offline to an average reference. All EEG data were processed with the MNE Python toolbox (Gramfort et al., 2014), the algorithm described herein, and custom scripts. These data have previously been reported(Tran et al., 2016), though all analyses presented here are novel using our new algorithmic approach.

EEG task and stimuli. Participants performed a visual working memory task. They were instructed to maintain central fixation and asked to respond using the index finger of their right hand. The visual working memory paradigm was slightly modified from the procedures used in Vogel and Machizawa (2004) (Vogel & Machizawa, 2004) as previously outlined (Voytek & Knight, 2010), where additional task details can be found. Participants were visually presented with a constant fixation cross in the center of the screen throughout the entire duration of the experiment. At the beginning of each trial, this cross would flash to signal the beginning of the trial. This was followed 350 ms later by one, two, or three (corresponding to the load level) differently colored squares for 180 ms, lateralized to either the left or right visual hemifield. After a 900 ms delay, a test array of the same number of colored squares appeared in the same spatial location. Participants were instructed to respond with a button press to indicate whether or not one item in the test array had changed color compared to the initial memory array. Each participant performed 8 blocks of 40 trials each.

EEG behavioral data analysis. Behavioral accuracy was assessed using a d' measure of sensitivity which takes into account the false alarm rate to correct for response bias (d' = Z(*hit rate*)-Z(*false alarm rate*)). To avoid mathematical constraints in the calculation of d', we applied a standard correction procedure, wherein, for any participants with a 100% hit rate or 0% false alarm rate, performance was adjusted such that 1/(2N) false alarms were added or 1/(2N) hits subtracted where necessary.

EEG Pre-processing. Each participant's EEG data were first filtered with a highpass filter at 1 Hz, and then decomposed using ICA (Bell & Sejnowski, 1995). Any ICA components that significantly correlated with HEOG and/or VEOG activity were automatically identified and

rejected. A two-minute segment of data from the beginning of the recording was extracted and analyzed as resting state data. Trials were epoched from -0.85 to 1.10 seconds relative to stimulus onset. All incorrect trials and trials with artifacts were excluded from subsequent analysis. The AutoReject procedure was used to estimate thresholds and automatically reject any trials with artifacts, as well as to interpolate bad channels (Jas et al., 2017).

EEG resting state data analysis. Power spectra were calculated for all channels, using Welch's method (Welch, 1967), for a two-minute segment of extracted resting state data from the beginning of the recording. These power spectra were fit using the algorithm, using the settings {peak_width_limits = [1,6], max_n_peaks = 6, min_peak_height = 0.05, peak_threshold = 1.5, aperiodic_mode = 'fixed'}. The average R^2 of spectral fits was 0.96, reflecting good fits, though one participant from the younger group was considered an outlier, with R^2 and absolute error of the fit more than 2.5 standard deviations away from the mean; this participant was dropped from further analyses in the resting condition. Estimated periodic spectral parameters were analyzed from a posterior channel of interest, Oz, chosen to capture visual cortical alpha activity. Aperiodic parameters were analyzed from channel Cz.

T-tests were performed to evaluate differences between age groups. For visualization purposes, periodic and/or aperiodic components were reconstructed for each participant's fitted parameters. To explore if aperiodic differences could drive frequency-specific power differences, *t*-tests were run at each frequency, comparing between younger and older adult group, for the power values from the reconstructed aperiodic-only signal. To compare participant-specific fits to canonical band analyses, the overlap of a Gaussian centered at 10 Hz with a +/-2 Hz bandwidth

(reflecting the common 8-12 Hz alpha range) was calculated with the individualized center frequency per participant, using a fixed +/-2 Hz bandwidth range. All *t*-tests are two-tailed.

EEG task data analysis. For task analyses, data were analyzed from visual cortical alpha electrodes contralateral to the hemifield of visual stimulus presentation (right hemifield stimuli: {P3, P5, P7, P9, PO3, PO7, O1}; left hemifield stimuli: {P4, P6, P8, P10, PO4, PO8, O2}). Only correct trials were analyzed, and trials were collapsed across presentation side. Trials were split up into the three segments of interest: baseline [-0.85 to -0.35 sec], early trial segment [0.10 to 0.60 sec], and late trial segment [0.50 to 1.00 sec].

For spectral parameterization analyses, PSDs were calculated across each segment, for each channel, and spectra were fit, using the same settings as the rest data. Fitted parameters were then averaged across channels, to arrive at one set of parameters per trial, per participant. For comparison, two canonical alpha band analyses were run, one in which trial data were filtered to the alpha range (8-12 Hz), and another in which the data were filtered +/- 2 Hz around an individualized alpha center frequency, identified as the frequency of peak power between the range 7-14 Hz. These filtered copies of the data were then epoched and Hilbert transformed to calculate analytic alpha amplitude. Average analytic alpha was calculated across each time segment. Evoked measures of each parameter (*i.e.*, canonical alpha, aperiodic-adjusted alpha power, and aperiodic offset and exponent) were calculated, in which the value of the parameter in the late trial was baseline-corrected by the measure of the parameter from the pre-trial baseline period for each investigated parameter.

To investigate which estimation technique (canonical band estimation vs. spectral parameterization) and which spectral parameter best predicted behavior, regression models

were used to predict d', per load, from canonical or spectral parameterization output measures, separately for each age group. We used a baseline behavioral model, predicting d' from the memory load (the number of presented items in the trial), and all models also used load as a covariate. To compare which features best predicted behavior, we predicted separate models, using 1) canonical alpha, 2) canonical alpha measured at an individualized frequency, 3) parameterized alpha, 4) parameterized aperiodic features. These models are described as:

$$d' = b_0 + b_1(load) + \varepsilon$$ baseline model

$$d' = b_0 + b_1(load) + b_2(\alpha_{pw(c)}) + \varepsilon$$ canonical alpha model

$$d' = b_0 + b_1(load) + b_2(\alpha_{pw(cif)}) + \varepsilon$$ individualized canonical alpha model

$$d' = b_0 + b_1(load) + b_2(\alpha_{pw(p)}) + \varepsilon$$ parameterized alpha model

$$d' = b_0 + b_1(load) + b_2(ap_{exp}) + b3(ap_{off}) + \varepsilon$$ aperiodic model

In the above, α_{pw} represents alpha power, and *c*, *icf*, *p* represent 'canonical', 'canonical' with individualized frequency', and 'parameterized', respectively, and ap represents aperiodic, with *exp* and *off* denoting exponent and offset respectively. All models were fit as ordinary least squares linear models. Model fitting and comparisons were done using the *statsmodels* module in Python. The F-test for overall significance of the model was used to evaluate whether each model provided a significant fit.

LFP data. LFP data used for algorithm validation came from two male rhesus monkeys (*Maccaca mulatta*) 4 to 5 years of age, collected for a previously reported experiment (methodological details can be found in the corresponding manuscript (Lara & Wallis, 2014)). All procedures were carried out in accord with the US National Institutes of Health guidelines and

the recommendations of the University of California, Berkeley Animal Care and Use Committee. Neuronal responses were recorded from PFC using arrays of 8-32 tungsten microelectrodes. Local field potentials were recorded with a 1 kHz sampling frequency and analyzed offline. LFP were isolated from the band-passed (0-100 Hz) recordings, and spectral fits were done on a channel-by-channel basis using Welch's method and the same settings used for the EEG analyses described above.

Results

Algorithm performance against simulated data

To investigate algorithm performance, we simulated realistic neural PSDs with known ground truth parameters. These simulated spectra consist of a combination of Gaussians, with variable center frequency, power, and bandwidth; an aperiodic component with varying offset and exponent; and noise. Algorithm performance was evaluated in terms of its ability to reconstruct the individual parameters used to generate the data (**Fig. 3;** see **Methods**). Individual parameter accuracy was considered, since the algorithm, without using the settings to limit the number of fitted peaks, can arbitrarily increase R^2 and reduce error. Thus, overall fit error should not be the sole method by which to assess algorithm performance, and should be considered together with the number of peaks fit. This is because, in the extreme, if the algorithm fits a peak at every frequency then the error between the center frequency of the true peak and the closest identified peak will be artificially low. In addition, global goodness-of-fit measures such as R^2 or mean squared error are not directly related to accuracy of individual parameter estimation.

Common analyses seek to identify and measure the most prominent oscillation in the power spectrum. To assess algorithm performance at this task, we began by simulating a single spectral peak with varying levels of both noise and aperiodic parameters (**Fig. 3A**). Algorithm performance is assessed by the absolute error of each of the reconstructed parameters: aperiodic offset and exponent (**Fig. 3B**), as well as center frequency, power, and bandwidth of the largest peak (**Fig. 3C**). Note that power as returned by the algorithm always refers to aperiodic-adjusted power—that is the magnitude of the peak *over and above* the aperiodic component.

Simulated aperiodic exponents ranged between [0.5, 2.0] au/Hz, and the median absolute error (MAE) of the algorithmically identified exponent remained below 0.1 au/Hz, even in the presence of high noise, with MAE increasing monotonically across noise levels (**Fig. 3B**). Spectral peaks were simulated with center frequencies between [3, 34] Hz, with peak power between [0.15, 0.4] au above the aperiodic component, and bandwidths between [1, 3 Hz] (see methods for full details). When identifying center frequency, MAE was within 1.25 Hz of the true peak for all tested noise levels. For peak power MAE remained below 0.1 au, and for bandwidth MAE was within 1.25 Hz, for even the largest noise scenarios. In both cases MAE increased monotonically with noise (**Fig. 3A**). Note that for bandwidth, a default algorithm parameter limits maximum bandwidth to 8.0 Hz (see **Methods**), which likely reduces MAE.

Another use case for the algorithm is to identify multiple oscillations (**Fig. 3D-F**). Here we assess performance as overall fit error, considered in combination with whether the algorithm finds the correct number of oscillations. In the presence of multiple simulated peaks (**Fig. 3D**), the median fit error increases monotonically as the number of peaks increases (**Fig. 3E**). Multiple simulated peaks can differ significantly in power and can overlap, increasing fit error. Despite this, the modal number of fit peaks matches the number of true simulated peaks (**Fig. 3E,F**).

Additional simulations tested algorithm performance across broader frequency ranges (**Fig. S2**). For the frequency range of 1-100 Hz, MAE was below 1.5 Hz for low frequency peaks (3-34 Hz), and below 4 Hz for high frequency peaks (50-90 Hz), across noise levels (**Fig. S2B**). Across larger frequency ranges, spectra often exhibit a 'knee', or bend in the aperiodic component of the data

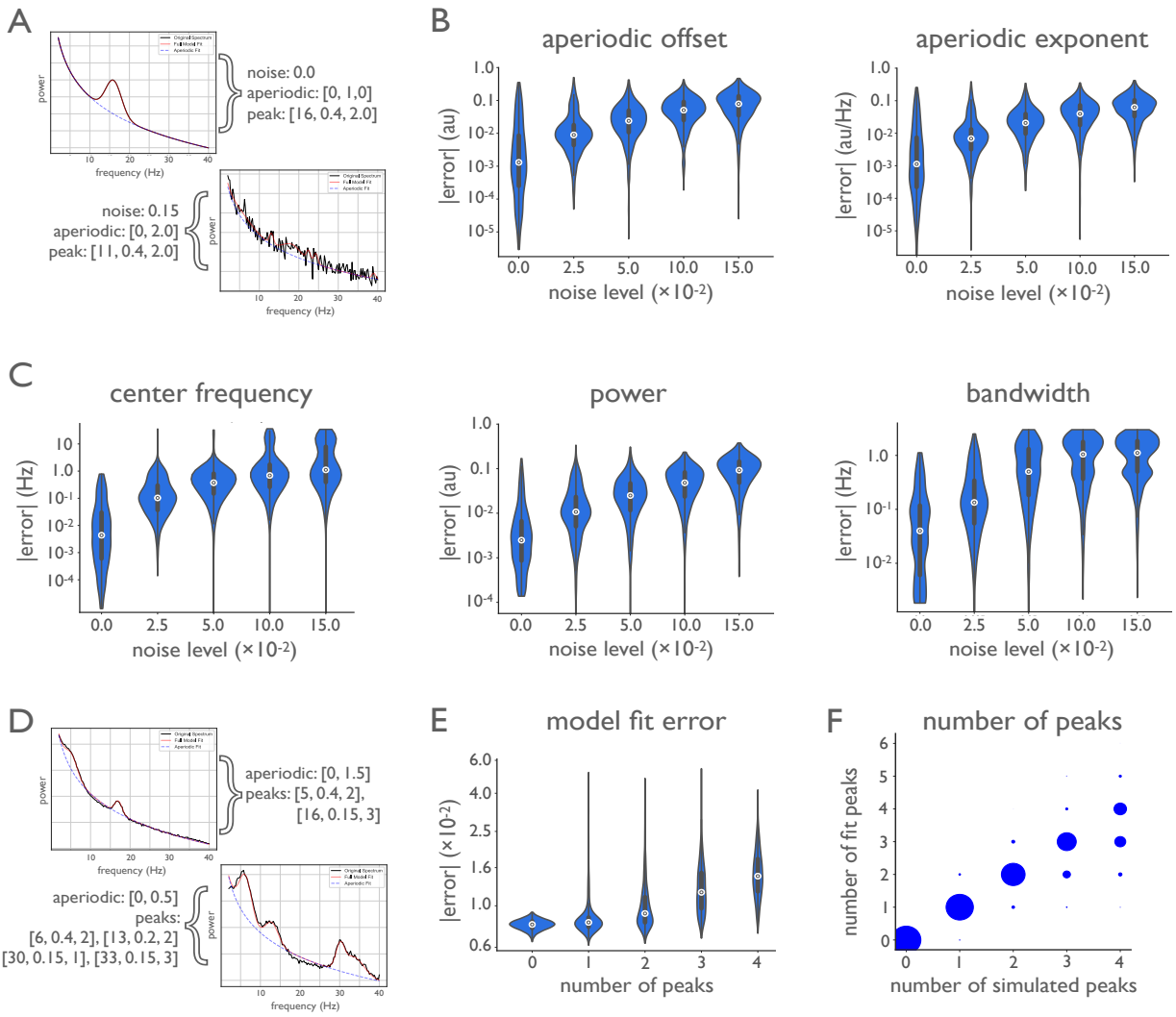

Figure 1.3 | Algorithm performance on simulated data. (**A-C**) Power spectra were simulated with one peak, at five distinct noise levels (1000 spectra per noise level). (**A**) Example spectra with simulation parameters are shown (black), as aperiodic [offset, exponent] and periodic [center frequency, power, bandwidth]. Spectral fits (red), for the one-peak simulations in a low- and high-noise scenario. Simulation parameters for plotted example spectra are noted. (**B**) Median absolute error (MAE) of the algorithmically identified aperiodic offset and exponent, across noise levels, as compared to ground truth. (**C**) MAE of the algorithmically identified peak parameters—center frequency, power, and bandwidth—across noise levels. In all cases, MAE increases monotonically with noise, but remains low. (**D-F**) A distinct set of power spectra were simulated to have different numbers of peaks (0-4, 1000 spectra per number of peaks) at a fixed noise level (0.01). (**D**) Example simulated spectra, with fits, for the multi-peak simulations. Conventions as in **A**. (**E**) Absolute model fit error for simulated spectra, across number of simulated peaks. (**F**) The number of peaks present in simulated spectra compared to the number of fitted peaks. All violin plots show full distributions, where small white dots represent median values and small box plots show median, first and third quartiles, and ranges. The algorithm imposes a 6.0 Hz maximum bandwidth limit in its fit, giving rise to the truncated errors for bandwidth in **C**. Note that the error axis is log-scaled in **B,C,E**.

(Gao et al., 2020; Miller et al., 2009) (see **Methods**). Knee locations were simulated between [0, 150] au, and MAE for the recovered parameters was below 15 au, while maintaining good performance for offset (MAE below 0.2) and exponent (MAE below 0.15) (**Fig. S2C**). Finally, the robustness of the algorithm was assessed against violations of model assumptions, including fitting no knee when a knee is present, non-Gaussian peaks, and non-sinusoidal oscillations (**Fig. S3**).

Algorithm performance against expert human labeling

Next, we examined algorithm performance against how experts identify peaks in PSDs. Because it is uncommon for human raters to manually measure the other spectral features parameterized by the algorithm, human raters experienced in oscillation research (n=9) identified only the center frequencies of peaks in human EEG and non-human primate LFP PSDs (**Fig. 4A,B**, see **Methods**). For many spectra there was strong consensus (e.g., **Fig. 4A**), but not for all (e.g., **Fig. 4B**). Performance was quantified in terms of precision, recall, and F_1 score, the latter of which combines precision and recall with equal weight (see **Methods**). This is a conservative approach that underestimates the abilities of the algorithm (which is optimized to best fit the entire spectrum, not just a peak's center frequency). Also important is that the definition of surrogate ground truth used here means that when human raters show disagreement regarding the center frequency of putative oscillations, the algorithm will be marked as incorrect (**Fig. 4B**).

Human labelers were relatively consistent in peak labeling for both EEG and LFP datasets, as evidenced by above-chance recall for each rater with the majority (**Fig. 4C**). Despite the disadvantages outlined above, the algorithm identified a similar number of peaks as the raters for both EEG (n=64 PSDs; humans, algorithm: 1.81, 1.71; t_{63}=0.77, p=0.44) and LFP (n=42

spectra, humans, algorithm: 1.05, 1.10; t_{41}=-0.47, p=0.64). The algorithm had comparable precision as humans for both EEG (humans, algorithm: 0.77, 0.81; z=0.18, p=1.0) and LFP (humans, algorithm: 0.83, 0.63; z=-1.44, p=0.38). The algorithm had slightly lower recall compared to humans for EEG (humans, algorithm: 0.87, 0.68; z=-2.15, p=0.092), and comparable recall for LFP (humans, algorithm: 0.86, 0.84; z=-0.22, p=0.99).

Raters also demonstrated a strong precision/recall tradeoff (Spearman □=-0.91, p=2.2×10^{-7}) (**Fig. 4C**). Such a tradeoff is common in search and classification, as most strategies to improve recall come at the cost of precision, and vice versa. At the extreme, for example, one could achieve perfect precision by marking only the most obvious, largest power, peak, but at the cost of failing to recall all other peaks. Or one could achieve perfect recall by marking every frequency as containing a peak, but at the cost of precision. For this reason, we assessed overall performance using the F_1 score, which equally weights precision and recall. The algorithm had comparable F_1 scores as humans for EEG (humans, algorithm: 0.79, 0.74; z=-0.44, p=0.96), and slightly lower F_1 scores for LFP (humans, algorithm: 0.83, 0.72; z=-2.16, p=0.087) (**Fig. 4D**).

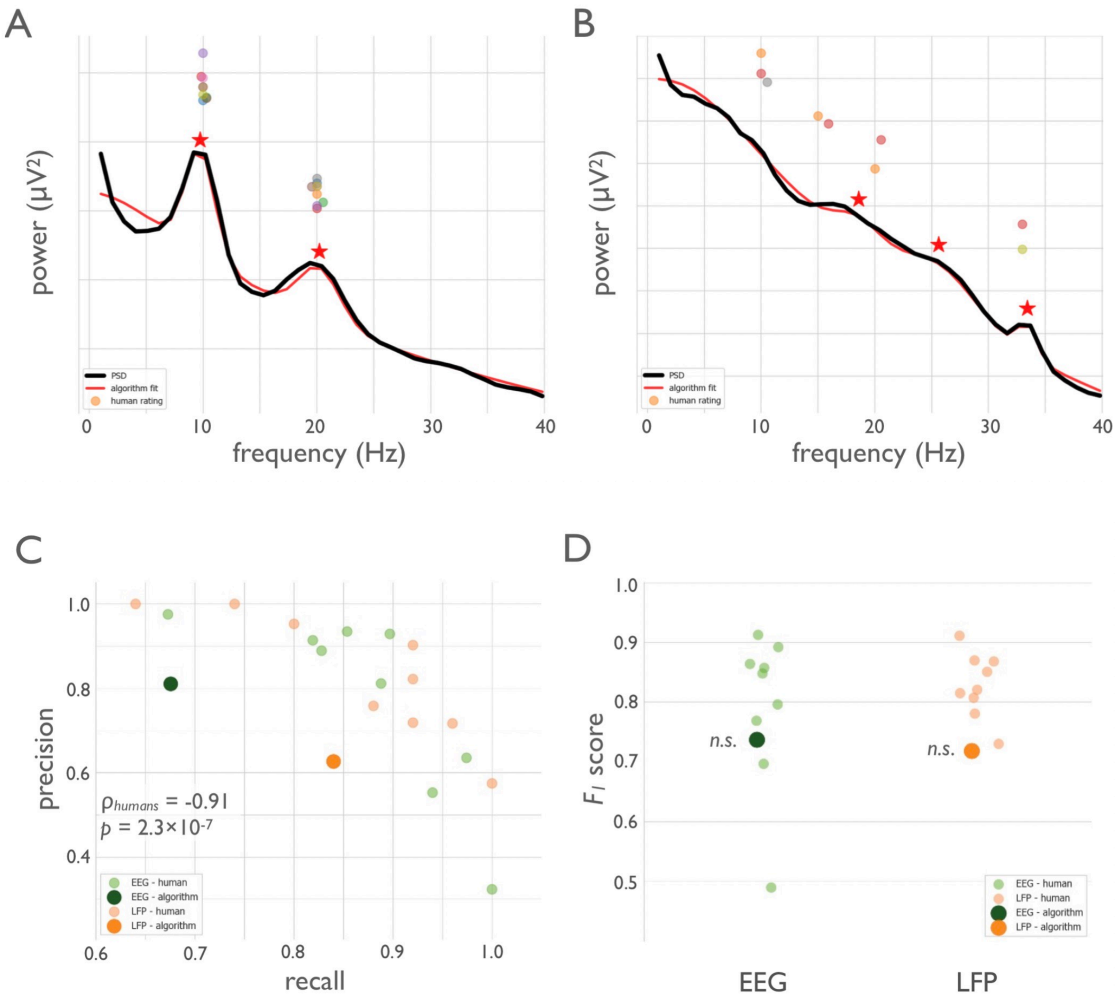

Figure 1.4 | Algorithm performance compared to human raters on real EEG and LFP data. (**A**,**B**) Examples of two different EEG spectra labeled by expert human raters, highlighting cases of strong (**A**) and weak (**B**) consensus amongst raters. The black line is the PSD of real data against which center frequency estimates were made. The red line is the algorithm fit; the red stars are the center frequencies identified by the algorithm. The dots are each individual expert's center frequency rating(s). Note that even when human consensus was low, with many identifying no peaks, as in **B**, the algorithm still provides an accurate fit (in terms of the R^2 fit and error). Nevertheless, the identified center frequencies in **B** would all be marked as false positives for the algorithm as compared to human majority rule, penalizing the algorithm. (**C**) Human raters show a strong precision/recall tradeoff, with some variability amongst raters. (**D**) Despite the penalty against the algorithm for potential overfitting, as in **B**, it performs comparably to the human majority rule. *n.s.:* algorithm not significantly different from human raters.

Age-related differences in spectral parameters

The practical utility of the algorithm was assessed across several EEG applications. First, we replicated and extend previous work looking at age-related differences in spectral parameters, such as alpha oscillations and aperiodic exponent, including how individualized parameters differ with aging (**Fig. 5**); then we examined whether task-related parameters are altered by working memory and aging (**Fig. 6**). To test this, we analyzed scalp EEG data from younger (n=16; 20-30 years) and older adults (n=14; 60-70 years) at rest and while performing a lateralized visual working memory task (see **Methods**).

Resting state analyses. Resting state alpha oscillations and aperiodic activity, as parameterized by the algorithm, were compared between age groups. First, we quantified how much individualized alpha parameters differed from canonical alpha. To do this, participant-specific alpha oscillations were reconstructed based on individual peak frequencies from channel Oz and were compared against a canonical 10 Hz-centered band. We observed considerable variation across participants (**Fig. 5A,B**, see **Methods**), as well as a significant difference between groups (overlap with canonical alpha: younger=84%, older=71%; t_{28}=2.27, p=0.031; Cohen's d=0.83) (**Fig. 5B**). Note that this manifests as a difference in alpha power between groups when using the canonical band analyses, though this is partly driven by more of older adult's alpha lying outside the canonical 8-12 Hz alpha range.

Older adults had lower (slower) alpha center frequencies than younger adults (younger=10.7 Hz, older=9.6 Hz; t_{28}=2.20, p=0.036; Cohen's d=0.79) and lower aperiodic-adjusted alpha power (younger=0.78 μV^2, older=0.45 μV^2; t_{28}=2.52, p=0.018; Cohen's d=0.93), though bandwidth did not differ between groups (younger=1.9 Hz, older=1.8 Hz; t_{28}=0.48,

p=0.632; Cohen's *d*=0.17) (**Fig. 5C**). The mean aperiodic-adjusted alpha power difference between groups was 0.33 μV^2/Hz whereas, when comparing total (not aperiodic-adjusted) alpha power, the mean difference was 0.45 μV^2/Hz. This demonstrates that, though alpha power changes with age, the magnitude of this change is exaggerated by conflating age-related alpha changes with age-related aperiodic changes.

Regarding aperiodic activity, older adults had lower aperiodic offsets (younger=-11.1 μV^2, older=-11.9 μV^2; t_{28}=6.75, *p*<0.0001; Cohen's *d*=2.45) and lower (flatter) aperiodic exponents (younger=1.43 μV^2/Hz, older=0.75 μV^2/Hz; t_{28}=7.19, *p*<0.0001; Cohen's *d*=2.63) (**Fig. 5E**). Participant-specific aperiodic components were reconstructed based on individual offset and exponent parameter fits from channel Cz, and used to compare frequency-by-frequency differences between groups (**Fig. 5D**). From reconstructions, significant differences were found between groups in the frequency ranges 1.0-10.5 Hz and 40.2-45.0 Hz (*p*<0.05, uncorrected *t*-tests at each frequency band). This demonstrates, in real data, how group differences in what would traditionally be considered to be oscillatory bands can actually be caused by aperiodic—non-oscillatory—differences between groups (*c.f.*, **Fig. 1**).

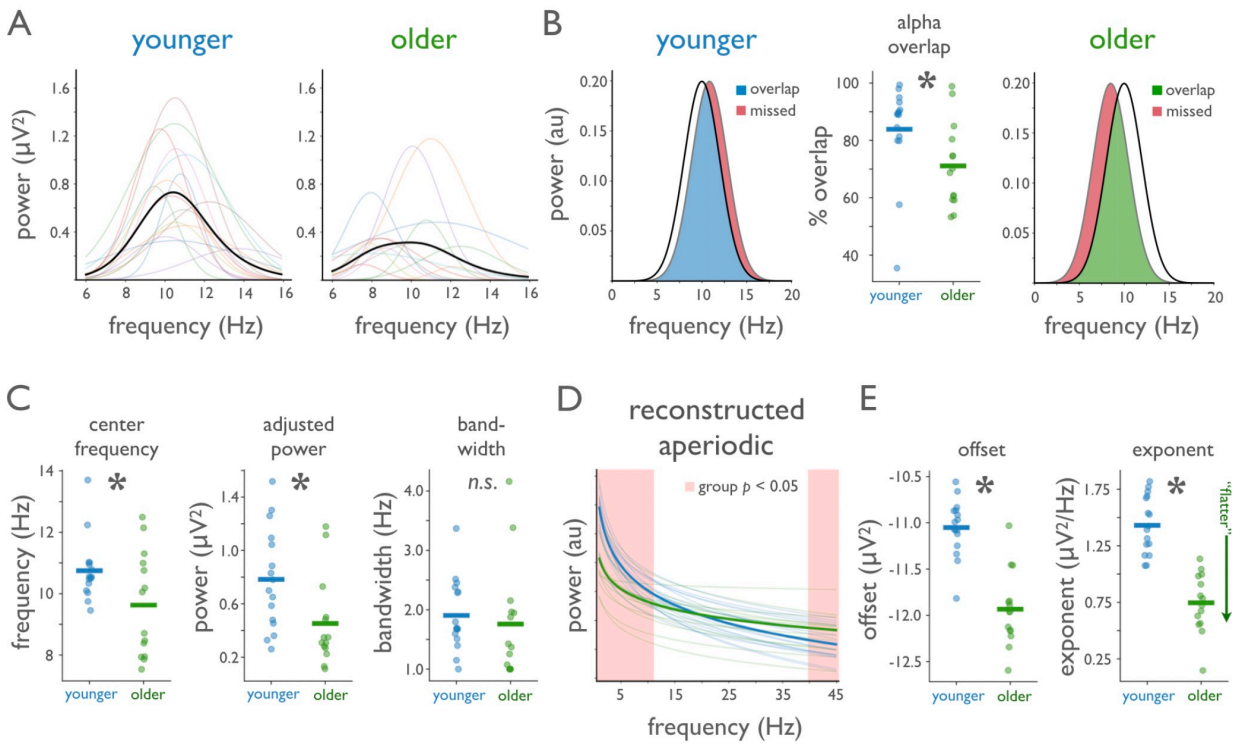

Figure 1.5 | Age-related shifts in spectral EEG parameters during resting state. (**A**) Visualization of individualized oscillations as parameterized by the algorithm, selected as highest power oscillation in the alpha (7-14 Hz) range from visual cortical EEG channel Oz for each participant. There are clear differences in oscillatory properties between age groups that are quantified in **C**. (**B**) A comparison of alpha captured by a canonical 10 ± 2 Hz band, as compared to the average deviation of the center frequency of the parameterized alpha, for the younger group (left, blue) and older group (right, green). In this comparison, the canonical band approach captures 84% of the parameterized alpha in the younger adult group, and only 71% in the older adult group, as quantified in the middle panel. Red represents the alpha power missed by canonical analysis, which disproportionately reflects more missed power in the older group. (**C**) Comparison of parameterized alpha center frequency, aperiodic-adjusted power, and bandwidth, split by age group. (**D**) Comparison of aperiodic components at channel Cz, per group. For this visualization, the aperiodic offset and exponent, per participant, were used to reconstruct an "aperiodic only" spectrum (removing the putative oscillations). Red shaded regions reflect areas where there are significant power differences at each frequency between groups ($p < 0.05$ uncorrected *t*-tests). In this comparison, significant group differences in both aperiodic offset and exponent (**E**) drive group-wise differences that otherwise appear to be band-specific in both low (< ~10 Hz) and high (> ~40 Hz) frequencies, when analyzed in a more traditional manner. Bars in **B**, **C**, **E** represent mean values while stars indicate statistically significant difference, at $p < 0.05$. *n.s.* not significant.

Working memory analyses. To evaluate whether parameterized spectra can predict behavioral performance, we analyzed a working memory task from the same dataset, in which participants had to remember the color(s) of briefly presented squares over a short delay period. We then attempted to predict behavioral performance, measured as d', from periodic and aperiodic parameters calculated as a difference measures between baseline and delay period (see **Methods** for full task and analysis details). Ordinary least squares linear regression models were fit to predict performance, and model comparisons were done to examine which spectral parameters and estimation approaches best predicted behavior (**Fig. 6A-C**). The most consistent model for predicting behavior across groups (adjusting for the number of parameters in the model) was one using only the two aperiodic parameters (offset and exponent; younger: $F_{(4, 46)}$=3.94, p = 0.0078, R_{adj}^2=0.19; older: $F_{(4, 37)}$=5.10, p=0.0023, R_{adj}^2=0.29). In the older adult group, the aperiodic-adjusted alpha power model was also a significant predictor ($F_{(3, 38)}$=7.70, p=0.0004, R_{adj}^2=0.33), performing better than a model using canonical alpha measures ($F_{(3, 38)}$=5.18, p=0.0042, R_{adj}^2=0.23). In the younger adult group, neither measure of alpha power significantly predicted behavior (**Fig. 6E**). This result highlights that, while traditional analyses of such tasks typically focus on alpha activity (Tran et al., 2016), we find that the more accurate prediction of behavior is from aperiodic activity, a pattern that may be misinterpreted as alpha dynamics in canonical analyses, in particular when there are spectral parameter differences between groups.

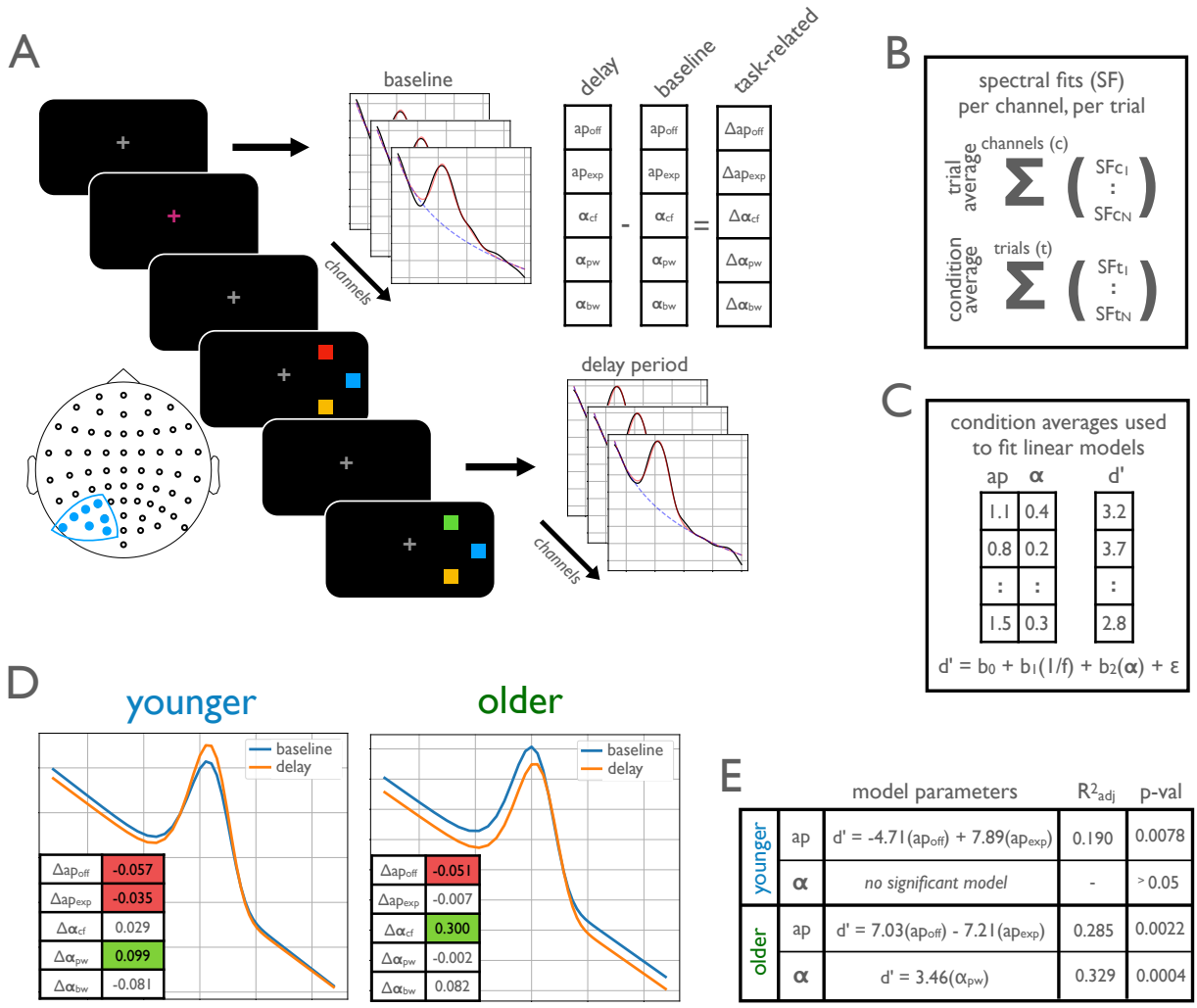

Figure 1.6 | Event-related spectral parameterization of working memory in aging. (**A**) Contralateral electrodes (filled blue dots on the electrode localization map) were analyzed in a working memory task, with spectral fits to delay period activity per channel, per trial, as well as to the pre-trial baseline period (see **Methods**). Task-related measures of each spectral parameter were computed by subtracting the baseline parameters from the delay period parameters. (**B**) Parameters were collapsed across channels, to provide a measure per trial, and collapsed across trials, to provide a measure per working memory load (condition). (**C**) For this analysis, condition average spectral parameters were used to predict behavioral performance, measured as d', per condition. (**D**) The average evoked difference in spectral parameters, between baseline and delay periods, for each group, presented as spectra reconstructed from the spectral fits, including aperiodic and oscillatory alpha parameters. The inset tables present the changes in each parameter, shaded if significant (one sample *t*-test, $p < 0.05$; green: positive weight; red: negative weight). (**E**) Parameters for behavioral models predicting behavioral performance for each group. All behavioral models use the evoked spectral parameters from **A**. Note that all behavioral models also include an intercept term, and a covariate for load.

Discussion

Despite the ubiquity of oscillatory analyses, there are several analytic assumptions that impact the physiological interpretation of prior oscillation research. Standard approaches for quantifying oscillations presume that oscillations are present, which may not be true (**Fig. S1**), and often rely on canonical frequency bands that presume that spectral power implies oscillatory power. These assumptions overlook the existence of aperiodic activity, which is itself dynamic, and so cannot be simply ignored as stationary noise. Aperiodic activity also has interesting demographic, cognitive, and clinical correlates, as well as physiological relevance, and so should also be explicitly parameterized and analyzed. Here we introduce a novel method for algorithmically extracting periodic and aperiodic components in electro- and magnetophysiological data that addresses these often-overlooked issues in cognitive and systems neuroscience.

We demonstrate this method with a series of applications, and highlight methodological points and novel findings. We show how apparent age-related differences in oscillatory power can be partially driven by shifts in oscillation center frequency (**Fig. 1C**). Specifically, we find that canonical alpha band analyses (*e.g.*, analyzing the 8-12 Hz range) fail to capture all of the oscillatory power within individual participants, and are systematically biased between groups (Lansbergen et al., 2011) (**Fig. 5B**). In our data, canonical alpha analyses miss a greater proportion of power in older adult's *true* alpha activity compared to younger adult's alpha, due to the fact that older adults tend to have slower (lower frequency) alpha (Obrist, 1954) (**Fig. 5A,B**). This is important, as traditional analyses using fixed bands fail to address inter-individual differences,

which has methodological consequences, and also ignores that variations in peak-frequencies within oscillation bands have functional correlates and are of theoretical interest(Mierau et al., 2017).

We also show how apparent oscillation power can be influenced by changes in the aperiodic exponent, for example in the case of age-related changes in the aperiodic exponent (Fig. 5D,E). Thus, though we replicate often-described age-related alpha power changes (Klimesch, 1999; Obrist, 1954), we find the magnitude of this effect, when analyzed for alpha power specifically, is more subtle than previously reported. This is because age-related changes in the aperiodic component also shift total narrowband alpha power, despite the fact that power in a narrowband *oscillation* has not changed relative to the aperiodic process (Voytek & Knight, 2015) (see Fig. S1A). We conclude that periodic activity is not the sole driver of the apparent ~10 Hz power differences in aging; and that the magnitude of alpha power differences have been systemically confounded by concomitant differences in aperiodic activity.

We also examined the utility of spectral parameterization in a cognitive context, analyzing EEG data from a visual working memory task (Fig. 6). While such studies often focus on oscillatory activity, in particular visual cortical alpha (Tran et al., 2016), recent computational work shows the importance of excitation/inhibition (EI) balance in working memory maintenance (Lim & Goldman, 2013). Given that the aperiodic exponent partially reflects EI balance (Gao et al., 2017), and is systematically altered in aging (Voytek et al., 2015), we hypothesized that the aperiodic component would predict working memory performance. We find that, across groups, event-related changes in the aperiodic parameters, rather than just oscillatory alpha, most consistently predict individual working memory performance. In contrast, delay period alpha parameters

tracked behavior among older, but not younger, adults. This suggests that there are categorical differences between groups regarding which spectral parameters track working memory outcomes, and that these features are easy to conflate—or miss—without explicit spectral parameterization, and highlights a novel finding of aperiodic activity predicting working memory performance in human EEG data.

This work raises interesting possibilities for how to interpret common findings. Intriguingly, when examined in the time-domain, differences in the aperiodic exponent manifest as raw voltage differences (Fig. S1A). It may be that observed differences between conditions, for example in event-related spectral perturbations or evoked potentials, are partially explainable by, or related to, differences in aperiodic exponent. This consideration is particularly important when comparing between groups, given that the aperiodic exponent varies across groups, including aging (Voytek et al., 2015) (Fig. 5D,E) and disease (Molina et al., 2020; Robertson et al., 2019).

The observation of within subject changes of the aperiodic exponent also has implications regarding the ubiquitous negative correlation between low frequency (<30 Hz) and high frequency (>40 Hz) activity (Mukamel et al., 2005), observed here in the EEG data (Fig. 5D). This is often interpreted as a push/pull relationship between low frequency oscillations and gamma, however spectral parameterization offers a different interpretation: a see-saw-like rotation of the spectrum at around 20-30 Hz due to a change in aperiodic activity. This results in decreased power in lower frequencies with a simultaneous increase in higher frequency power. Here it would be a mischaracterization to say that there was a task-related decrease in low frequency oscillations, because that need not be the feature that was truly altered; instead, the aperiodic

exponent changed, manifesting as the spectrum "rotating" around a specific frequency point. This has been observed to occur in a task-related manner in human visual cortex (Podvalny et al., 2015).

Across the gamma range, there can be both narrowband activity and broadband shifts (Bartoli et al., 2019). There may also be high variability of narrowband frequencies within participants such that averaging across those bands decreases detectability overall statistical power (Muthukumaraswamy et al., 2010). Parameterizing spectra allows for detecting narrowband peaks, and inferring whether narrow- and/or broadband aspects of the data are changing. This may also be useful for analyses such as phase-amplitude coupling (PAC), which have provided a powerful means for probing the potential mechanisms of neural communication (Canolty & Knight, 2010; de Hemptinne et al., 2015; van der Meij et al., 2012; Voytek et al., 2015). These analyses typically rely on fixed frequency bands, which is problematic given that multiple-oscillator PAC exhibits different phase coupling frequencies by cortical region (van der Meij et al., 2012). Using spectral parameterization to characterize oscillatory components may allow for better identifying phase coupling modes across brain regions, task, and time, thus increasing the specificity and accuracy of cross-frequency coupling analyses.

Altogether, the parameterization algorithm provides a principled method for quantifying the neural power spectrum, increasing analytical power by disentangling periodic and aperiodic components. This allows researchers to take full advantage of the rich variability present in neural field potential data, rather than treating that variability as noise. These spectral features reflect distinct properties of the data, but may also be inter-related, given the evidence that the aperiodic exponent and band powers can be correlated (Muthukumaraswamy & Liley, 2018; Tran

et al., 2020). This highlights the need for careful parameterization to adjudicate between individual spectral features and their relationship to cognitive, clinical, demographic, and physiological data.

Though the algorithm itself is agnostic to underlying physiological generators of the periodic and aperiodic components, it can be leveraged to investigate theories and interpretations of them. For example, changes in the aperiodic exponent may relate to a shift in the balance of the transmembrane currents in the input region, such as a shift in EI balance (Gao et al., 2017). In oscillations, traditional canonical frequency band analyses commit researchers to the idea that those predefined bands have functional roles, rather than considering the underlying physiological mechanisms that generate different spectral features. Spectral parameterization across scales, and in combination with other measures, may allow us to better link macroscale electrophysiology to microscale synaptic and firing parameters (Barbieri et al., 2014; Reimann et al., 2013), providing a better understanding of the relationship between microscale synaptic dynamics and different components in field potential signals, from microscale LFP, to mesoscale intracranial EEG, to macroscale EEG and MEG (Buzsáki et al., 2012).

While there are other methods for measuring periodic and aperiodic activity, none jointly parameterize aperiodic and periodic components. Some methods focus on identifying individual differences in oscillations, however, they are mostly restricted to detecting the peak frequency within a specific sub-band (Haegens et al., 2014). This has resulted in a broad literature looking at variation within canonical bands, most commonly peak alpha frequency within and across individuals (Haegens et al., 2014; Mierau et al., 2017). However, such approaches often assume

only one peak within a band, does not generalize across broad frequencies, and/or ignores aperiodic activity (Pascual Marqui et al., 1987), perpetuating the conflation of aperiodic and periodic processes. Other approaches attempt to control for the aperiodic component when identifying oscillations, but do not parameterize both the aperiodic and periodic features together. Often, these methods treat the aperiodic component as a nuisance variable (Blankertz et al., 2010), for example by correcting for it via spectral whitening (Groppe et al., 2013), rather than a feature to be explicitly modeled and parameterized. For example, an approach called BOSC (Better OSCillation Detector) (Hughes et al., 2012) fits a line to the PSD to determine a power threshold in an attempt to isolate oscillations, but does not parameterize the aperiodic signal. The irregular-resampling auto-spectral analysis (IRASA) method, which seeks to explicitly separate the periodic component through a resampling procedure (Wen & Liu, 2016), also does not parameterize the aperiodic signal. In developing the current algorithm, we found that linear spectral fits, such as used in BOSC and often applied with IRASA, do not perform as well as the approach presented here. Other methods, such as principal component variants, require manual component selection (Miller et al., 2012). Collectively, the current method addresses existing shortcomings by explicitly parameterizing periodic and aperiodic signals, flexibly fitting multiple peaks and different aperiodic functions, without requiring extensive manual tuning or supervision.

There are some practical considerations to keep in mind when applying this method. The model, as proposed, is applicable to multiple kinds of datasets, ranging from LFP to EEG and MEG. Different modalities, and different frequency ranges, may require different settings for optimal fitting, and fits should always be evaluated for goodness-of-fit. Detailed notes and

instructions for applying the algorithm to different modalities, assessing model fits, and tuning parameters are all available in the tool's online documentation[vi]. There are also caveats to consider when interpreting model parameters. Notably, while the presence of power above the aperiodic component suggests that there is an oscillation at that frequency, a spectral peak does not always imply that there is an oscillation at that frequency (Cole & Voytek, 2017). For example, sharp wave rhythms, such as the sawtooth-like waves seen in hippocampus or the sensorimotor mu rhythm, will manifest as narrowband power at harmonics of the fundamental frequency (Cole & Voytek, 2017) (Fig. S3 G-I). Similarly, the lack of an observed peak over and above the aperiodic component does not definitively imply the complete absence of an oscillation. There could be very low power oscillations, highly variable oscillatory properties, and/or rare burst events or within a long time series (Izhikevich et al., 2018), that do not exhibit as clear spectral peaks. To address these possibilities, spectral parameterization can be complemented with time-domain analysis approaches (Cole & Voytek, 2019).

In conclusion, application of our algorithm shows that different physiological processes, including changes in the exponent or offset of the aperiodic component or periodic oscillatory changes, are often conflated (Caplan et al., 2015). Our approach allows for disambiguating distinct changes in the data by parameterizing aperiodic and periodic features, allowing for investigations of how these features relate to cognitive functioning in health, aging, and disease, as well as their underlying physiological mechanisms. The proposed algorithm is validated with simulated data, and its utility demonstrated on a series of data applications. Because of the

[vi] https://fooof-tools.github.io/

speed and ease of the algorithm and the interpretability of the fitted parameters, this tool opens avenues for the high-throughput, large-scale analyses that will be critical for data-driven approaches to neuroscientific research (Voytek, 2016).

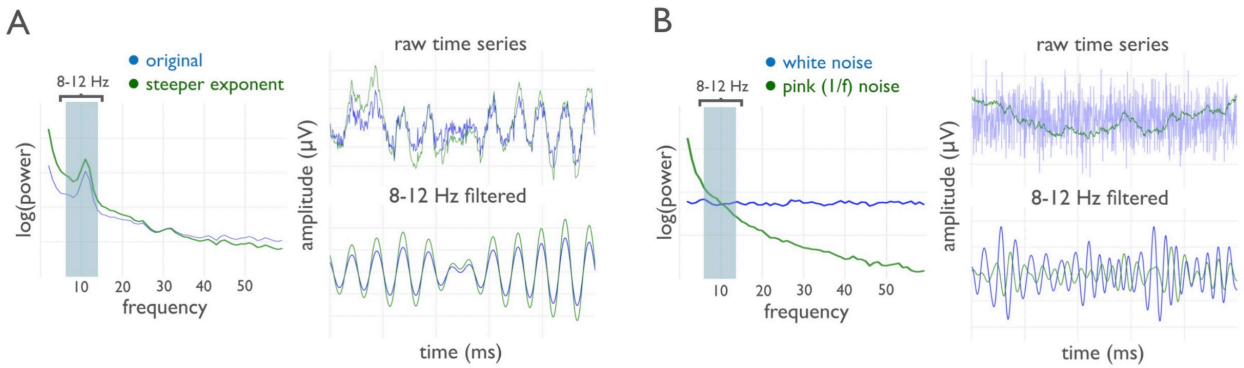

Supplementary Figure 1.1 | False oscillatory power changes and illusory oscillations. (**A**) Here we took a real neural PSD (blue) and artificially introduced a change in the aperiodic exponent, similar to what is seen in healthy aging (Voytek et al., 2015). This PSD was then inverted back to the time domain (right panels). The exponent change manifests as amplitude differences in the time domain. This affects apparent narrowband power when an *a priori* filter is applied. This is despite the fact that the true oscillatory power *relative* to the aperiodic component is unaffected. (**B**) Even when no oscillation is present, such as the case with the white and pink (1/f) noise examples here (blue and green, respectively), narrowband filtering gives rise to illusory oscillations where no periodic feature exists in the actual signal, by definition.

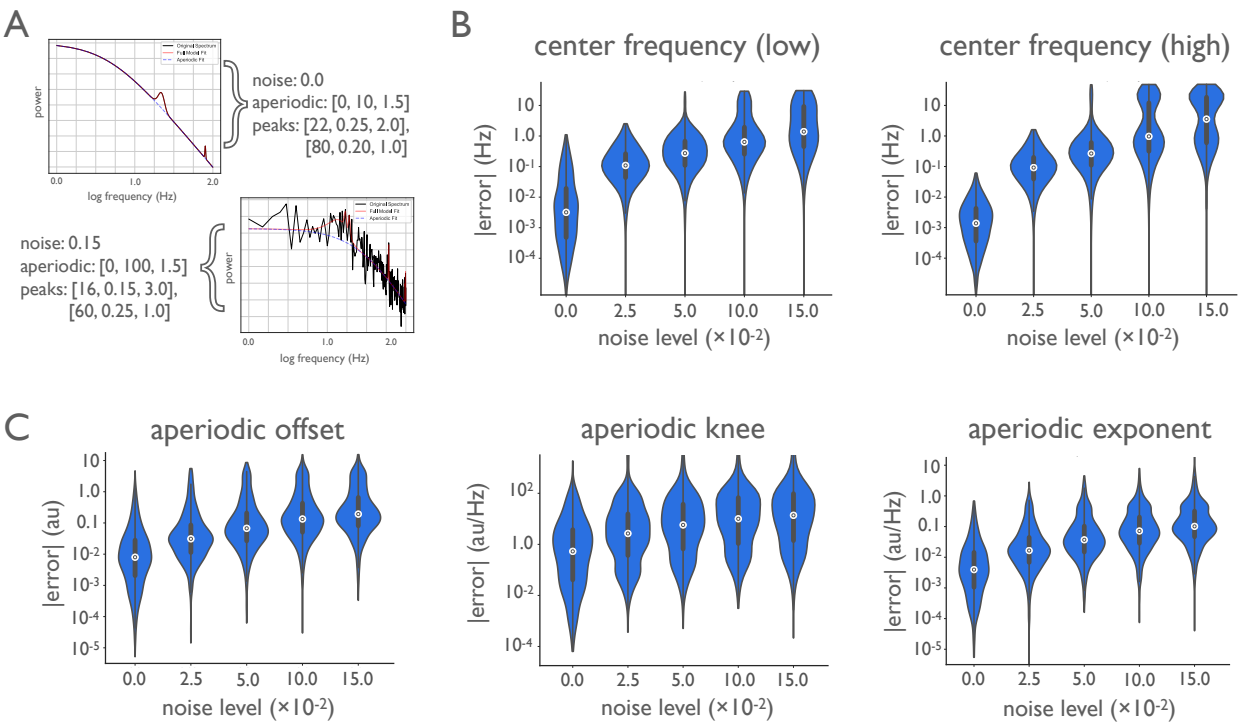

Supplementary Figure 1.2 | Algorithm performance on simulated data across a broader frequency range. (**A-C**) Power spectra were simulated across the frequency range (1-100 Hz), with two peaks, one in a low range, and one in a high range (see **Methods**), across five distinct noise levels (1000 spectra per noise level). (**A**) Example power spectra with simulation parameters as aperiodic [offset, knee, exponent] and periodic [center frequency, power, bandwidth] (**B**) Absolute error of algorithmically identified peak center frequency, separated for the low (3-35 Hz) and high range (50-90 Hz) peaks. (**C**) Absolute error of algorithmically identified aperiodic parameters, offset, knee, and exponent. Note that the error axis is log-scaled in **B,C**.

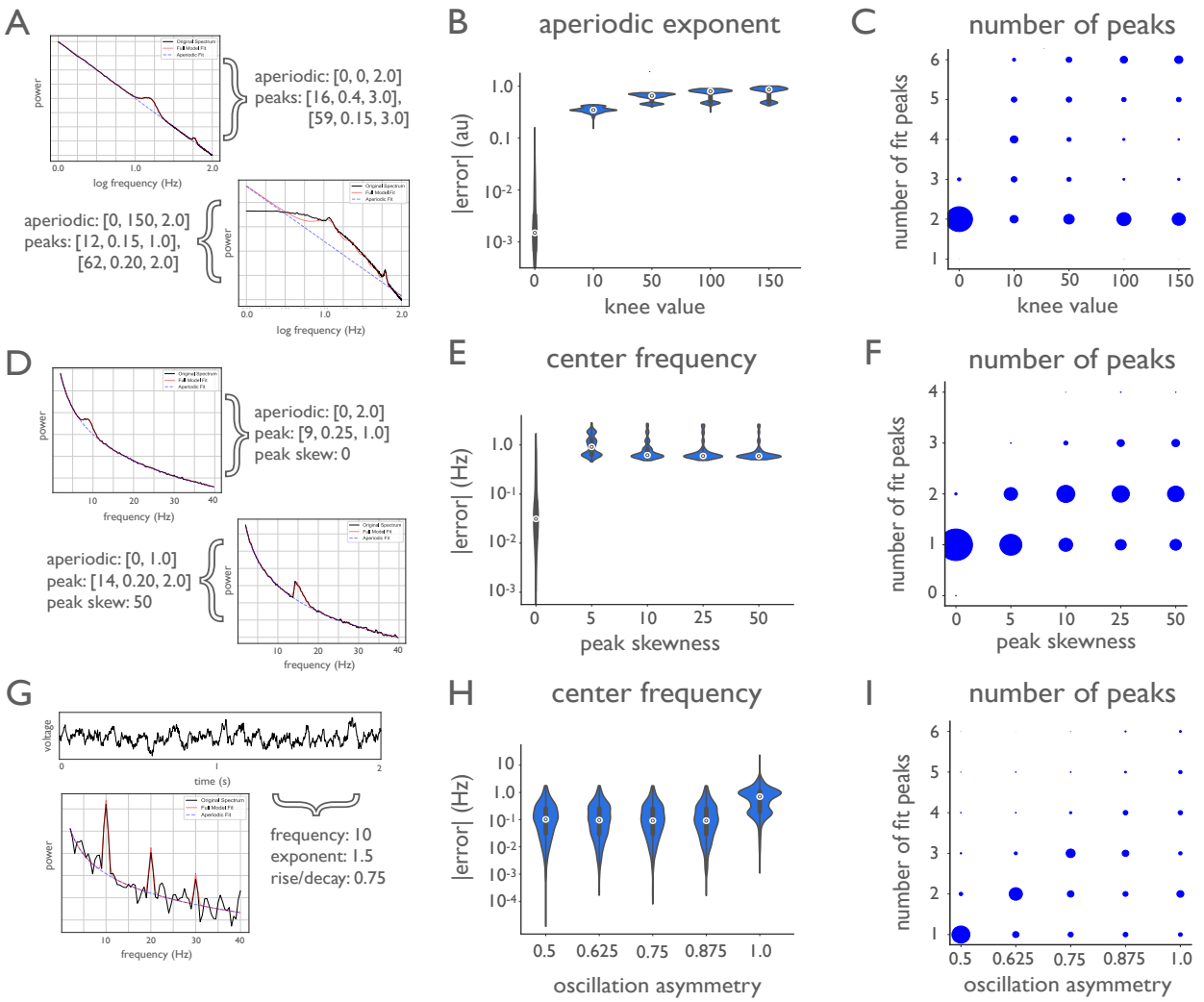

Supplementary Figure 1.3 | Algorithm performance on simulated data that violate model assumptions (**A-C**) Power spectra were simulated across a broader frequency range (1-100 Hz), with two peaks, one in a low range, and one in a high range across five distinct knees values (1000 spectra per knee value). These power spectra were fit with the model set in 'fixed' mode to evaluate how sensitive performance is to aperiodic mode. (**A**) Example power spectra with simulation parameters as aperiodic [offset, knee, exponent] and periodic [center frequency, power, bandwidth]. (**B**) Absolute error of algorithmically identified aperiodic exponent, across power spectra with different knee values. (**C**) The number of peaks fit by the model, across different knee values. (**D-F**) A distinct set of simulations were created in which power spectra were created with asymmetric or skewed peaks, across five distinct skew levels (1000 spectra per skew level). (**D**) Example simulated spectra, with fits and parameter definitions, showing two different skew levels. (**E**) Absolute error of algorithmically identified peak center frequency, across power spectra with different peak skewness values. (**F**) The number of peaks fit by the model, across peak skewness. Note that all spectra in this set have one peak. (**G-I**) A distinct set of simulations, in which time series were generated with asymmetric oscillations in the time domain, from which power spectra were calculated, across five distinct levels of oscillation asymmetry (1000 spectra per asymmetry value). (**G**) Example simulation of an asymmetric oscillation, simulated in the time domain, and the associated power spectrum. (**H**) Absolute error of algorithmically identified peak center frequency, across oscillation asymmetry values. (**I**) The number of peaks fit by the model, compared across oscillation asymmetry values. Note that the error axis is log-scaled in **B,E,H**.

Supplementary Table 1.1 | Algorithm parameters

name	description	units	default value	API accessible?
peak_width_limits	Bounds on the [min, max] peak bandwidth.	hertz	[0.5, 12]	Yes
max_n_peaks	Maximum number of peaks to fit.	integer	Infinite	Yes
min_peak_height	Absolute minimum power threshold for peaks.	log power	0.0	Yes
peak_threshold	Relative minimum power threshold for peaks.	std	2.0	Yes
aperiodic_mode	Whether to fit the aperiodic component with a knee parameter.	'fixed' or 'knee'	'fixed'	Yes
_ap_percentile_thresh	Power percentile to select points to fit aperiodic component.	percentage	2.5	No
_ap_guess	Seed values for aperiodic fitting.	float	[None, 0, None]	No
_bw_std_edge	Threshold for dropping peaks close to the edge.	gaussian std	1.0	No
_gauss_overlap_thresh	Threshold for dropping overlapping peaks.	gaussian std	0.75	No
_cf_bound	Bound on centre-frequency for multi-gaussian fit.	gaussian std	1.5	No

References

Barbieri, F., Mazzoni, A., Logothetis, N. K., Panzeri, S., & Brunel, N. (2014). Stimulus Dependence of Local Field Potential Spectra: Experiment versus Theory. *Journal of Neuroscience*, *34*(44), 14589–14605. https://doi.org/10.1523/JNEUROSCI.5365-13.2014

Bartoli, E., Bosking, W., Chen, Y., Li, Y., Sheth, S. A., Beauchamp, M. S., Yoshor, D., & Foster, B. L. (2019). Functionally Distinct Gamma Range Activity Revealed by Stimulus Tuning in Human Visual Cortex. *Current Biology*, *29*(20), 3345-3358.e7. https://doi.org/10.1016/j.cub.2019.08.004

Becker, R., Van de Ville, D., & Kleinschmidt, A. (2018). Alpha Oscillations Reduce Temporal Long-Range Dependence in Spontaneous Human Brain Activity. *The Journal of Neuroscience*, *38*(3), 755–764. https://doi.org/10.1523/JNEUROSCI.0831-17.2017

Bell, A. J., & Sejnowski, T. J. (1995). An information-maximisation approach to blind separation and blind deconvolution. *Neural Computation*.

Blankertz, B., Sannelli, C., Halder, S., Hammer, E. M., Kübler, A., Müller, K.-R., Curio, G., & Dickhaus, T. (2010). Neurophysiological predictor of SMR-based BCI performance. *NeuroImage*, *51*(4), 1303–1309. https://doi.org/10.1016/j.neuroimage.2010.03.022

Bullock, T. H. (1981). Neuroethology deserves more study of evoked responses. *Neuroscience*.

Bullock, T. H., Mcclune, M. C., & Enright, J. T. (2003). Are the electroencephalograms mainly rhythmic? Assessment of periodicity in wide-band time series. *Neuroscience*, *121*(1), 233–252. https://doi.org/10.1016/S0306-4522(03)00208-2

Buzsáki, G., Anastassiou, C. A., & Koch, C. (2012). The origin of extracellular fields and currents—EEG, ECoG, LFP and spikes. *Nature Reviews Neuroscience*, *13*(6), 407–420. https://doi.org/10.1038/nrn3241

Buzsaki, G., & Draguhn, A. (2004). Neuronal Oscillations in Cortical Networks. *Science*, *304*(5679), 1926–1929. https://doi.org/10.1126/science.1099745

Buzsáki, G., Logothetis, N., & Singer, W. (2013). Scaling Brain Size, Keeping Timing: Evolutionary Preservation of Brain Rhythms. *Neuron*, *80*(3), 751–764. https://doi.org/10.1016/j.neuron.2013.10.002

Canolty, R. T., & Knight, R. T. (2010). The functional role of cross-frequency coupling. *Trends in Cognitive Sciences*, *14*(11), 506–515. https://doi.org/10.1016/j.tics.2010.09.001

Caplan, J. B., Bottomley, M., Kang, P., & Dixon, R. A. (2015). Distinguishing rhythmic from non-rhythmic brain activity during rest in healthy neurocognitive aging. *NeuroImage*, *112*, 341–352. https://doi.org/10.1016/j.neuroimage.2015.03.001

Cole, S. R., Donoghue, T., Gao, R., & Voytek, B. (2019). NeuroDSP: A package for neural digital signal processing. *Journal of Open Source Software*, *4*(36), 1272. https://doi.org/10.21105/joss.01272

Cole, S. R., & Voytek, B. (2017). Brain Oscillations and the Importance of Waveform Shape. *Trends in Cognitive Sciences*, *21*(2), 137–149. https://doi.org/10.1016/j.tics.2016.12.008

Cole, S. R., & Voytek, B. (2019). Cycle-by-cycle analysis of neural oscillations. *Journal of Neurophysiology*, *122*(2), 849–861. https://doi.org/10.1152/jn.00273.2019

Crone, N. (1998). Functional mapping of human sensorimotor cortex with electrocorticographic spectral analysis. I. Alpha and beta event- related desynchronization. *Brain*, *121*(12), 2271–2299. https://doi.org/10.1093/brain/121.12.2271

de Hemptinne, C., Swann, N. C., Ostrem, J. L., Ryapolova-Webb, E. S., San Luciano, M., Galifianakis, N. B., & Starr, P. A. (2015). Therapeutic deep brain stimulation reduces cortical phase-amplitude coupling in Parkinson's disease. *Nature Neuroscience*, *18*(5), 779–786. https://doi.org/10.1038/nn.3997

Dustman, R. E., Shearer, D. E., & Emmerson, R. Y. (1993). EEG and event-related potentials in normal aging. *Progress in Neurobiology*, *41*(3), 369–401. https://doi.org/10.1016/0301-0082(93)90005-D

Engel, A. K., Fries, P., & Singer, W. (2001). Dynamic predictions: Oscillations and synchrony in top–down processing. *Nature Reviews Neuroscience*, *2*(10), 704–716. https://doi.org/10.1038/35094565

Freeman, W. J., & Zhai, J. (2009). Simulated power spectral density (PSD) of background electrocorticogram (ECoG). *Cognitive Neurodynamics*, *3*(1), 97–103. https://doi.org/10.1007/s11571-008-9064-y

Fries, P. (2005). A mechanism for cognitive dynamics: Neuronal communication through neuronal coherence. *Trends in Cognitive Sciences*, *9*(10), 474–480. https://doi.org/10.1016/j.tics.2005.08.011

Gao, R. (2016). Interpreting the electrophysiological power spectrum. *Journal of Neurophysiology*, *115*(2), 628–630. https://doi.org/10.1152/jn.00722.2015

Gao, R., Lucas van den Brink, R., Pfeffer, T., & Voytek, B. (2020). Neuronal timescales are functionally dynamic and shaped by cortical microarchitecture. *BioRxiv*, 41.

Gao, R., Peterson, E. J., & Voytek, B. (2017). Inferring synaptic excitation/inhibition balance from field potentials. *NeuroImage*, *158*, 70–78. https://doi.org/10.1016/j.neuroimage.2017.06.078

Gramfort, A., Luessi, M., Larson, E., Engemann, D. A., Strohmeier, D., Brodbeck, C., Parkkonen, L., & Hämäläinen, M. S. (2014). MNE software for processing MEG and EEG data. *NeuroImage*, *86*, 446–460. https://doi.org/10.1016/j.neuroimage.2013.10.027

Groppe, D. M., Bickel, S., Keller, C. J., Jain, S. K., Hwang, S. T., Harden, C., & Mehta, A. D. (2013). Dominant frequencies of resting human brain activity as measured by the electrocorticogram. *NeuroImage*, *79*, 223–233. https://doi.org/10.1016/j.neuroimage.2013.04.044

Haegens, S., Cousijn, H., Wallis, G., Harrison, P. J., & Nobre, A. C. (2014). Inter- and intra-individual variability in alpha peak frequency. *NeuroImage*, *92*, 46–55. https://doi.org/10.1016/j.neuroimage.2014.01.049

He, B. J. (2014). Scale-free brain activity: Past, present, and future. *Trends in Cognitive Sciences*, *18*(9), 480–487. https://doi.org/10.1016/j.tics.2014.04.003

He, W., Donoghue, T., Sowman, P., Seymour, R. A., Brock, J., Crain, S., Voytek, B., & Hillebrand, A. (2019). Co-Increasing Neuronal Noise and Beta Power in the Developing Brain. *BioRxiv*, 49.

Hughes, A. M., Whitten, T. A., Caplan, J. B., & Dickson, C. T. (2012). BOSC: A better oscillation detection method, extracts both sustained and transient rhythms from rat hippocampal recordings. *Hippocampus*, *22*(6), 1417–1428. https://doi.org/10.1002/hipo.20979

Izhikevich, L., Gao, R., Peterson, E., & Voytek, B. (2018). Measuring the average power of neural oscillations. *BioRxiv*. https://doi.org/10.1101/441626

Jas, M., Engemann, D. A., Bekhti, Y., Raimondo, F., & Gramfort, A. (2017). Autoreject: Automated artifact rejection for MEG and EEG data. *NeuroImage*, *159*, 417–429. https://doi.org/10.1016/j.neuroimage.2017.06.030

Jasper, H., & Penfield, W. (1949). Electrocorticograms in man: Effect of voluntary movement upon the electrical activity of the precentral gyrus. *Archiv Für Psychiatrie Und Nervenkrankheiten*, *183*(1–2), 163–174. https://doi.org/10.1007/BF01062488

Klimesch, W. (1999). EEG alpha and theta oscillations reflect cognitive and memory performance: A review and analysis. *Brain Research Reviews*, *29*(2–3), 169–195. https://doi.org/10.1016/S0165-0173(98)00056-3

Kopell, N. J., Gritton, H. J., Whittington, M. A., & Kramer, M. A. (2014). Beyond the Connectome: The Dynome. *Neuron*, *83*(6), 1319–1328. https://doi.org/10.1016/j.neuron.2014.08.016

Lansbergen, M. M., Arns, M., van Dongen-Boomsma, M., Spronk, D., & Buitelaar, J. K. (2011). The increase in theta/beta ratio on resting-state EEG in boys with attention-deficit/hyperactivity disorder is mediated by slow alpha peak frequency. *Progress in Neuro-Psychopharmacology and Biological Psychiatry*, *35*(1), 47–52. https://doi.org/10.1016/j.pnpbp.2010.08.004

Lara, A. H., & Wallis, J. D. (2014). Executive control processes underlying multi-item working memory. *Nature Neuroscience*, *17*(6), 876–883. https://doi.org/10.1038/nn.3702

Lim, S., & Goldman, M. S. (2013). Balanced cortical microcircuitry for maintaining information in working memory. *Nature Neuroscience*, *16*(9), 1306–1314. https://doi.org/10.1038/nn.3492

Manning, J. R., Jacobs, J., Fried, I., & Kahana, M. J. (2009). Broadband Shifts in Local Field Potential Power Spectra Are Correlated with Single-Neuron Spiking in Humans. *Journal of Neuroscience*, *29*(43), 13613–13620. https://doi.org/10.1523/JNEUROSCI.2041-09.2009

Mierau, A., Klimesch, W., & Lefebvre, J. (2017). State-dependent alpha peak frequency shifts: Experimental evidence, potential mechanisms and functional implications. *Neuroscience*, *360*, 146–154. https://doi.org/10.1016/j.neuroscience.2017.07.037

Miller, K. J., Hermes, D., Honey, C. J., Hebb, A. O., Ramsey, N. F., Knight, R. T., Ojemann, J. G., & Fetz, E. E. (2012). Human Motor Cortical Activity Is Selectively Phase-Entrained on Underlying Rhythms. *PLoS Computational Biology*, *8*(9), e1002655. https://doi.org/10.1371/journal.pcbi.1002655

Miller, K. J., Sorensen, L. B., Ojemann, J. G., & den Nijs, M. (2009). Power-Law Scaling in the Brain Surface Electric Potential. *PLoS Computational Biology*, *5*(12), e1000609. https://doi.org/10.1371/journal.pcbi.1000609

Molina, J. L., Voytek, B., Thomas, M. L., Joshi, Y. B., Bhakta, S. G., Talledo, J. A., Swerdlow, N. R., & Light, G. A. (2020). Memantine Effects on Electroencephalographic Measures of Putative Excitatory/Inhibitory Balance in Schizophrenia. *Biological Psychiatry: Cognitive Neuroscience and Neuroimaging*, S2451902220300471. https://doi.org/10.1016/j.bpsc.2020.02.004

Mukamel, R., Gelbard, H., Arieli, A., Hasson, U., Fried, I., & Malach, R. (2005). Coupling Between Neuronal Firing, Field Potentials, and fMRI in Human Auditory Cortex. *Science*, *309*(5736), 951–954. https://doi.org/10.1126/science.1110913

Muthukumaraswamy, S. D., & Liley, D. TJ. (2018). 1/f electrophysiological spectra in resting and drug-induced states can be explained by the dynamics of multiple oscillatory relaxation processes. *NeuroImage*, *179*, 582–595. https://doi.org/10.1016/j.neuroimage.2018.06.068

Muthukumaraswamy, S. D., Singh, K. D., Swettenham, J. B., & Jones, D. K. (2010). Visual gamma oscillations and evoked responses: Variability, repeatability and structural MRI correlates. *NeuroImage*, *49*(4), 3349–3357. https://doi.org/10.1016/j.neuroimage.2009.11.045

Obrist, W. D. (1954). The electroencephalogram of normal aged adults. *Electroencephalography and Clinical Neurophysiology*, *6*, 235–244. https://doi.org/10.1016/0013-4694(54)90025-5

Pascual Marqui, R. D., Valdés-Sosa, P. A., & Alvarez-Amador, A. (1987). A Parametric Model for Multichannel EEG Spectra. *International Journal of Neuroscience*, 11.

Podvalny, E., Noy, N., Harel, M., Bickel, S., Chechik, G., Schroeder, C. E., Mehta, A. D., Tsodyks, M., & Malach, R. (2015). A unifying principle underlying the extracellular field potential spectral responses in the human cortex. *Journal of Neurophysiology*, *114*(1), 505–519. https://doi.org/10.1152/jn.00943.2014

Reimann, M. W., Anastassiou, C. A., Perin, R., Hill, S. L., Markram, H., & Koch, C. (2013). A Biophysically Detailed Model of Neocortical Local Field Potentials Predicts the Critical Role of Active Membrane Currents. *Neuron*, *79*(2), 375–390. https://doi.org/10.1016/j.neuron.2013.05.023

Robertson, M. M., Furlong, S., Voytek, B., Donoghue, T., Boettiger, C. A., & Sheridan, M. A. (2019). EEG Power Spectral Slope differs by ADHD status and stimulant medication exposure in early childhood. *Journal of Neurophysiology*, jn.00388.2019. https://doi.org/10.1152/jn.00388.2019

Samaha, J., & Postle, B. R. (2015). The Speed of Alpha-Band Oscillations Predicts the Temporal Resolution of Visual Perception. *Current Biology*, *25*(22), 2985–2990. https://doi.org/10.1016/j.cub.2015.10.007

Tran, T. T., Hoffner, N. C., LaHue, S. C., Tseng, L., & Voytek, B. (2016). Alpha phase dynamics predict age-related visual working memory decline. *NeuroImage*, *143*, 196–203. https://doi.org/10.1016/j.neuroimage.2016.08.052

Tran, T. T., Rolle, C. E., Gazzaley, A., & Voytek, B. (2020). Linked Sources of Neural Noise Contribute to Age-related Cognitive Decline. *Journal of Cognitive Neuroscience*, *0*(0), 1–110. https://doi.org/10.1162/jocn_a_01584

van der Meij, R., Kahana, M., & Maris, E. (2012). Phase-Amplitude Coupling in Human Electrocorticography Is Spatially Distributed and Phase Diverse. *Journal of Neuroscience*, *32*(1), 111–123. https://doi.org/10.1523/JNEUROSCI.4816-11.2012

Veerakumar, A., Tiruvadi, V., Howell, B., Waters, A. C., Crowell, A. L., Voytek, B., Posse, P. R., Denison, L., Rajendra, J. K., Edwards, J. A., Bijanki, K. R., Choi, K. S., & Mayberg, H. S. (2019). Field potential 1/f activity in the subcallosal cingulate region as a candidate signal for monitoring deep brain stimulation for treatment resistant depression. *Journal of Neurophysiology*, 25.

Vogel, E. K., & Machizawa, M. G. (2004). Neural activity predicts individual differences in visual working memory capacity. *Nature*, *428*(6984), 748–751. https://doi.org/10.1038/nature02447

Voytek, B., & Knight, R. T. (2010). Prefrontal cortex and basal ganglia contributions to visual working memory. *Proceedings of the National Academy of Sciences*, *107*(42), 18167–18172. https://doi.org/10.1073/pnas.1007277107

Voytek, B., Kramer, M. A., Case, J., Lepage, K. Q., Tempesta, Z. R., Knight, R. T., & Gazzaley, A. (2015). Age-Related Changes in 1/f Neural Electrophysiological Noise. *Journal of Neuroscience*, *35*(38), 13257–13265. https://doi.org/10.1523/JNEUROSCI.2332-14.2015

Voytek, B. (2016). The Virtuous Cycle of a Data Ecosystem. *PLOS Computational Biology*, *12*(8), e1005037. https://doi.org/10.1371/journal.pcbi.1005037

Voytek, B., Kayser, A. S., Badre, D., Fegen, D., Chang, E. F., Crone, N. E., Parvizi, J., Knight, R. T., & D'Esposito, M. (2015). Oscillatory dynamics coordinating human frontal networks in support of goal maintenance. *Nature Neuroscience*, *18*(9), 1318–1324. https://doi.org/10.1038/nn.4071

Voytek, B., & Knight, R. T. (2015). Dynamic Network Communication as a Unifying Neural Basis for Cognition, Development, Aging, and Disease. *Biological Psychiatry*, *77*(12), 1089–1097. https://doi.org/10.1016/j.biopsych.2015.04.016

Welch, P. (1967). The use of fast Fourier transform for the estimation of power spectra: A method based on time averaging over short, modified periodograms. *IEEE Transactions on Audio and Electroacoustics*, *15*(2), 70–73. https://doi.org/10.1109/TAU.1967.1161901

Wen, H., & Liu, Z. (2016). Separating Fractal and Oscillatory Components in the Power Spectrum of Neurophysiological Signal. *Brain Topography*, *29*(1), 13–26. https://doi.org/10.1007/s10548-015-0448-0

Winawer, J., Kay, K. N., Foster, B. L., Rauschecker, A. M., Parvizi, J., & Wandell, B. A. (2013). Asynchronous Broadband Signals Are the Principal Source of the BOLD Response in Human Visual Cortex. *Current Biology*, *23*(13), 1145–1153. https://doi.org/10.1016/j.cub.2013.05.001

Chapter 2

Frequency Band Ratios Conflate Periodic and Aperiodic Neural Activity

Abstract

Band ratio measures, computed as the ratio of power between two frequency bands, are a common analysis measure in neuro-electrophysiological recordings. Band ratio measures are typically interpreted as reflecting quantitative measures of periodic, or oscillatory, activity. This assumes that the measure reflects relative powers of distinct periodic components that are well captured by predefined frequency ranges. However, electrophysiological signals contain periodic components and a 1/f-like aperiodic component, the latter of which contributes power across all frequencies. Here, we investigate whether band ratio measures truly reflect oscillatory power differences, and/or to what extent ratios may instead reflect other periodic changes—such as in center frequency or bandwidth—and/or aperiodic activity. In simulation, we investigate how band ratio measures relate to changes in multiple spectral features, and show how multiple periodic and aperiodic features influence band ratio measures. We validate these findings in human electroencephalography (EEG) data, comparing band ratio measures to parameterizations of power spectral features, and find that multiple disparate features influence ratio measures. For example, the commonly applied theta / beta ratio is most reflective of differences in aperiodic activity, and not oscillatory theta or beta power. Collectively, we show that periodic and aperiodic features can create the same observed changes in band ratio

measures, and that this is inconsistent with their typical interpretations as measures of periodic power. We conclude that band ratio measures are a non-specific measure, conflating multiple possible underlying spectral changes, and recommend explicit parameterization of neural power spectra as a more specific approach.

Introduction

Frequency band ratio measures, in which a ratio of power is calculated between pre-specified frequency bands, are a common analysis measure in cognitive and clinical neuroscience. For example, a consistent line of research investigates the theta / beta ratio as a potential biomarker for executive function, and in particular attentional processing (Angelidis et al., 2016; Gordon et al., 2018; Lubar, 1991; van Son et al., 2019). Other work has explored using ratio measures in learning and memory (Kim et al., 2016; Nokia et al., 2008; Trammell et al., 2017), age related changes (Clarke et al., 2001; Gasser et al., 1988; Matoušek & Petersén, 1973), and automated sleep scoring (Costa-Miserachs et al., 2003; Krakovská & Mezeiová, 2011; Reed et al., 2017).

Band ratio measures are also common in clinical neuroscience, in studies seeking biomarkers for diagnosis, clinical monitoring, and potential intervention. Band ratio measures are commonly used in investigations of attention-deficit hyperactivity disorder (Arns et al., 2013; Loo & Makeig, 2012; Lubar, 1991; Snyder & Hall, 2006). Other investigations into the potential clinical utility of band ratio measures include anesthesia (Long et al., 1989), multiple sclerosis (Keune et al., 2017), cerebral ischemia (Sheorajpanday et al., 2009), and Parkinson's disease (Geraedts et al., 2018). Band ratio measures have also been applied in studies of mild-cognitive impairment, dementia, and Alzheimer's (Bennys et al., 2001; Moretti et al., 2013; Penttilä et al., 1985), recently reviewed in (Cassani et al., 2018), and have also been applied in studies of autism (Wang et al., 2016) and psychotic disorders (Howells et al., 2018).

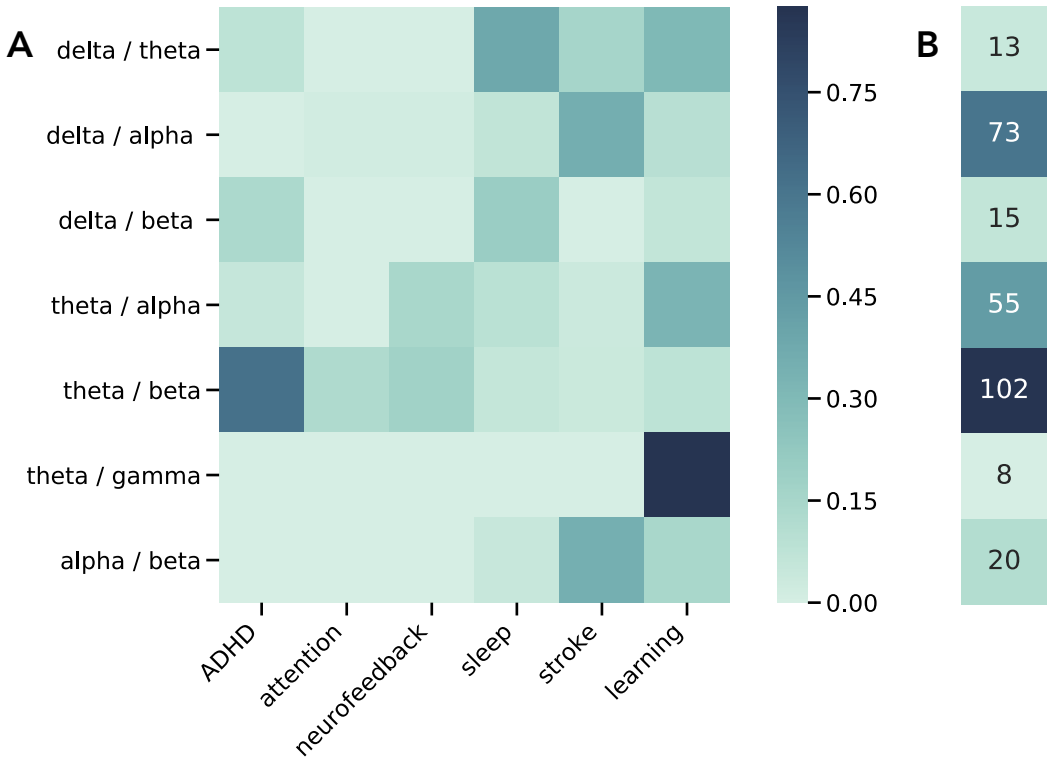

Figure 2.1. Literature Analysis of Band Ratio Related Articles. A) Associations between published journal articles referring to band ratio measures and cognitive and clinical associations. Each cell represents the proportion of articles referring to a specified band ratio measure that also mentions the corresponding association term. **B)** Total counts of the number of articles mentioning each band ratio measure.

Collectively, band ratio measures are used across basic, clinical, and applied neuroscience. This is corroborated by an automated literature search that quantified the number of published articles that reference band ratio measures (Figure 1), finding over 250 articles. Given the popularity of these measures, it is important to investigate their methodological properties and assumptions.

Studies using band ratio measures typically compute power in pre-defined frequency bands, and then calculate a ratio measure between them. The result is then analyzed for potential correlations with features of interest. Such analyses typically interpret band ratio measures as

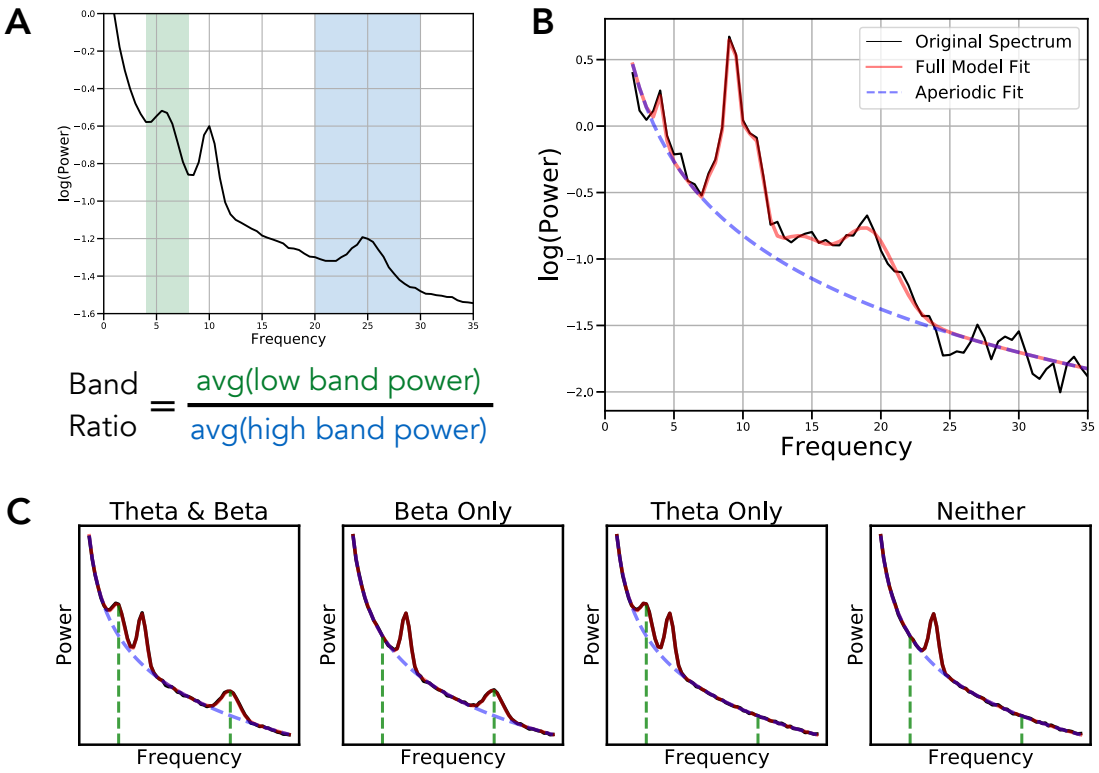

Figure 2.2. Overview of Band Ratio Measures and Spectral Parameters. A) An example power spectrum in which shaded regions reflect the theta (4-8 Hz) and beta band (20-30 Hz) respectively. Band ratio measures, such as the theta / beta ratio are calculated by dividing the average power between these two bands. **B)** An example of a parameterized power spectrum, in which aperiodic activity is separated from measured periodic components. This is an example spectrum from EEG data, in which peaks in theta, alpha, and beta power are present. **C)** Examples of simulated power spectra with and without component oscillations of the theta / beta ratio. Black lines indicate the simulated data, with red line reflecting the model fit, the dashed blue line indicating the aperiodic component of the model fit, and the green lines indicating the location of canonical theta and beta oscillations. Band ratio measures, though intended to measure periodic activity, will reflect power at the pre-determined frequencies regardless of whether there is evidence of periodic activity at those frequencies.

reflecting periodic power, under the assumption that pre-specified frequency bands specifically measure oscillatory activity.

However, a known problem with applying predefined frequency bands uniformly across all participants is that variation in center frequencies can lead to misestimations of band powers (Lansbergen et al., 2011). These potential confounds between different periodic features of the

data challenge the notion that band ratio measures relate specifically to periodic power (see Figure 3A).

A broader issue is the implicit assumption that pre-defined frequency bands reflect only periodic activity, and that measuring the average power of a frequency range specifically captures periodic power. This assumption is in general invalid, as electrophysiological activity includes not only periodic components, but 1/f-like aperiodic activity (Haller et al., 2018; B. J. He, 2014). This 1/f-like activity, henceforth referred to as the 'aperiodic component', has power at all frequencies, meaning there will always be power in a given frequency range, but is not comprised solely of periodic activity (see Figure 2B).

Therefore, power in a given frequency range, reflects, at least in part, aperiodic activity, and only partially, if at all, periodic activity. A marker that there is actual periodic power in a signal is that there should be a band specific peak over and above this aperiodic component (Buzsáki et al., 2013). To specifically measure this periodic component of the signal, one should measure the power of overlying peaks relative to the aperiodic component of the signal (Haller et al., 2018). Band ratio measures, as currently applied, do not address the confound of ubiquitous aperiodic activity in neural signals. Aperiodic neural activity is known to be variable both within (Podvalny et al., 2015) and between (Voytek et al., 2015) individuals, which raises the possibility that band ratio measures may capture and reflect differences in aperiodic activity within and between individuals (see Figure 3B).

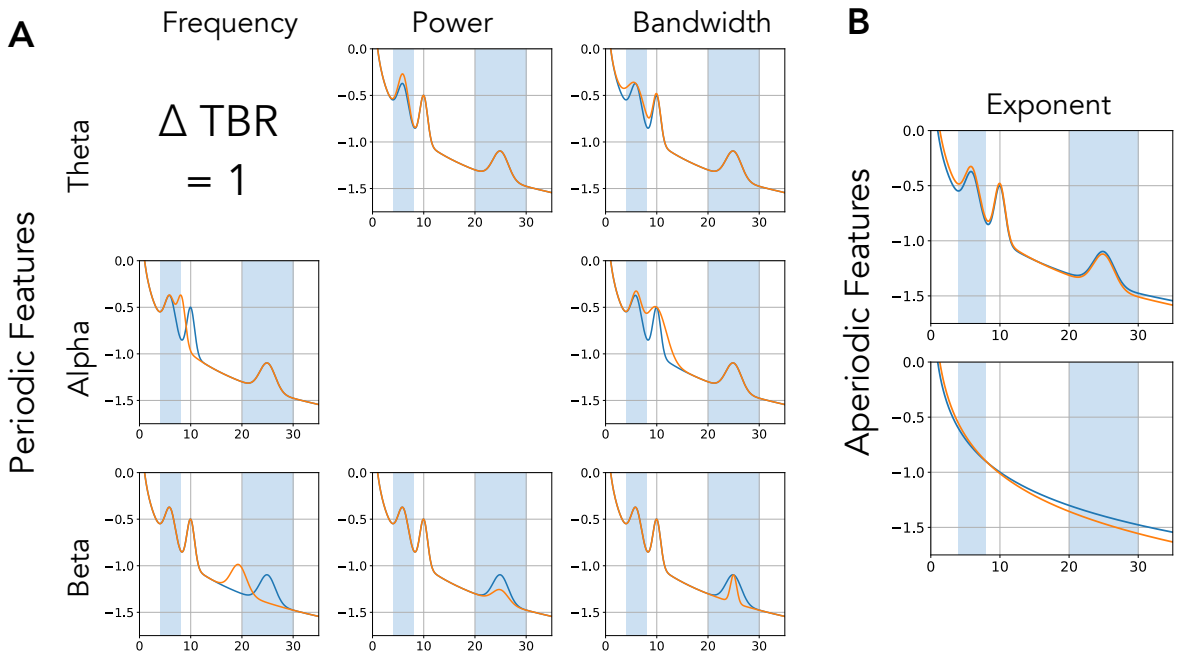

Figure 2.3. Equivalent Band Ratio Differences from Distinct Changes. Simulations demonstrating the underdetermined nature of band ratio measures. In each case, the power spectrum plotted in orange has the same difference of measured theta / beta ratio, indicated as Δ TBR, from the reference spectrum, in blue. This difference in ratio can arise from changes in multiple different features of the data, including a shift in: **A)** periodic parameters such as the center frequency, power or bandwidth of oscillations, and/or from a shift in; **B)** aperiodic properties of the data, in this case the aperiodic exponent. Differences in aperiodic activity can induce differences in measured band ratios, even without any periodic components present (bottom panel).

In summary, band ratio measures are a common measure that are interpreted as reflecting periodic power. However, variations in periodic parameters and/or aperiodic activity, with or without oscillations even being present, can influence band ratio measures (Figure 2C). This suggests that band ratio measures are underdetermined, whereby a change in one or many different features of the data may drive analogous differences in band ratio measures (Figure 3). If so, typical interpretations of band ratio measures are unsupported, and band ratio measures may be uninterpretable, as there are many possible underlying causes of measured differences.

Methods

In this investigation we examined whether the conception of band ratios as measures that specifically reflect periodic power is supported. This question is motivated by considering that periodic properties of electrophysiological data are highly variable, often violating the assumptions of predefined frequency bands, and also that they also co-exist with variable and dynamic aperiodic activity (Haller et al., 2018). To investigate this, we examined the properties and validity of band ratio measures, including, 1) how are band ratio measures influenced by different features of periodic activity, including center frequency, power and bandwidth, and 2) how are band ratio measures influenced by changes in aperiodic properties of the data, including the aperiodic exponent and offset. To do so, we used simulated data and an EEG dataset, and calculated band ratio measures, comparing these measurements to other quantifications of the data in order to investigate which properties of the data band ratio measures are sensitive to.

Analyses were done using Python (version 3.7), including common libraries numpy, pandas, scipy, matplotlib and seaborn for analysis and visualization. The MNE library was used for managing and processing EEG data (Gramfort et al., 2014). Custom code was used to calculate band ratio measures and perform analyses. All code for this project is available in the project repository (https://github.com/voytekresearch/bandratios).

2.1 Literature Analysis

The literature analysis was done using the 'Literature Scanner' (LISC) Python toolbox (Donoghue, 2019). Briefly, this toolbox allows for collecting and analyzing literature data by curating search terms of interest, gathering related articles from available databases, and

analyzing the results. For this analysis, a list of band ratio terms (e.g., "theta / beta ratio") and related association terms (e.g., "attention"), with relevant synonyms and exclusion words, was manually curated. Searches were performed to determine the number of articles in the PubMed database that reference these terms in their abstract, and the number of co-occurrences of band ratio terms with association terms. Association scores were calculated as the proportion of articles referencing a band ratio measure that also mention one of the included association terms.

2.2 Spectral Measures

Band ratio measures are usually calculated from absolute power values, averaged across canonical frequency bands. For all analyses, canonical frequency bands were defined as: theta (4-8 Hz), alpha (8-13 Hz), beta (13-30 Hz). In this study, band ratios were calculated from power spectra by dividing mean power across the low band range by the mean power across the high band range. For all analyses, we calculated the theta / beta ratio, theta / alpha ratio, and alpha / beta ratio. Ratio measures are often log-transformed, as they typically display a non-normal, skewed distribution. Where log-transformations of ratio values were used in analyses or visualizations, it is noted.

As a comparison to band ratio measures, periodic (oscillatory) and aperiodic properties of power spectra were characterized using the fitting-oscillations-&-one-over-f (FOOOF) toolbox (Haller et al., 2018) for parameterizing neural power spectra. Briefly, this tool measures both the aperiodic component of neural power spectra, described by the exponent and offset, and periodic peaks, described by the center frequency (CF), power (PW) and bandwidth (BW) of identified peaks. Band ratio measures were compared to the outputs of these parameterizations, to evaluate which parameters of the data the band ratio measures are sensitive to and primarily

reflect. We also computed 'parameterized ratios' which were ratio measures computed between the power of identified peaks from the parameterization procedure, as a measure of the ratio of isolated periodic power between bands, after controlling for aperiodic activity.

2.3 Simulations

Neural power spectra were simulated to match the statistics of electrophysiological neural data, by combining a 1/f-like aperiodic component with overlying peaks of periodic activity, with overlying noise (Haller et al., 2018). The aperiodic component describes the 1/f-like characteristic of neural power spectra and is entirely described by the aperiodic 'exponent' and 'offset.' The aperiodic exponent, meaning the χ in $\frac{1}{f^{\chi}}$, describes the steepness of the 1/f, and the 'offset,' describes the vertical translation of the aperiodic component. Periodic components describe putative oscillations that display power above the aperiodic component. Periodic components are simulated as Gaussians, and are described by a 'center frequency' (CF) in hertz; peak 'power' (PW), over and above the aperiodic component, in arbitrary units (au); and 'bandwidth' (BW) which describes the width of the peak, also measured in hertz. The simulation, for a power spectrum *P*, is described as:

$$P = L + \sum G_n$$

in which *L* is the aperiodic component, described as

$$L = b - \log\left(f^{x}\right)$$

where b is the offset and χ is the exponent. Note that in these formulations, power is in log10 spacing. In linear power, the exponent would be written as $1/f^{x}$, hence the label of one-over f.

Periodic components are added, whereby each peak is described as a Gaussian, as:

$$G_n = a * \exp\left(\frac{-(f-c)^2}{2 * w^2}\right)$$

in which *c* is the peak center frequency, and *a* and *w* are the height and width of the gaussian, equivalent to the power and bandwidth of the peak. For both the aperiodic and periodic components, f is the array of frequencies of the power spectrum.

Spectra were simulated for the frequency range of 1-35 Hz, with 0.5 Hz frequency resolution. Default aperiodic and periodic parameter values were chosen to capture physiologically realistic values. These default values, as well as the ranges that parameters were simulated across for each parameter, for each frequency band, are given in tables 1 & 2. A small amount of normally distributed noise (0.005 au) was added per frequency to all spectra.

To measure how spectral parameters relate to band ratio measures, spectra were simulated where a single parameter was varied across a range while the remaining parameters were kept at their default values. From these spectra the theta / beta, theta / alpha and alpha / beta ratio measures were calculated to track how individual parameters relate to ratio measures. Since CF, PW, and BW are specific to a peak, they were individually varied for both low-band and high-band peaks.

We then studied how band ratio measures are affected by interacting changes in spectral parameters. Simulated power spectra were created where two parameters from the set {CF, PW, BW, EXP} were simultaneously varied across their respective ranges. All combinations of paired parameter simulations were calculated, and then analyzed by calculating band ratio measures and examining which how simulated properties influence measured values. The default

parameter settings and ranges remained the same as the single parameter simulations (as in Tables 1 & 2).

Table 2.1 Simulated Periodic Parameters Each parameter is given a default value, used when this parameter is included but not varied, and a range and increment, which define the range of simulated values when this parameter is systematically varied.

		Theta	Alpha	Beta
CF	Default	6	10	21.5
	Range	4 - 8	8 - 13	13 - 30
	Increment	0.25	0.25	1
PW	Default	0.5	0.5	0.5
	Range	0 - 1.0	0 - 1.0	0 - 1.0
	Increment	0.1	0.1	0.1
BW	Default	0.1	0.1	0.1
	Range	0.2 - 0.4	0.2 - 0.4	0.2 - 0.4
	Increment	0.2	0.2	0.2

Table 2.2 Simulated Aperiodic Parameters Same description as Table 1, for the aperiodic parameters

	Default	Range	Increment
Offset	0	0 - 2.5	0.25
Exponent	1	0 - 3	0.2

2.4 EEG Data Analysis

To further examine how various spectral parameters affect band ratio measures, in real data, we used the openly available 'Multimodal Resource for Studying Information Processing in the Developing Brain', or MIPDB, dataset of human EEG data released by the Child Mind Institute (Langer et al., 2017). The study population is a community sample of children and adults (n = 126, age range = 6-44, age mean = 15.79, age standard deviation = 8.03, number of males = 69). Data for each subject includes resting state and task EEG data, behavioral measures, and eye tracking data. EEG data was collected on a 128 channel Geodesic Hydrocel system, from which the outermost channels, around the chin and neck, were excluded, leaving a standard 111 channel setup. For the current investigation, we analyzed eyes-closed resting state data. Of the 126 participants in the dataset, 9 did not include resting state data collection, as indicated by the dataset description, and were therefore excluded. In addition, a further 6 participants were excluded from this analysis due to missing the resting state recording file (1 subject) or not having enough resting data events to analyze (5 participants) leaving 111 participants included in the final analysis.

In the resting state protocol, participants were instructed to fixate on a central cross, and open or close their eyes when they heard a beep, alternating between 20 second blocks of eyes open and 40 second blocks of eyes closed. The dataset includes a pre-processed and artifact corrected copy of the data, which was used here, with full details of the pre-processing described in (Langer et al., 2017). Briefly, bad electrodes were identified and interpolated, eye artifacts were regressed out of the EEG from EOG electrodes, and a PCA approach was used to remove

sparse noise from the data. We further identified flat channels (channels with no data) and interpolated them, and re-referenced data to a common average reference.

For the current analyses, we used the eyes closed resting state data, and extracted the time period of 5 – 35 seconds within the 40 second eyes closed resting segments, excluding the 5 seconds post and prior to eye opening. We used the first block for each participant for analysis. Power spectra were calculated for each channel using Welch's method, using 2 second windows with 25% overlap.

We then parameterized the calculated power spectra to return estimates of periodic and aperiodic parameters. The model parameterization we used is agnostic to frequency bands, fitting peaks wherever they're found in the frequency spectrum regardless of canonical band definitions (Haller et al., 2018). We determined that activity was contained in a band if the peak of an oscillation was contained in the aforementioned band definitions. Settings for parameterizing power spectra are as follows: the width for a detected peak was bound between 1 - 8 Hz, with a maximum number of detectable peaks set at 8, a minimum threshold for detecting a peak set at 0.1 au, the threshold for detecting was set at the default value of 2 standard deviations above the noise floor, and spectra were fit in 'fixed' aperiodic mode, without a knee. Parameterizations were evaluated for quality, including manual checks, and using goodness-of-fit metrics, including the r-squared between spectrum models and original data, which had mean value of 0.9732, indicating good fits.

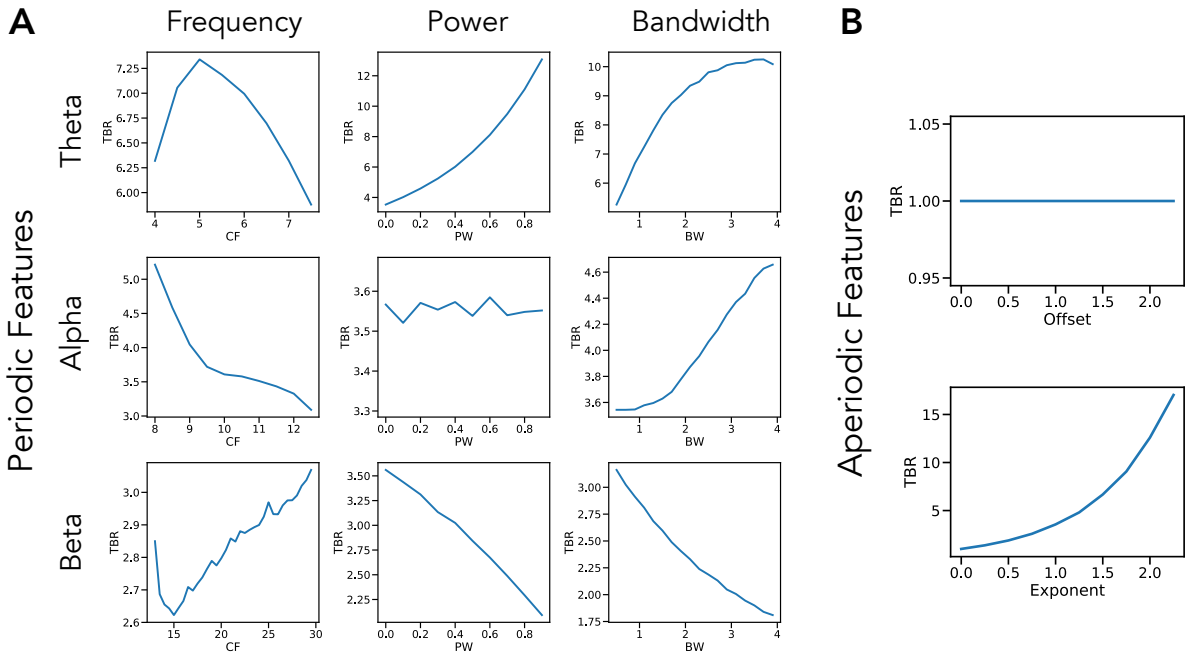

Figure 2.4. Single Parameter Simulations. Simulations of changes in measured theta / beta ratio as individual parameters are varied, including: **A)** periodic parameters and **B)** aperiodic parameters. Changes in theta center frequency show an increase in theta / beta ratio as the heightened activity is better captured in the canonical band, then decreases as activity leaves the band. Increasing theta power and bandwidth both increase theta / beta ratio while increasing beta power and bandwidth decreases theta / beta ratio. The center frequency and bandwidth of alpha peaks also influences measured theta / beta ratio, even though alpha is not supposed to be included in the measure. Beta parameters essentially have the inverse effect of changes in theta parameters. Changes in aperiodic exponent also substantially impact measured theta / beta ratio, though offset has no effect. Note that the layout of this figure corresponds to Figure 3, in which examples of how each parameter influences measured theta / beta ratio can be seen.

2.5 Statistical Analyses

For all band ratio measures, we calculated Spearman correlations between spectral parameters, including center frequency, power and bandwidth of each oscillation band, as well as the aperiodic exponent, across all channels. We do not report correlations to aperiodic offset, as offset shifts by themselves do not affect ratio measures (see simulation results). In addition,

we calculated Spearman correlations between each ratio measure and participants' ages, and between spectral parameters and age.

For all computed correlations, we applied bootstrapping approaches to compute confidence intervals for each reported measure and, where appropriate, to test the difference between correlation magnitudes (Wilcox, 2016). Confidence intervals were computed by resampling, with replacement, and computing correlations for each resample, which creates a distribution from which confidence intervals can be computed. For all bootstraps, 5000 resamples were used, and 95% confidence intervals were computed. In addition, differences between correlations were using bootstrapping. To do so, differences of correlations were computed on resamples, creating a distribution of bootstrapped differences of correlations, which can be used to test if the measured difference is significantly different from zero. The distribution of difference measures was used to compute an empirical p-value, testing a two-sided comparison of if the measured value is significantly different from zero.

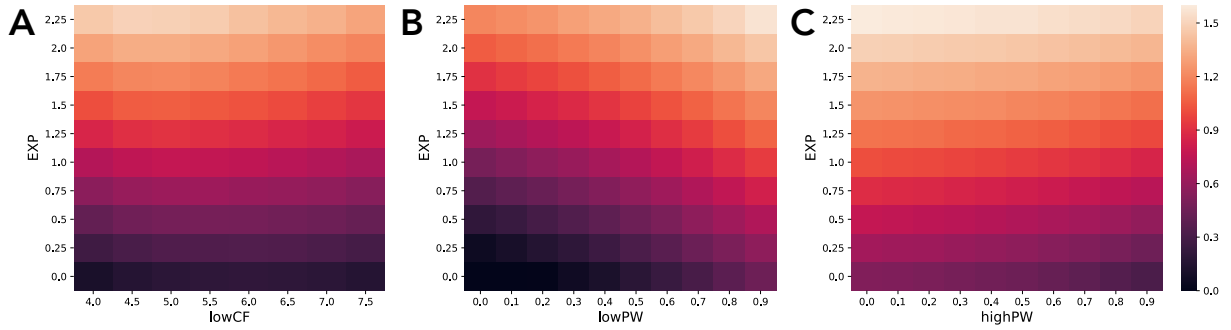

Figure 2.5. Interacting Parameter Simulations. Measured theta / beta ratio values in simulations as two spectral parameters are varied together. Ratio measures are plotted in log10 space due to their skewed distributions. Combinations plotted are aperiodic exponent with low band center frequency **(A)**, as well as with low band power **(B)** and high band power **(C)**. All combinations of varying parameters influence measured band ratio values.

Results

3.1 Simulation Results

We started by investigating, in simulation, the extent to which band ratios capture periodic power as typically interpreted, and/or to what extent they are potentially related to other periodic or aperiodic spectral parameters. Measured theta / beta ratios across simulations in which one spectral parameter was changed at a time, are reported in Figure 4. As expected, when examining periodic changes (Figure 4A) the theta / beta ratio is strongly driven by power of theta and beta oscillations. However, ratio measures can also be influenced by the center frequency and bandwidth of the theta and beta peaks. We also replicate previous work showing that the center frequency of the alpha peak can impact measures of theta / beta ratio, (Lansbergen et al., 2011), and extend this to include alpha bandwidth. For aperiodic changes (Figure 4B), we see that the aperiodic exponent has a significant effect on measured ratio values, but that the offset has no effect.

Collectively, we see that a wide range of different parameter changes can affect measured ratios. In this case, 8 of the 10 parameters alter theta / beta band ratio, with the only exceptions being the aperiodic offset, which changes power equally between ratio bands, and power in the non-included band, in this case alpha (for the theta / beta ratio). Of note, however, is that the scale of these effects can be quite different, with the power of the included bands and the aperiodic exponent having the biggest impacts. Simulations for other band ratio measures are consistent with those for the theta / beta ratio, and are available in the project repository.

We further explored simulations of pairwise combinations of parameter changes, to investigate how ratio measures are affected by concomitant changes in multiple parameters (Figure 5). These simulations include, for example, measured theta / beta band ratios as the aperiodic exponent and theta center frequency both vary, showing an interaction between them (Figure 5A). We can see how changes in aperiodic exponent interact with power changes in the lower (Figure 5B) and higher (Figure 5C) bands. These simulations also demonstrate that both features have an impact on measured ratios, and allow a comparison of scale, showing, for example, that although the influence of low band power and aperiodic exponent is of a similar magnitude, when compared to high band power, the effect of aperiodic exponent changes is relatively much larger. Collectively, through these simulations, we see that changes in different spectral parameters can interact and drive different patterns of differences in measured band ratios. Further simulations of interacting parameters across all other combinations are available in the project repository.

3.2 EEG Data Results

We next analyzed EEG data recorded during resting state, and compared band ratio measures to parameterized power spectral features. For all correlations here, we report results across all channels. Re-running these analyses with channel groups, using frontal, central, and parietal sub-selections all showed qualitatively similar patterns, the results of which are available in the project repository.

For the theta / beta ratio, within periodic spectral parameters we find, as expected, that the strongest relationship is between theta / beta ratio and theta power (r = 0.34, CI_{95}: [0.15, 0.52], $p < 0.001$) with a similar magnitude correlation with beta power (r = -0.28, CI_{95}: [-0.46, -0.09], $p < 0.01$). When ignoring direction (taking the absolute value of the correlations), the magnitude of the correlations between theta / beta ratio and theta and beta power is not significantly different (Δr = 0.06, CI_{95}: [-0.25, 0.36], p = 0.69). When considering aperiodic parameters, we find a much stronger relationship between theta / beta ratio and aperiodic exponent (r = 0.77, CI_{95}: [0.66, 0.84] $p < 10^{-20}$). This correlation is of a significantly higher magnitude (ignoring direction) than the correlation to theta power (Δr = 0.42, CI_{95}: [0.22, 0.62], $p < 10^{-35}$) or beta power (Δr = 0.48, CI_{95}: [0.26, 0.70], $p < 10^{-35}$). The full set of spectral parameter correlations is available in Figure 6A.

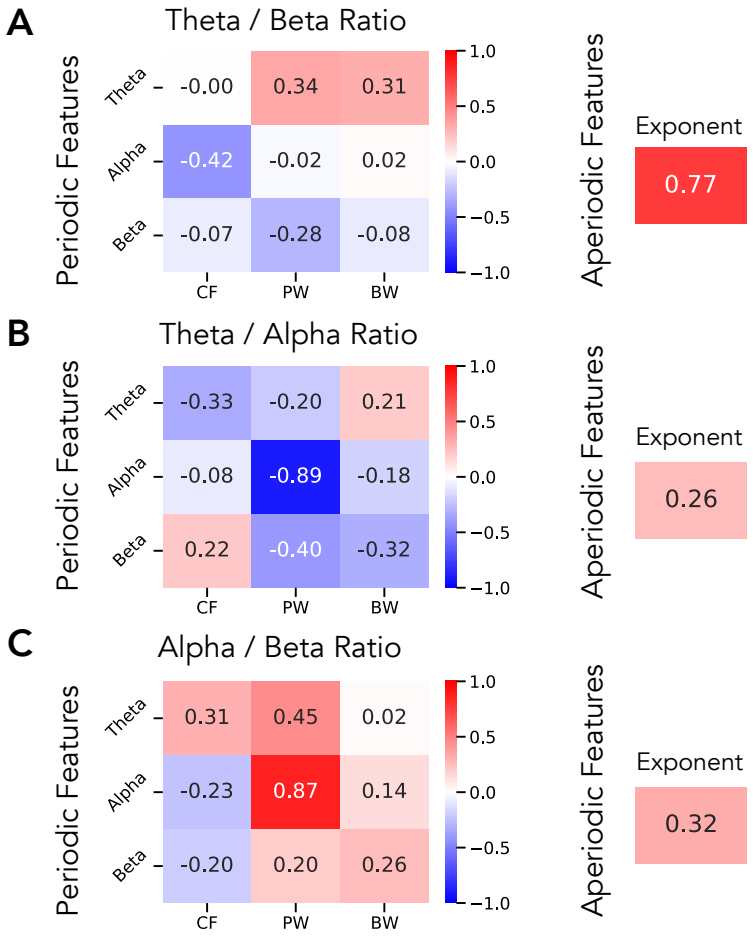

Figure 2.6. Correlations between Spectral Parameters and Band Ratio Measures in EEG Data. In a large EEG dataset, correlation results are reported for band ratios as compared to the periodic (left) and aperiodic (right) parameters for the **(A)** theta / beta ratio, **(B)** theta / alpha ratio and **(C)** alpha / beta ratio. In **(A)**, these results show that the theta / beta ratio is most strongly correlated with the aperiodic exponent, and less related to power in the theta or beta. In contrast, **(B)** and **(C)** show that any ratio measure that includes an alpha band is most strongly correlated to alpha power, meaning any alpha ratio is mostly reflecting just alpha power.

In contrast, for the theta / alpha ratio, the highest correlation across both periodic and aperiodic spectral parameters was for alpha power (r = -0.89, CI_{95}: [-0.93, -0.84], $p < 10^{-35}$), with a much lower correlation to aperiodic exponent (r = 0.26, CI_{95}: [0.09, 0.42], $p < 0.01$), with a significant difference of correlation magnitude between the two (Δr = 0.63, CI_{95}: [0.45, 0.82], p

$< 10^{-35}$). This pattern of correlations was also similar for the alpha / beta ratio, with a strong correlation with alpha ($r = 0.87$, CI_{95}: [0.79, 0.92], $p < 10^{-30}$), and a much weaker one with aperiodic exponent ($r = 0.32$, CI_{95}: [0.14, 0.49], $p < 0.001$), again reflecting a significant difference in correlation magnitude ($\Delta r = 0.54$, CI_{95}: [0.35, 0.73], $p < 10^{-35}$). Spectral parameter correlations for the theta / alpha ratio and alpha / beta ratio are available in Figure 6B & 6C respectively.

We also calculated average ratio measures and spectral parameters for each channel, across the group. Topographies of these measures are plotted in Figure 7. Here we can see, for example, that the spatial topography of the theta / beta ratio is most similar to that of the aperiodic exponent, with a strong spatial correlation ($r = 0.77$, CI_{95}: [0.66, 0.84], $p < 10^{-20}$) between them. Notably, the magnitude of the correlation of theta / beta ratio to theta power ($r = 0.52$, CI_{95}: [0.38, 0.64], $p < 0.001$) and beta power ($r = 0.32$, CI_{95}: [0.15, 0.48], $p < 0.001$) are both significantly less than the correlation of theta / beta ratio to aperiodic exponent (theta power vs. exponent: $\Delta r = -0.24$, CI_{95}: [-0.39, -0.11], $p < 0.01$; beta power vs exponent: $\Delta r = -0.44$, CI_{95}: [-0.56, -0.33], $p < p < 10^{-35}$).

The topography of alpha / beta ratio is nearly identical to the topography of alpha power ($r = 0.98$, CI_{95}: [0.95, 0.98], $p < 10^{-70}$). Similarly, there is a strong inverse relation between the theta / alpha ratio and alpha power ($r = -0.92$, CI_{95}: [-0.95, -0.87], $p < 10^{-45}$). In these cases, the correlation of theta / alpha ratio to alpha power was significantly greater than to aperiodic exponent ($\Delta r = -0.19$, CI_{95}:[-0.28, -0.11], $p < p < 10^{-35}$), and the correlation between alpha / beta ratio and alpha power was also significantly greater than to aperiodic exponent ($\Delta r = 0.11$, CI_{95}: [0.07, 0.17], $p < p < 10^{-35}$).

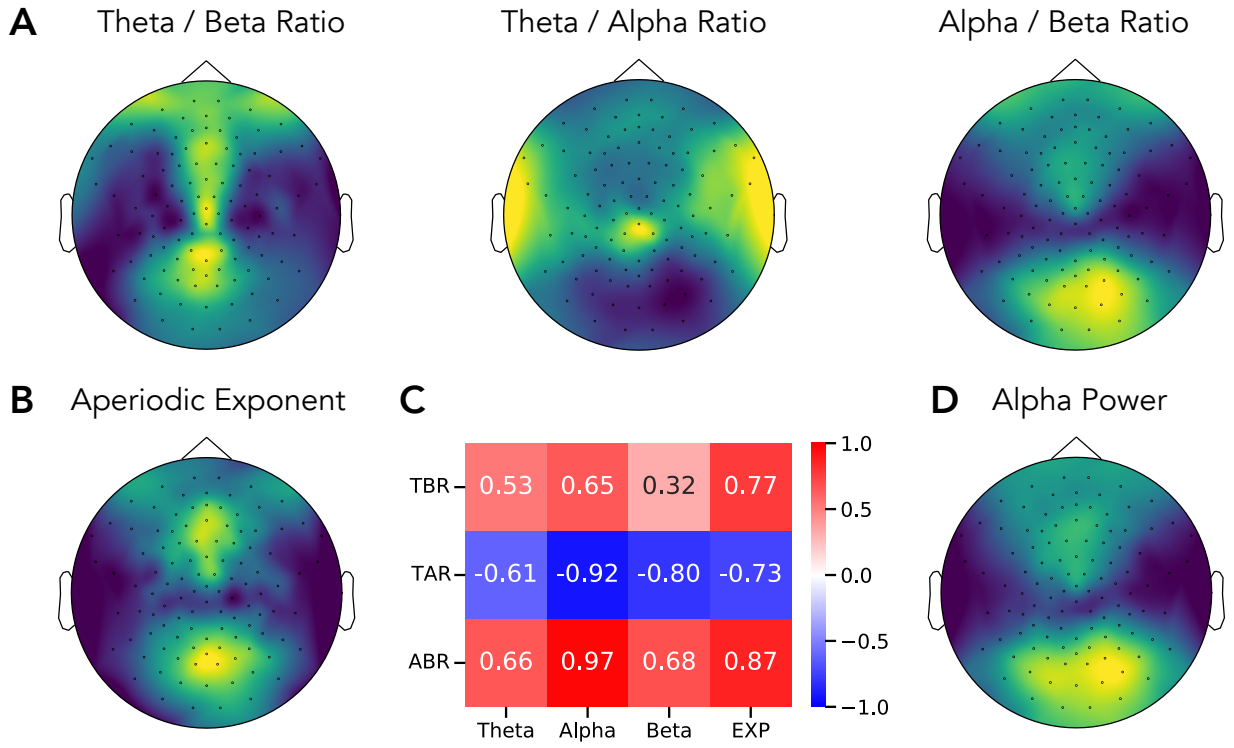

Figure 2.7. Topographies of Band Ratio Measures and Spectral Parameters. Topographical maps of the **A)** ratios measures, including the theta / beta ratio, theta / alpha ratio and alpha / beta ratio. For comparison, the topography of the aperiodic exponent **(B)** and of alpha power **(D)** are also presented. Each topography is scaled to relative range of the data, with higher values plotted in lighter colors (yellow). **C)** The spatial correlation between topographies of each ratio measure to spectral parameters including power of theta, alpha and beta, and the aperiodic exponent (EXP).

We also calculated how each measure correlated with age. The theta / beta ratio was found to be highly correlated with age (r = -0.67, CI_{95}: [-0.76, -0.54], $p < 10^{-15}$), with the negative correlation indicating that older adults have higher theta / beta ratios. The theta / alpha ratio also had a significant correlation with age (r = -0.37, CI_{95}: [-0.51, -0.20], p = 0.0001), but the alpha / beta ratio was not significantly correlated with age (r = -0.12, CI_{95}: [-0.30, 0.08], p = 0.22). For spectral parameters, the aperiodic exponent was found to be highly correlated with age (r = 0.68, CI_{95}: [-0.77, -0.57], $p < 10^{-15}$), consistent with previous reports (W. He et al., 2019; Voytek

et al., 2015). There was not a significant difference in the magnitude of the correlation of theta / beta ratio and age, and that of the aperiodic exponent and age (Δr = 0.01, CI_{95}: [-0.01, 0.0], p = 0.18).

We also calculated correlations between parameterized ratios (ratios computed on isolated periodic power) and age. We found that the parameterized theta / beta ratio (r = -0.12, CI_{95}: [-0.29, 0.05], p = 0.21), parameterized theta / alpha ratio (r = -0.13, CI_{95}: [-0.31, 0.05], p = 0.18), and parameterized alpha / beta ratio (r = -0.08, CI_{95}: [-0.28, 0.11], p = 0.38) were all non-significantly correlated with age. This is consistent with correlations between band ratio measures and age being driven by the influence of aperiodic activity, since no relation is found with isolated periodic power.

Discussion

4.1 Methodological Discussion Points

Through investigations of both simulated and real data, we find that frequency band ratio measures, though typically applied and interpreted as reflecting the relative periodic power of distinct frequency bands, can actually reflect a large number of distinct changes in the underlying data. These band ratio measures therefore capture multiple different changes in periodic and aperiodic properties. Part of this stems from the use of predefined frequency bands of interest, as has been previously reported (Lansbergen et al., 2011; Saad et al., 2018). Here, we replicate and extend this finding, showing how center frequency, and also oscillatory bandwidth, can influence band ratio measures in ways that can be misinterpreted as reflecting power differences. In addition, we show how frequency band ratio measures may commonly capture, at least partially, aperiodic components of electrophysiological data.

Specifically, we used a parameterization model conceiving of the power spectrum as the combination of an aperiodic, 1/f-like spectrum, characterized by an offset and exponent, with overlying periodic 'peaks', each characterized by a center frequency, power (over and above the aperiodic component) and bandwidth measure. With this approach, we show many of these parameters can affect band ratio measures in simulation. When applied to real data, we find that different parameters do affect ratio measures, with different patterns for different ratio measures. For example, theta / beta ratio measures mostly reflect aperiodic exponent, whereas theta / alpha and alpha / beta ratios mostly reflect alpha power. In no ratio measures did we find evidence that the measure primarily reflects power within both specified bands.

Given the underdetermined nature of band ratio measures in the face of multiple features of the data that may be changing, we conclude that band ratio measures are not an appropriate measure for characterizing electrophysiological data, at least not in isolation. This is because they are uninterpretable in terms of knowing which component(s) of the data they actually reflect. We therefore recommend complementary or alternate approaches, such as parameterizing neural power spectra (Haller et al., 2018). Such approaches allow for specifically measuring periodic and aperiodic components and therefore a more precise quantification and identification of which features of the data vary within and between individuals.

A prior recommendation, that attempts to address center frequency differences (Lansbergen et al., 2011), is that band ratio measures should use individualized frequency bands (Saad et al., 2018). It should be noted that the recommended approach, originally proposed by (Klimesch, 1999), is to use individualized bands based on an alpha band anchor point, whereby theta and beta can be defined as below and above the observed alpha peak. Though this addresses some issues with varying alpha center frequency, it does not specifically establish if there is a defined theta or beta peak, over and above aperiodic power, nor does it identify specific center frequencies should such periodic activity be present. Because this approach also does not separate aperiodic from periodic power, individualized peak detection, especially when anchored to alpha peaks, is insufficient to address the problems highlighted here.

It has previously been reported that ratio measures are stable and have high test-retest reliability within individuals (Angelidis et al., 2016; Monastra et al., 2001; Ohlund, 2000). This is not necessarily in conflict with the finding here that band ratio measures may reflect many distinct features of the data; stable test-retest reliability merely suggests that whichever feature(s) are

captured by band ratios within a given subject are themselves stable. However, that band ratios across individuals, and in particular across different populations, may reflect different properties of the data may well help explain why there has been difficulty in reproducing several findings using band ratios. For example, recent failures to replicate band ratio measures include follow ups on previously reported relations with trait anxiety (van Son et al., 2018) or attentional control (van Son et al., 2019). In clinical work, there have been inconsistent findings relating the theta / beta ratio to ADHD (Liechti et al., 2013; Ogrim et al., 2012). It is possible that when investigating varying populations, different features of the data may be driving different observed ratio measures, and this may relate to the significant variance of band ratio measures and their correlates found across studies.

4.2 Interpretation Related Discussion Points

Band ratio measures are often conceptualized as capturing the proportion of a 'slower' frequency band relative to some 'faster' one, and are often interpreted as a relative 'slowing' of neural activity (eg: Monastra, Lubar, & Linden, 2001; Poza, Hornero, Abásolo, Fernández, & Mayo, 2008) or as a shift of power from one band to another (eg: Gasser, Verleger, Bächer, & Sroka, 1988). Other interpretations focus on interpreting and investigating ratio measures in terms of changes within the component bands, for example interpreting a decrease in theta / beta ratio as changes in the theta or beta band (eg: Clarke et al., 2013), which conceptualizes one or more distinct changes in periodic bands. All of these conceptualizations consider that band ratios reflect periodic power.

In this work, we challenge the notion that ratio measures can be assumed to reflect periodic changes. While they can, and sometimes do, reflect changes in periodic power, they

also reflect other parameters, and are often highly influenced by aperiodic activity. This is consistent with observations that helped motivate the use band ratio measures, for instance of correlated changes across frequency bands (Lubar, 1991). These observed correlated changes across frequency bands can be explained parsimoniously as a change in aperiodic activity. Changes in aperiodic exponent influences power across all frequencies and therefore induces correlations between any two measured frequency regions. This notion is somewhat consistent with the interpretations of ratios reflecting 'substitutions' of power between bands (Gasser et al., 1988), in the sense that one process explains the changes across different frequency regions – though the conception that this is a shift of periodic activity is inconsistent with our findings.

These findings cast doubt on prior reports that use band ratio measures and interpret them as primarily reflecting periodic power. Where such studies are reproducible, recontextualization of such findings should consider multiple possible interpretations, including, for example that, a) there is a true change in the power ratio of activity between distinct frequency bands reflecting periodic activity, b) there is a difference in periodic parameters other than power, such as in center frequency and/or bandwidth, c) there are differences in aperiodic activity, or, d) some combination of the above. Based on data analyzed, the theta / beta ratio is most likely to reflect aperiodic activity, whereas the theta / alpha and alpha / beta ratios are most likely to primarily reflect alpha power. That said, ratio measures could vary across studies in what they reflect, and/or reflect interactions between parameters. Re-evaluations of prior work and/or follow up investigations should seek to re-evaluate such data to investigate which features, in each case, are driving the measured changes in band ratios, and update interpretations accordingly.

In this investigation we replicated the consistently reported finding that band ratio measures vary systematically with age (Angelidis et al., 2016; Bresnahan et al., 1999; Buyck & Wiersema, 2014; Clarke et al., 2001; Gasser et al., 1988; Monastra et al., 2001; Ogrim et al., 2012; Putman et al., 2010). We also replicate that aperiodic activity varies systematically with age (W. He et al., 2019; Voytek et al., 2015). The EEG dataset analyzed here consists of young participants, and the pattern of findings is also consistent with recent work showing that changes in aperiodic activity across age better explain developmental patterns compared to prior reports of correlated changes across multiple distinct oscillation bands (W. He et al., 2019). Since band ratio measures are highly correlated with aperiodic activity (especially the theta / beta ratio), the relation of band ratios to age could be explained as a consequence of band ratio measures reflecting aperiodic activity. This interpretation is supported by the finding that parameterized ratios, using the isolated periodic power, do not correlate with age. The noted relation of band ratios to age is therefore likely to be a confound of aperiodic activity.

Overall, the EEG data analyzed here suggests that ratio measures, and the theta / beta ratio in particular, often largely reflects aperiodic activity. As well as the relationship of aperiodic activity and band ratio measures to age, this is also consistent with other reports that find that correlates of band ratio measures may relate to aperiodic activity. For example, when band ratios are used in sleep scoring, it is typically done with the delta / theta ratio, which we predict likely also captures aperiodic changes. This would be consistent with recent reports that aperiodic activity changes systematically with sleep (Lendner et al., 2020). Collectively, these shared correlates are consistent with the suggestion that band ratio measures likely often reflect aperiodic activity.

A key prediction, if ratio measures often reflect aperiodic properties, is that the reported findings will not be specific to the frequency ranges used to measure the ratios, as aperiodic effects should exist across all frequencies. Indeed, correlated change across frequency bands is one of the observations that led to the popularity of band ratio measures (Lubar, 1991). It has also been reported that distinct ratio measures across different frequency bands show similar patterns, for example that both delta / beta and theta / beta ratios relate to cognitive correlates (Schutter & Van Honk, 2005; Tortella-Feliu et al., 2014), both theta / alpha and theta / beta have been reported to relate to ADHD (Barry et al., 2003), and multiple different ratios show similar patterns in investigations of Alzheimer's disease (Poza et al., 2008). In cases such as these, in which different band ratio measures show approximately similar trends across a wide array of band pairs, a plausible interpretation is that these findings do not reflect correlated changes across multiple distinct frequency bands, but rather that they are all capturing frequency-agnostic aperiodic shifts.

Band ratio measures are also used as target for manipulation in neurofeedback paradigms. In such designs, findings are also consistent with the possibility that targeting ratios at least partially manipulates aperiodic properties, rather than targeting oscillation bands specifically. For example, a recent report showed that targeting beta in a feedback design also induces power changes in the alpha band (Jurewicz et al., 2018), which challenges the possibility of targeting different bands independently. Where investigations probe the specificity of neurofeedback protocols, non-specific effects have been reported, such as an effect on beta from a theta / alpha protocol (Egner et al., 2004), and changes in alpha when using a theta / beta

protocol (Bazanova et al., 2018; Limin Yang et al., 2015), all of which is consistent with ratios reflecting aperiodic activity.

If a considerable proportion of the variance of band ratios measures is due to aperiodic properties, and not well described or interpreted as band specific changes, then it becomes an open question to ask what the physiological interpretation should be, and therefore how these findings should be interpreted. One hypothesis is that the aperiodic properties of neural time series may relate the relative balance of excitatory and inhibitory activity (Gao et al., 2017). Though further work is required to explore this hypothesis and how it relates to measurements done with band ratios, this does suggest a potential link between what has been measured in band ratios, as a correlate of various cognitive markers and disease states, and potential interpretations related to excitation and inhibition. A more general review of aperiodic properties in neural data, sometimes referred to 'scale-free' activity, is available in (B. J. He, 2014).

In the case of ADHD, the theta / beta ratio has been a focus of much research (see reviews in Arns, Conners, & Kraemer, 2013 & Snyder & Hall, 2006), including being investigated as a potential diagnostic marker (Snyder et al., 2015). Findings have been inconsistent, with a reported lack of reliability across studies (Arns et al., 2013), and a practice advisory against using the theta / beta ratio as a diagnostic marker for ADHD (Gloss et al., 2016). These inconsistent findings could potentially be explained by our findings, with the prediction that the theta / beta measure is non-specific and inconsistent in how it is capturing different features of the data across subjects and studies, and that it is overall likely to be highly influenced by aperiodic activity. Indeed, it has recently been reported in a population of ADHD subjects that aperiodic properties

are correlated with theta / beta ratio measures, and that aperiodic measures better relate to disease state and medication status than any ratio measures (Robertson et al., 2019).

We therefore recommend that particular attention should be paid to ratio measures applied in clinical applications, in which the pursuit of biomarkers based on non-specific and unreliable measures could hinder, rather than ameliorate, clinical practice. For other clinical disorders that have been investigated with band ratio measures, such as Alzheimer's disease (Cassani et al., 2018), or psychotic disorders (Howells et al., 2018), investigations should follow up on which underlying features best explain changes in ratio measures, and update interpretations and future work on biomarkers accordingly.

A notable exception, as we found in analyzed EEG data, to ratio measures reflecting aperiodic shifts is in cases in which ratio measures include the alpha band. When the alpha band is included in the ratio, band ratio measures tend to primarily reflect alpha power. This is likely due to the prominence of the alpha band, where alpha is typically present across participants, has very high power, and is dynamic. Thus, it is logical that ratio measures that include the alpha band largely reflect alpha dynamics, as we observed here. This effect may also be exaggerated in our analysis, as we are analyzing eyes closed data, in which alpha power is most prominent, though the pattern of results is consistent when re-computed on eyes open data. Investigations in which ratio measures such as delta / alpha or theta / alpha are used should investigate to what extent the dominant effect they are capturing is alpha dynamics. Overall, we recommend that reports from studies using band ratios including alpha should consider if the findings are likely to be largely explained by alpha dynamics.

Conclusion

Frequency band ratio measures are a common analysis approach applied to neural field data, including EEG, MEG, ECoG and LFP. Band ratio approaches have been applied across many domains, including in basic research investigating executive functions, learning and memory, and sleep; in clinical investigations including investigating ADHD and dementia; and in applied work leveraging them for neurofeedback applications. Though typically interpreted as a normalized measure reflecting the relative power of distinct periodic components, here we show that band ratio measures can reflect not only multiple features of periodic neural activity, including the center frequency, power and bandwidth of periodic components, but can also be driven by variations in aperiodic activity. This is demonstrated both in simulation and in the analysis of a large EEG dataset, in which we show how multiple spectral features relate to measured band ratios, making them an imprecise metric. For example, the most dominant contributor to the theta / beta ratio is the aperiodic exponent, whereas the theta / alpha and alpha / beta ratio predominantly reflect alpha power. Overall, band ratio measures are found to be underdetermined, and so across participants, recording modalities, species, and contexts may reflect different components of the signal. This makes comparisons with band ratio measures difficult, if not impossible, and questions their typical interpretations as reflecting periodic activity. As an alternative, we recommend that parameterization of neural power spectra is able to better capture which components of neural signals vary and relate to features of interest, without conflating changes in periodic and aperiodic activity, as band ratio measures do.

References

Angelidis, A., van der Does, W., Schakel, L., & Putman, P. (2016). Frontal EEG theta/beta ratio as an electrophysiological marker for attentional control and its test-retest reliability. *Biological Psychology*, *121*, 49–52. https://doi.org/10.1016/j.biopsycho.2016.09.008

Arns, M., Conners, C. K., & Kraemer, H. C. (2013). A Decade of EEG Theta/Beta Ratio Research in ADHD: A Meta-Analysis. *Journal of Attention Disorders*, *17*(5), 374–383. https://doi.org/10.1177/1087054712460087

Barry, R. J., Clarke, A. R., & Johnstone, S. J. (2003). A review of electrophysiology in attention-deficit/hyperactivity disorder: I. Qualitative and quantitative electroencephalography. *Clinical Neurophysiology*, *114*(2), 171–183. https://doi.org/10.1016/S1388-2457(02)00362-0

Bazanova, O. M., Auer, T., & Sapina, E. A. (2018). On the Efficiency of Individualized Theta/Beta Ratio Neurofeedback Combined with Forehead EMG Training in ADHD Children. *Frontiers in Human Neuroscience*, *12*. https://doi.org/10.3389/fnhum.2018.00003

Bennys, K., Rondouin, G., Vergnes, C., & Touchon, J. (2001). Diagnostic value of quantitative EEG in Alzheimer's disease. *Neurophysiologie Clinique*, *31*(3), 153–160. https://doi.org/10.1016/S0987-7053(01)00254-4

Bresnahan, S. M., Anderson, J. W., & Barry, R. J. (1999). Age-related changes in quantitative EEG in attention-deficit / hyperactivity disorder. *Biological Psychiatry*, *46*(12), 1690–1697. https://doi.org/10.1016/S0006-3223(99)00042-6

Buyck, I., & Wiersema, J. R. (2014). State-related electroencephalographic deviances in attention deficit hyperactivity disorder. *Research in Developmental Disabilities*, *35*(12), 3217–3225. https://doi.org/10.1016/j.ridd.2014.08.003

Buzsáki, G., Logothetis, N., & Singer, W. (2013). Scaling Brain Size, Keeping Timing: Evolutionary Preservation of Brain Rhythms. *Neuron*, *80*(3), 751–764. https://doi.org/10.1016/j.neuron.2013.10.002

Cassani, R., Estarellas, M., San-Martin, R., Fraga, F. J., & Falk, T. H. (2018). Systematic Review on Resting-State EEG for Alzheimer's Disease Diagnosis and Progression Assessment. *Disease Markers*, *2018*, 1–26. https://doi.org/10.1155/2018/5174815

Clarke, A. R., Barry, R. J., Dupuy, F. E., McCarthy, R., Selikowitz, M., & Johnstone, S. J. (2013). Excess beta activity in the EEG of children with attention-deficit/hyperactivity disorder: A disorder of arousal? *International Journal of Psychophysiology*, *89*(3), 314–319. https://doi.org/10.1016/j.ijpsycho.2013.04.009

Clarke, A. R., Barry, R. J., McCarthy, R., & Selikowitz, M. (2001). Age and sex effects in the EEG: Development of the normal child. *Clinical Neurophysiology*, *112*(5), 806–814. https://doi.org/10.1016/S1388-2457(01)00488-6

Costa-Miserachs, D., Portell-Cortés, I., Torras-Garcia, M., & Morgado-Bernal, I. (2003). Automated sleep staging in rat with a standard spreadsheet. *Journal of Neuroscience Methods*, *130*(1), 93–101. https://doi.org/10.1016/S0165-0270(03)00229-2

Donoghue, T. (2019). LISC: A Python Package for Scientific Literature Collection and Analysis. *Journal of Open Source Software*, *4*(41), 1674. https://doi.org/10.21105/joss.01674

Egner, T., Zech, T. F., & Gruzelier, J. H. (2004). The effects of neurofeedback training on the spectral topography of the electroencephalogram. *Clinical Neurophysiology*, *115*(11), 2452–2460. https://doi.org/10.1016/j.clinph.2004.05.033

Gao, R., Peterson, E. J., & Voytek, B. (2017). Inferring synaptic excitation/inhibition balance from field potentials. *NeuroImage*, *158*, 70–78. https://doi.org/10.1016/j.neuroimage.2017.06.078

Gasser, T., Verleger, R., Bächer, P., & Sroka, L. (1988). Development of the EEG of school-age children and adolescents. I. Analysis of band power. *Electroencephalography and Clinical Neurophysiology*, *69*(2), 91–99. https://doi.org/10.1016/0013-4694(88)90204-0

Geraedts, V. J., Marinus, J., Gouw, A. A., Mosch, A., Stam, C. J., van Hilten, J. J., Contarino, M. F., & Tannemaat, M. R. (2018). Quantitative EEG reflects non-dopaminergic disease severity in Parkinson's disease. *Clinical Neurophysiology*, *129*(8), 1748–1755. https://doi.org/10.1016/j.clinph.2018.04.752

Gloss, D., Varma, J. K., Pringsheim, T., & Nuwer, M. R. (2016). Practice advisory: The utility of EEG theta/beta power ratio in ADHD diagnosis: Report of the Guideline Development, Dissemination, and Implementation Subcommittee of the American Academy of Neurology. *Neurology*, *87*(22), 2375–2379. https://doi.org/10.1212/WNL.0000000000003265

Gordon, S., Todder, D., Deutsch, I., Garbi, D., Getter, N., & Meiran, N. (2018). Are resting state spectral power measures related to executive functions in healthy young adults? *Neuropsychologia*, *108*, 61–72. https://doi.org/10.1016/j.neuropsychologia.2017.10.031

Gramfort, A., Luessi, M., Larson, E., Engemann, D. A., Strohmeier, D., Brodbeck, C., Parkkonen, L., & Hämäläinen, M. S. (2014). MNE software for processing MEG and EEG data. *NeuroImage*, *86*, 446–460. https://doi.org/10.1016/j.neuroimage.2013.10.027

Haller, M., Donoghue, T., Peterson, E., Varma, P., Sebastian, P., Gao, R., Noto, T., Knight, R. T., Shestyuk, A., & Voytek, B. (2018). Parameterizing neural power spectra. *BioRxiv*. https://doi.org/10.1101/299859

He, B. J. (2014). Scale-free brain activity: Past, present, and future. *Trends in Cognitive Sciences*, *18*(9), 480–487. https://doi.org/10.1016/j.tics.2014.04.003

He, W., Donoghue, T., Sowman, P. F., Seymour, R. A., Brock, J., Crain, S., Voytek, B., & Hillebrand, A. (2019). Co-Increasing Neuronal Noise and Beta Power in the Developing Brain. *BioRxiv*, 49. https://doi.org/10.1101/839258

Howells, F. M., Temmingh, H. S., Hsieh, J. H., van Dijen, A. V., Baldwin, D. S., & Stein, D. J. (2018). Electroencephalographic delta/alpha frequency activity differentiates psychotic disorders: A study

of schizophrenia, bipolar disorder and methamphetamine-induced psychotic disorder. *Translational Psychiatry*, *8*(1). https://doi.org/10.1038/s41398-018-0105-y

Jurewicz, K., Paluch, K., Kublik, E., Rogala, J., Mikicin, M., & Wróbel, A. (2018). EEG-neurofeedback training of beta band (12–22 Hz) affects alpha and beta frequencies – A controlled study of a healthy population. *Neuropsychologia*, *108*, 13–24. https://doi.org/10.1016/j.neuropsychologia.2017.11.021

Keune, P. M., Hansen, S., Weber, E., Zapf, F., Habich, J., Muenssinger, J., Wolf, S., Schönenberg, M., & Oschmann, P. (2017). Exploring resting-state EEG brain oscillatory activity in relation to cognitive functioning in multiple sclerosis. *Clinical Neurophysiology*, *128*(9), 1746–1754. https://doi.org/10.1016/j.clinph.2017.06.253

Kim, J., Goldsberry, M. E., Harmon, T. C., & Freeman, J. H. (2016). Developmental Changes in Hippocampal CA1 Single Neuron Firing and Theta Activity during Associative Learning. *PLOS ONE*, *11*(10), e0164781. https://doi.org/10.1371/journal.pone.0164781

Klimesch, W. (1999). EEG alpha and theta oscillations reflect cognitive and memory performance: A review and analysis. *Brain Research Reviews*, *29*(2), 169–195. https://doi.org/10.1016/S0165-0173(98)00056-3

Krakovská, A., & Mezeiová, K. (2011). Automatic sleep scoring: A search for an optimal combination of measures. *Artificial Intelligence in Medicine*, *53*(1), 25–33. https://doi.org/10.1016/j.artmed.2011.06.004

Langer, N., Ho, E. J., Alexander, L. M., Xu, H. Y., Jozanovic, R. K., Henin, S., Petroni, A., Cohen, S., Marcelle, E. T., Parra, L. C., Milham, M. P., & Kelly, S. P. (2017). A resource for assessing information processing in the developing brain using EEG and eye tracking. *Scientific Data*, *4*, 170040. https://doi.org/10.1038/sdata.2017.40

Lansbergen, M. M., Arns, M., van Dongen-Boomsma, M., Spronk, D., & Buitelaar, J. K. (2011). The increase in theta/beta ratio on resting-state EEG in boys with attention-deficit/hyperactivity disorder is mediated by slow alpha peak frequency. *Progress in Neuro-Psychopharmacology and Biological Psychiatry*, *35*(1), 47–52. https://doi.org/10.1016/j.pnpbp.2010.08.004

Lendner, J. D., Helfrich, R. F., Mander, B. A., Romundstad, L., Lin, J. J., Walker, M. P., Larsson, P. G., & Knight, R. T. (2020). An electrophysiological marker of arousal level in humans. *ELife*, *9*, e55092. https://doi.org/10.7554/eLife.55092

Liechti, M. D., Valko, L., Müller, U. C., Döhnert, M., Drechsler, R., Steinhausen, H.-C., & Brandeis, D. (2013). Diagnostic Value of Resting Electroencephalogram in Attention-Deficit/Hyperactivity Disorder Across the Lifespan. *Brain Topography*, *26*(1), 135–151. https://doi.org/10.1007/s10548-012-0258-6

Limin Yang, Wenya Nan, Xiaoting Qu, Feng Wan, Pui-In Mak, Peng Un Mak, Vai, M. I., Yong Hu, & Rosa, A. (2015). Beta/theta ratio neurofeedback training effects on the spectral topography of EEG. *37th Annual International Conference of the IEEE Engineering in Medicine and Biology Society (EMBC)*, 4741–4744. https://doi.org/10.1109/EMBC.2015.7319453

Long, C. W., Shah, N. K., Loughlin, C., Spydell, J., & Bedford, R. F. (1989). A Comparison of EEG Determinants of Near-Awakening from Isoflurane and Fentanyl Anesthesia: Spectral Edge, Median Power Frequency, and **δ** Ratio. *Anesthesia & Analgesia*, *69*(2), 169–173. https://doi.org/10.1213/00000539-198908000-00005

Loo, S. K., & Makeig, S. (2012). Clinical Utility of EEG in Attention-Deficit/Hyperactivity Disorder: A Research Update. *Neurotherapeutics*, *9*(3), 569–587. https://doi.org/10.1007/s13311-012-0131-z

Lubar, J. F. (1991). Discourse on the development of EEG diagnostics and biofeedback for attention-deficit/hyperactivity disorders. *Biofeedback and Self-Regulation*, *16*(3), 201–225. https://doi.org/10.1007/BF01000016

Matoušek, M., & Petersén, I. (1973). Automatic evaluation of EEG background activity by means of age-dependent EEG quotients. *Electroencephalography and Clinical Neurophysiology*, *35*(6), 603–612. https://doi.org/10.1016/0013-4694(73)90213-7

Monastra, V. J., Lubar, J. F., & Linden, M. (2001). The development of a quantitative electroencephalographic scanning process for attention deficit-hyperactivity disorder: Reliability and validity studies. *Neuropsychology*, *15*(1), 136–144. https://doi.org/10.1037//0894-4105.15.1.136

Moretti, D. V., Paternicò, D., Binetti, G., Zanetti, O., & Frisoni, G. B. (2013). EEG upper/low alpha frequency power ratio relates to temporo-parietal brain atrophy and memory performances in mild cognitive impairment. *Frontiers in Aging Neuroscience*, *5*. https://doi.org/10.3389/fnagi.2013.00063

Nokia, M. S., Penttonen, M., Korhonen, T., & Wikgren, J. (2008). Hippocampal theta (3–8Hz) activity during classical eyeblink conditioning in rabbits. *Neurobiology of Learning and Memory*, *90*(1), 62–70. https://doi.org/10.1016/j.nlm.2008.01.005

Ogrim, G., Kropotov, J., & Hestad, K. (2012). The quantitative EEG theta/beta ratio in attention deficit/hyperactivity disorder and normal controls: Sensitivity, specificity, and behavioral correlates. *Psychiatry Research*, *198*(3), 482–488. https://doi.org/10.1016/j.psychres.2011.12.041

Ohlund, B. (2000). *An Investigation of the Reliability and Validity of Theta/Beta Ratio Measurement* [PhD Thesis]. Arizona State University.

Penttilä, M., Partanen, J. V., Soininen, H., & Riekkinen, P. J. (1985). Quantitative analysis of occipital EEG in different stages of Alzheimer's disease. *Electroencephalography and Clinical Neurophysiology*, *60*(1), 1–6. https://doi.org/10.1016/0013-4694(85)90942-3

Podvalny, E., Noy, N., Harel, M., Bickel, S., Chechik, G., Schroeder, C. E., Mehta, A. D., Tsodyks, M., & Malach, R. (2015). A unifying principle underlying the extracellular field potential spectral responses in the human cortex. *Journal of Neurophysiology*, *114*(1), 505–519. https://doi.org/10.1152/jn.00943.2014

Poza, J., Hornero, R., Abásolo, D., Fernández, A., & Mayo, A. (2008). Evaluation of spectral ratio measures from spontaneous MEG recordings in patients with Alzheimer's disease. *Computer Methods and Programs in Biomedicine*, *90*(2), 137–147. https://doi.org/10.1016/j.cmpb.2007.12.004

Putman, P., van Peer, J., Maimari, I., & van der Werff, S. (2010). EEG theta/beta ratio in relation to fear-modulated response-inhibition, attentional control, and affective traits. *Biological Psychology*, *83*(2), 73–78. https://doi.org/10.1016/j.biopsycho.2009.10.008

Reed, C. M., Birch, K. G., Kamiński, J., Sullivan, S., Chung, J. M., Mamelak, A. N., & Rutishauser, U. (2017). Automatic detection of periods of slow wave sleep based on intracranial depth electrode recordings. *Journal of Neuroscience Methods*, *282*, 1–8. https://doi.org/10.1016/j.jneumeth.2017.02.009

Robertson, M. M., Furlong, S., Voytek, B., Donoghue, T., Boettiger, C. A., & Sheridan, M. A. (2019). EEG Power Spectral Slope differs by ADHD status and stimulant medication exposure in early childhood. *Journal of Neurophysiology*. https://doi.org/10.1152/jn.00388.2019

Saad, J. F., Kohn, M. R., Clarke, S., Lagopoulos, J., & Hermens, D. F. (2018). Is the Theta/Beta EEG Marker for ADHD Inherently Flawed? *Journal of Attention Disorders*, *22*(9), 815–826. https://doi.org/10.1177/1087054715578270

Schutter, D. J. L. G., & Van Honk, J. (2005). Electrophysiological ratio markers for the balance between reward and punishment. *Cognitive Brain Research*, *24*(3), 685–690. https://doi.org/10.1016/j.cogbrainres.2005.04.002

Sheorajpanday, R. V. A., Nagels, G., Weeren, A. J. T. M., van Putten, M. J. A. M., & De Deyn, P. P. (2009). Reproducibility and clinical relevance of quantitative EEG parameters in cerebral ischemia: A basic approach. *Clinical Neurophysiology*, *120*(5), 845–855. https://doi.org/10.1016/j.clinph.2009.02.171

Snyder, S. M., & Hall, J. R. (2006). A Meta-analysis of Quantitative EEG Power Associated With Attention-Deficit Hyperactivity Disorder: *Journal of Clinical Neurophysiology*, *23*(5), 441–456. https://doi.org/10.1097/01.wnp.0000221363.12503.78

Snyder, S. M., Rugino, T. A., Hornig, M., & Stein, M. A. (2015). Integration of an EEG biomarker with a clinician's ADHD evaluation. *Brain and Behavior*, *5*(4), e00330. https://doi.org/10.1002/brb3.330

Tortella-Feliu, M., Morillas-Romero, A., Balle, M., Llabrés, J., Bornas, X., & Putman, P. (2014). Spontaneous EEG activity and spontaneous emotion regulation. *International Journal of Psychophysiology*, *94*(3), 365–372. https://doi.org/10.1016/j.ijpsycho.2014.09.003

Trammell, J. P., MacRae, P. G., Davis, G., Bergstedt, D., & Anderson, A. E. (2017). The Relationship of Cognitive Performance and the Theta-Alpha Power Ratio Is Age-Dependent: An EEG Study of Short Term Memory and Reasoning during Task and Resting-State in Healthy Young and Old Adults. *Frontiers in Aging Neuroscience*, *9*. https://doi.org/10.3389/fnagi.2017.00364

van Son, D., De Blasio, F. M., Fogarty, J. S., Angelidis, A., Barry, R. J., & Putman, P. (2019). Frontal EEG theta/beta ratio during mind wandering episodes. *Biological Psychology*, *140*, 19–27. https://doi.org/10.1016/j.biopsycho.2018.11.003

van Son, D., Schalbroeck, R., Angelidis, A., van der Wee, N. J. A., van der Does, W., & Putman, P. (2018). Acute effects of caffeine on threat-selective attention: Moderation by anxiety and EEG theta/beta ratio. *Biological Psychology*, *136*, 100–110. https://doi.org/10.1016/j.biopsycho.2018.05.006

Voytek, B., Kramer, M. A., Case, J., Lepage, K. Q., Tempesta, Z. R., Knight, R. T., & Gazzaley, A. (2015). Age-Related Changes in 1/f Neural Electrophysiological Noise. *Journal of Neuroscience*, *35*(38), 13257–13265. https://doi.org/10.1523/JNEUROSCI.2332-14.2015

Wang, Y., Sokhadze, E. M., El-Baz, A. S., Li, X., Sears, L., Casanova, M. F., & Tasman, A. (2016). Relative Power of Specific EEG Bands and Their Ratios during Neurofeedback Training in Children with Autism Spectrum Disorder. *Frontiers in Human Neuroscience*, *9*. https://doi.org/10.3389/fnhum.2015.00723

Wilcox, R. R. (2016). Comparing dependent robust correlations. *British Journal of Mathematical and Statistical Psychology*, *69*(3), 215–224. https://doi.org/10.1111/bmsp.12069

Chapter 3

Variability of Periodic and Aperiodic Electrophysiological Activity across the Human Cortex

Abstract

Electrophysiological activity displays both periodic (oscillatory) and aperiodic (1/f-like) activity. Both of these components have been implicated in healthy brain functioning and disease states, and display significant variation both within and between subjects. However, there are some limitations to prior work investigating the variability of periodic and aperiodic neural activity, including that i) many common analyses approaches do not explicitly separate periodic and aperiodic activity, and thus potentially conflate these two distinct components ii) periodic activity is typically examined using pre-defined frequency bands that may not accurately reflect oscillation occurrence and frequency variation, which limits precise quantification and comparison and iii) concomitant variability in aperiodic neural activity is rarely considered and analyzed. In this work, we apply a novel parameterization approach that addresses these limitations by characterizing periodic and aperiodic activity from neural power spectra. We apply this approach across several EEG and MEG datasets, and report on patterns of within and between subject variability, noting, for example: i) between subject variability in the occurrence, center frequency, aperiodic-adjusted power and bandwidth variation of neural oscillations, ii) within subject topographical variation of periodic activity, and dynamics between state, iii)

between subject patterns of variability of aperiodic activity, and iv) within subject variability of aperiodic activity, whereby aperiodic activity varies systematically across the cortex as well as between task and rest states. These analyses present a detailed overview of within and between subject variation in neural field data, much of which may be missed by common analysis approaches, and demonstrates the utility of applying spectral parameterization to large datasets.

Introduction

Electro-magnetic neural field recordings, reflecting aggregate activity across large populations of neurons, are commonly recorded in neuroscientific investigations of human brain activity, such is as recorded by magnetoencephalography (MEG) or electroencephalography (EEG). Such data contains both periodic activity, which are rhythmic patterns of aggregate synaptic activity across groups of neurons (Buzsáki et al., 2012; Wang, 2010), and aperiodic activity that has no characteristic periodicity, contributing power across all frequencies (Haller et al., 2018; B. J. He, 2014).

Aperiodic activity in neural field data is often termed 1/f or 1/f-like activity, as it follows a $1/f^{\chi}$ distribution in the frequency domain. Aperiodic activity is known to be variable within and between subjects, for example, relating to age between subjects (W. He et al., 2019; Voytek & Knight, 2015), and task performance within subjects (Podvalny et al., 2015). The provenance and putative functional roles of aperiodic activity are active areas of investigation, and it has been proposed that aspects of aperiodic activity potentially relate to the excitation / inhibition (EI) balance in neural circuits (Gao et al., 2017), and to timescales of neural processing (Gao et al., 2020).

Despite its ubiquity and potential interpretations, relatively little work has explored the properties and variability of aperiodic neural activity. Some early investigations started by mapping 1/f properties across the cortex (Freeman et al., 2003; Pritchard, 1992), including in newborn babies (Fransson et al., 2013), as well as comparing across species (Freeman & Zhai, 2009). Though recent work has increasingly started to investigate aperiodic neural activity as a

potentially interesting feature of investigation, there is still a relative lack of work exploring intra- and inter-individual variation of such activity. One recent investigation of individual variability found that it varies between subjects to the extent that individuals can be identified based on patterns of aperiodic activity (Demuru & Fraschini, 2020).

In comparison to aperiodic activity, periodic activity, or neural oscillations, have been much more heavily studied. Periodic activity is a ubiquitous feature of neural field data, and has been proposed to play important roles in neural computation and cognition (Buzsáki & Draguhn, 2004). Disruptions of periodic activity are implicated across numerous psychiatric and neurological disorders (Voytek & Knight, 2015). Functional interpretations of periodic activity typically consider that oscillations may be involved in functional organization, organizing information through time (VanRullen, 2016), and/or between regions (Fries, 2005; Varela et al., 2001).

Periodic neural activity is typically conceptualized and analyzed in terms of distinct frequency bands. These bands are typically described as delta (0.5 - 4 Hz), theta (4 - 8 Hz), alpha (8 - 13 Hz), beta (13 - 30 Hz), low gamma (30 - 80 Hz) and high gamma (80 - 150), though band definitions often vary. Prior work has examined patterns and topographies of these bands across the cortex, including in MEG (Cox et al., 2018; Demirtas et al., 2018; Niso et al., 2016a), and ECoG (Frauscher et al., 2018a). Such work has shown group level patterns of cortical activity – for example, that theta activity is typically most prominent in the frontal lobe, beta is focused in central sensorimotor regions, and alpha dominates in the occipital cortex.

Between subject variability of periodic activity can occur across distinct features, such as in their power, frequency, and spatial distribution. Patterns of oscillatory power have been

reported to vary systematically with age (Hashemi et al., 2016), including in ways that predict cognitive performance (Vlahou et al., 2014). Another common feature of investigation is the peak frequency, in particular of alpha, which also varies with age (Lindsley, 1938), and is considered to be a stable neurophysiological trait (Grandy et al., 2013). Variations of peak frequency relate to behavioral reaction times (Surwillo, 1961) and cognitive task demands (Haegens et al., 2014).

In terms of individual variability, it has been noted that individuals have identifiable 'oscillatory signatures' (Näpflin et al., 2007). Using EEG data, participants can be identified from their power spectra, in particular based on alpha activity (Del Pozo-Banos et al., 2014). These individual differences are robust and consistent, showing stability, including across sessions, in both MEG (Martín-Buro et al., 2016), and EEG (Fingelkurts et al., 2006). Oscillation measures also show high test-retest reliability in task scenarios, including movement related beta activity (Espenhahn et al., 2017), auditory related steady state oscillations (Tan et al., 2015), and working memory and vigilance tasks (McEvoy et al., 2000).

Altogether, a large body of work supports that there exists robust, consistent, and behaviorally significant variability of periodic activity, both within and between subjects. This activity co-exists with aperiodic activity, that itself also exhibits significant variability. Despite these findings, a large amount of work on neural field data often ignores this variability, by analyzing group level and averaged measures. Even work that does consider between subject variability, often still ignores within subject variation. For example, many investigations and analyses implicitly presume within subject stability of features of interest, and yet recent work has shown, for example, that alpha frequency and power can vary systematically with time spent on a task (Benwell et al., 2019).

Altogether, there is significant variability of both periodic and aperiodic activity, that is often under-appreciated and under-explored. The majority of investigations apply and investigate group level measures, without considering individual variability. This is often compounded by methodological limitations, even in work that does consider individual variability. These limitations include that analyses typically i) do not explicitly measure and separate periodic and aperiodic activity, which is liable to conflate changes between the two components, ii) apply predefined frequency ranges, which both presumes that oscillations are present (which may not be true), and makes assumptions about their center frequency, and iii) do not acknowledge and investigate if and how aperiodic activity itself can vary.

Here we seek to further investigate the variability of both aperiodic and periodic activity, while addressing these methodological limitations. This is done by measuring and accounting for concomitant periodic and aperiodic activity, allowing for separating these components, in order to examine the variability of each one. In doing so, we apply approaches that do not presume oscillatory presence or frequency, but rather specifically quantifying oscillatory frequency and power. This allows us to measure variability of both periodic and aperiodic activity. Applying these methods allows for examining within and between subject variability, allowing for systematic comparisons and estimating typical values and ranges within and between brain regions, conditions, and populations.

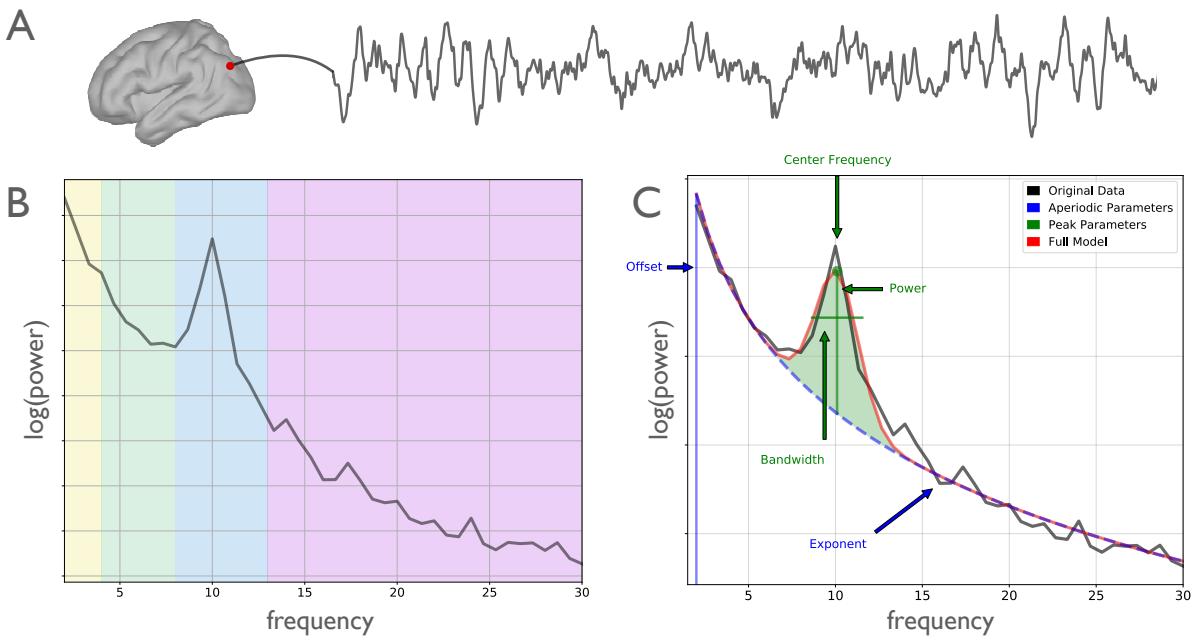

Figure 3.1 | Overview of data and analyses. (**A**) Example of a (simulated) time series of electrical activity recorded from the cortex. (**B**) The power spectrum of the data in A, with shading indicating pre-defined oscillation bands, including delta (2-4 Hz - shown in yellow), theta (4-8 Hz - green), alpha (8-13 Hz - blue), and beta (13-30 Hz - purple). (**C**) The same power spectrum as B, parameterized for periodic and aperiodic activity. Each parameter identified and quantified by the parameterization is labelled. Each identified peak is parameterized by its center frequency, aperiodic adjusted power (power over and above the aperiodic component), and bandwidth. Note that peaks are detected without applying any predefined frequency regions of interests. The aperiodic component is parameterized by the 'offset', or global broadband power, and the 'exponent', which is the value of χ in $1/f^{\chi}$, which reflects the pattern of power across frequencies. Note that the aperiodic exponent is equivalent to the slope, 'a' of the power spectrum, which can be computed from the log-log spectrum, and is sometimes reported in other work as the 'spectral slope', and has the equivalence $\chi = -a$. For this spectrum, the algorithm identifies a peak of activity in the alpha band, whereas activity in all other bands is explained by the aperiodic component. The simulated data was simulated as a bursty alpha oscillation with a 10 Hz center frequency, over aperiodic activity with an exponent of 1.75 a.u. The measured parameters from the algorithm are a peak with a center frequency of 10.1 Hz, and aperiodic exponent of 1.76 a.u.

Methods

In this work, we revisit the investigation of variability in neural field data, addressing limitation of prior work by i) explicitly measuring and separating both periodic & aperiodic activity, ii) detecting and measuring periodic neural activity without using predefined frequency bands, and iii) explicitly measuring the variability of aperiodic activity, all while quantitatively measuring spectral features of interest across multiple datasets and contexts. To do so, we analyzed several EEG and MEG datasets, applying a spectral parameterization algorithm to quantify periodic and aperiodic activity, and examine within and between subject variability of the resultant measures.

The majority of the analyses were done using the Python programming language (version 3.7), including common libraries numpy, pandas, scipy, matplotlib and seaborn for analysis and visualization. The MEG data was preprocessed in Matlab (r2017a), using the Brainstorm analyses toolbox (Tadel et al., 2011a). The EEG data was processed using the MNE toolbox (Gramfort et al., 2014). Analysis functions and time series simulations were used from the NeuroDSP Python toolbox (Cole et al., 2019). Parameterization of neural power spectra was done with the FOOOF toolbox (Haller et al., 2018). All code used for this project is available in the project repositories.

For all analyses, power spectrum parameterization was applied to quantify aperiodic and periodic activity (Haller et al., 2018). Briefly, this process conceptualizes and operationally defines oscillations as power (or 'bumps') over and above the aperiodic 1/f-like component of the data. This aperiodic component is parameterized, after which a search procedure detects and any regions of frequency-specific power, reflecting putative periodic activity (Fig 1C). These peaks

are detected and parameterized without using pre-specified frequency bands, providing quantified measures of the center-frequency, power (relative to the aperiodic component) and bandwidth of each identified peak. After isolating and removing these overlying peaks, a new estimate of the aperiodic component is calculated, providing an estimate of the global spectrum offset and aperiodic exponent (Fig 1C). This algorithm has settings, including bounds that can be set on the number and width of the detected peaks, power thresholds for detecting peaks, and a setting for the form of the aperiodic component.

2.1 Local EEG Dataset

An initial dataset of EEG data was analyzed from a project investigating the role of cortical oscillations in visual perception, henceforth referred to as the 'local' EEG dataset. Data included resting state segments and EEG data while subjects performed a lateralized visual detection task, modelled on a task that has been previously described (Busch et al., 2009). Briefly, subjects had to attend to a central fixation cross, and respond to peripherally presented flashes of lights. For the current investigation, task activity was only analyzed as 'task blocks' (as compared to resting state) with no analyses of trial related activity or behavioral performance. During the rest blocks, subjects were instructed to close their eyes, and hold still, for two-minute segments. EEG data was collected for 29 subjects (age range = [18, 28], 18 female) using a 64 channel BrainVision system, using standard 10-20 EEG electrode placement, and recorded with a sampling rate of 5000 Hz, and later down-sampled to 500 Hz. 15 of the subjects were recorded in a protocol with 2 rest blocks and 10 task blocks, while the remaining 14 subjects had 1 rest block and 12 task blocks.

The EEG data was decomposed using ICA (Bell & Sejnowski, 1995), after applying a 1 Hz high-pass filter. Any ICA components that were significantly correlated with EOG activity were automatically identified and rejected. Bad channels were identified and interpolated. Two-minute segments were extracted from each rest and task block, for each subject. Power spectral densities were calculated per subject, per state, per block and per channel for each segment of data, using the Welch's method, using 4 second windows, half-second overlap, with a Hamming window (Welch, 1967). Power spectra were parameterized across the frequency range of (3 – 30 Hz), using settings {peak_width_limits=[1,6], max_n_peaks=6, min_peak_height=0.075, peak_threshold=1.0, aperiodic_mode='fixed'}. Extracted peaks were post-hoc grouped into frequency bands, defined as theta (2-7Hz), alpha (8-14Hz), beta (15-30Hz) chosen to reflect approximate band ranges in the data (see Fig. 3A). Aperiodic parameters, offset and exponent, were also collected, per power spectrum.

2.2 ChildMind EEG Dataset

Additional EEG data was analyzed from the openly available 'Multimodal Resource for Studying Information Processing in the Developing Brain' (MIPDB) dataset from the Child Mind Institute (Langer et al., 2017), which will be referred to as the `ChildMind` dataset. The dataset includes EEG data, behavioral measures, and eye tracking for a community sample of children and adults (n = 126, age range = 6-44, age mean = 15.79, age standard deviation = 8.03, number of males = 69). For this project, we analyzed the resting state EEG data, which was collected on a 128 channel Geodesic Hydrocel system, with the peripheral channels dropped, leaving a 111-channel montage, with a sampling rate of 500 Hz. Of the 126 participants in the dataset, 9 did not include resting state data collection, as indicated by the dataset description, and were

therefore excluded. In addition, a further 6 participants were excluded from this analysis due to missing the resting state recording file (1 subject) or not having enough resting data events to analyze (5 participants) leaving 111 participants included in the final analysis.

In the resting state paradigm of the ChildMind dataset, participants were instructed to fixate on a central cross, and open and close their eyes at the sound of a beep, alternating between 20 second segments of eyes open and 40 second segments of eyes closed. The dataset includes a pre-processed and artifact corrected copy of the data, which was used here, with full details of the pre-processing described in (Langer et al., 2017). Briefly, bad electrodes were identified and interpolated, eye artifacts were regressed out of the EEG from EOG electrodes, and a PCA approach was used to remove sparse noise from the data. We further identified flat channels (channels with no data) and interpolated them, and re-referenced data to a common average reference.

For each 20 second eyes-open block, we extracted data from 2-18 seconds avoiding the time points around the time when eyes were opened and closed. Similarly, for each 40 second eyes-closed segment, we extracted the time region of 5-35 seconds. Power spectra were calculated, for each subject, for each block, and for each channel, using Welch's method, using 2 second windows and half second overlap, with a Hamming window (Welch, 1967). These spectra were then parameterized, across the frequency range of 3-35 Hz, using settings {peak_width_limits=[1,6], max_n_peaks=6, min_peak_height=0.05, peak_threshold=2.0, aperiodic_mode='fixed'}. We computed the average spectra across all blocks, separately for eyes-open and eyes-closed data, and also parameterized these average spectra, using the same settings.

2.3 MEG Dataset

We additionally analyzed magnetoencephalography (MEG) data, which was chosen as it provides high temporal-resolution, non-invasive recordings of human cortical activity, that can be localized using source projection. Open-access resting-state MEG data, as well as corresponding T1-weighted MRIs for each participant, were accessed from the young adult dataset from the Human Connectome Project database (Van Essen et al., 2013). Briefly, a subset of 95 participants from the HCP had MEG recordings. Of this group, 80 participants met our quality control procedures and were included in the analyses here (ages 22-35; 35 female). Participants were excluded due to missing resting state recordings, missing anatomical scans needed for source projection, or due to excessive artifacts. One participant was rejected post fitting due to being an outlier on goodness-of-fit and/or aperiodic parameters (more than 3 standard deviations from the group mean). For each participant, the first available rest recording was used, comprising approximately 6 minutes of eyes open, resting state data. Full details of the data collection are available elsewhere (Van Essen et al., 2012).

MEG data were pre-processed following best-practice guidelines (Gross et al., 2013), using the Brainstorm software toolbox (Tadel et al., 2011b). Cardiac and eye related artifacts (blinks and saccades) were automatically detected from ECG and EOG traces respectively and removed from the data using signal-space projections (SSP) from data segments selected from around each artifactual event (Nolte & Curio, 1999) using default parameters in Brainstorm. All MEG data were manually inspected for any remaining artifacts, and any contaminated segments were marked as bad, and not included in any further analysis. Cleaned, pre-processed resting state data were then epoched into 5 second segments.

Using the segmentation procedures available in Freesurfer (Fischl, 2012), each participants' T1-weighted anatomical MRI scan was used to construct scalp and cortical surfaces. Individual high-resolution surfaces were down-sampled to 7501 vertices using Brainstorm to serve as cortical reconstructions for MEG source imaging. Structural MRI images were co-registered with the MEG recordings using anatomical landmarks (nasion, and pre-auricular points) and digitized head points available from the recording, which were automatically aligned in Brainstorm, and then manually checked and tuned, as needed.

For source-projection, the overlapping-sphere technique (Huang et al., 1999) for forward modelling of the neural magnetic fields was used, using perpendicularly oriented current dipoles for each individual's anatomy (Baillet et al., 2001). Source projections were calculated using Brainstorm's weighted minimum norm estimate (wMNE) applied to the preprocessed sensor data. Empty room recordings, also available from the HCP, were used as an empirical estimate of the noise for each MEG sensor, in the wMNE projection. For group analysis, individual source maps were then geometrically registered to the ICBM152 brain template, a non-linear average of 152 participants (Fonov et al., 2009), using Brainstorm's multilinear registration technique.

For each epoch, a power spectra were estimated using an adapted version of Welch's method, which averaged across the individual FFTs using the median, as opposed to the mean, in order to deal with the skewed nature of power value distributions (Izhikevich et al., 2018), using a window size of 2 seconds. For each participant, at every vertex, a power spectrum was calculated from source-projected data, on the group template brain. Power values were then averaged across all available epochs to obtain one power spectrum per vertex, per individual.

Following pre-processing, source projection, and spectral analysis, we had power spectral representations of resting state activity at each of 7501 vertices for each of the 80 participants, projected on a template brain. Each of these spectra were then fit across the frequency range [2, 40], with settings {peak_width_limits=[1,6], max_n_peaks=6, min_peak_height=0.1, peak_threshold=2, aperiodic_mode='fixed'}, providing an aperiodic exponent and offset value per vertex as well as a list of extracted peaks (if found) per vertex, per participant. In rare cases, the algorithm can fail to converge on a solution and thus does not provide a fit. This was the case for a total of 4 spectra out of 600,080. For any spectrum for which this happened, that vertex for that participant was set as having no detected peaks, and the aperiodic exponent was interpolated as the mean value of all successful fits from that participant.

To analyze and visualize the putative oscillation results, all extracted peaks were *post hoc* sorted into pre-defined oscillation bands of theta (3-7 Hz), alpha (7-14 Hz), and beta (15-30 Hz). These ranges were chosen to capture the approximate clusters of peaks in the extracted data (see Fig. 3C). To do so, per vertex and per participant, peak output parameters were selected, for each band, if they corresponded to a peak with a center frequency within the band limits. If there was no peak within that range, that vertex was set as having no oscillation of that band. If more than one peak was found for the given range, the highest power peak was selected. From this band-specific data, we then created group maps for each oscillation band across all vertices. For each band we extract two maps: an oscillation power map as well as an oscillation probability map, which is the percent of the group that had a peak within that band at that vertex.

We then calculated a power-normalized "oscillation score". To do so, for each band, the average peak power value at each vertex, across all participants, was divided by the maximum average power value from the distribution of all vertices, such that the vertex that displays the highest band power across the group receives a score of 1, and every other vertex receives a normalized score between 0 and 1. This power ratio was then multiplied, vertex-by-vertex, with the oscillation probability topography. The resultant oscillation score is a bounded measure that can take values between 0 and 1, whereby a maximal score of 1 reflects that every participant has an oscillation in the specified band at the specified vertex, and that oscillation has the greatest average power at that vertex. Scores lower than 1 reflect increased variation in the presence and/or relative power of oscillations across the group.

Note that oscillation scores lower than 1 cannot, by themselves, be disambiguated in terms of where the variability lies. For example, an oscillation score of approximately 0.5 could reflect either a location in which oscillations tend to be of maximal power, but are only observed across approximately half the group, or oscillations that are consistent across the entire group, at about half the maximal power, or some middle ground between the two. These situations can be disambiguated by examining both the oscillation probability and power ratio maps separately. We then calculated the Pearson correlation between the topographies of oscillation scores for each band as well as the correlation between each band's oscillation score and the aperiodic exponent topography.

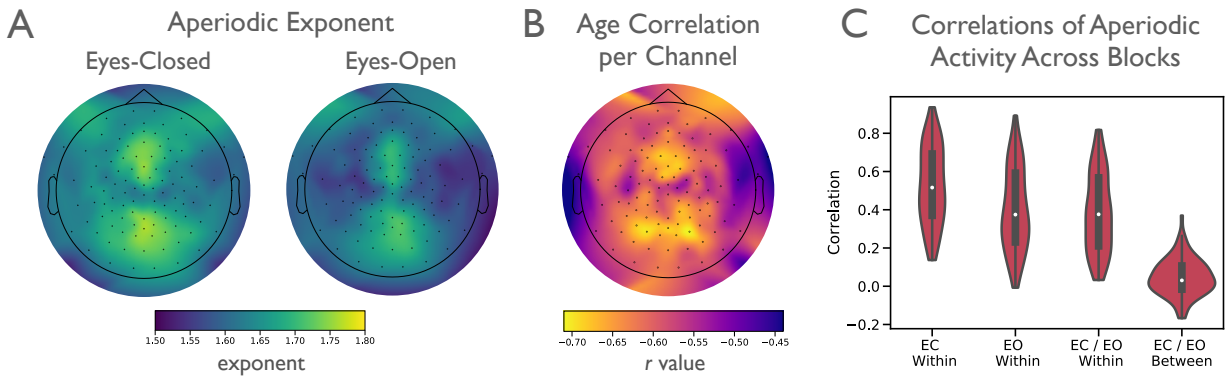

Figure 3.2 | Aperiodic activity in EEG data (**A**) Topography of aperiodic exponent, for both eyes-open and eyes-closed resting state data. (**B**) Correlation between age and aperiodic exponent, computed per channel. (**C**) Correlation of the aperiodic exponent across blocks. EC and EO denote 'eyes-closed' and 'eyes-open' respectively. EC / EO means correlations between the two states. 'Within' indicates a comparison within subjects, and 'Between' indicates between subjects. All data in this figure is from the ChildMind Dataset.

2.4 Statistics & Analyses

Group level measures and topographies were calculated by averaging features across channels or vertices. Comparisons between spectral features were compared with t-tests, using related samples tests for within subject comparisons. All tests were two-tailed. Effect sizes were computed with Cohens-d. Correlations were computed as Spearman's correlations.

Results

3.1 Overall Results

The aperiodic exponent exhibited variability between subjects and datasets, with a difference in aperiodic exponents found between the ChildMind EEG dataset (mean=1.67, std=0.33), and MEG dataset (mean=0.83, std=0.23). Some of the differences between groups may be due to age variation, as there were significant negative correlations between aperiodic exponent with age, in both the ChildMind EEG dataset ($r=-0.66$, $p=<1x10^{-12}$), and in the MEG dataset ($r=-0.46$, $p<1x10^{-4}$). Note that the ChildMind dataset is predominantly children, whereas the MEG dataset is young adults.

The aperiodic exponent was found to be stable within individuals, though with notable variation topographically and across states. In the ChildMind EEG dataset, the aperiodic exponent was greater centrally, in particular along the anterior to posterior axis (**Fig. 2A**). This topographical pattern was consistent in rest data with eyes-open and eyes-closed. There was also a topographical pattern to where the aperiodic exponent most highly correlated with age (**Fig. 2B**). There was a small but significant difference between subjects averaged aperiodic exponent between eyes open and eyes closed resting states ($t=2.37$, $p=0.020$, cohens-d=0.15). We also computed the correlation of aperiodic exponent values between blocks, within subjects (**Fig. 2C**). We find strong correlations of within-subjects repeat measures of aperiodic activity including with the eyes-closed state, (average correlation: 0.53), within the eyes-open (average correlation: 0.40), and between eyes open and closed conditions (average correlation: 0.38). By

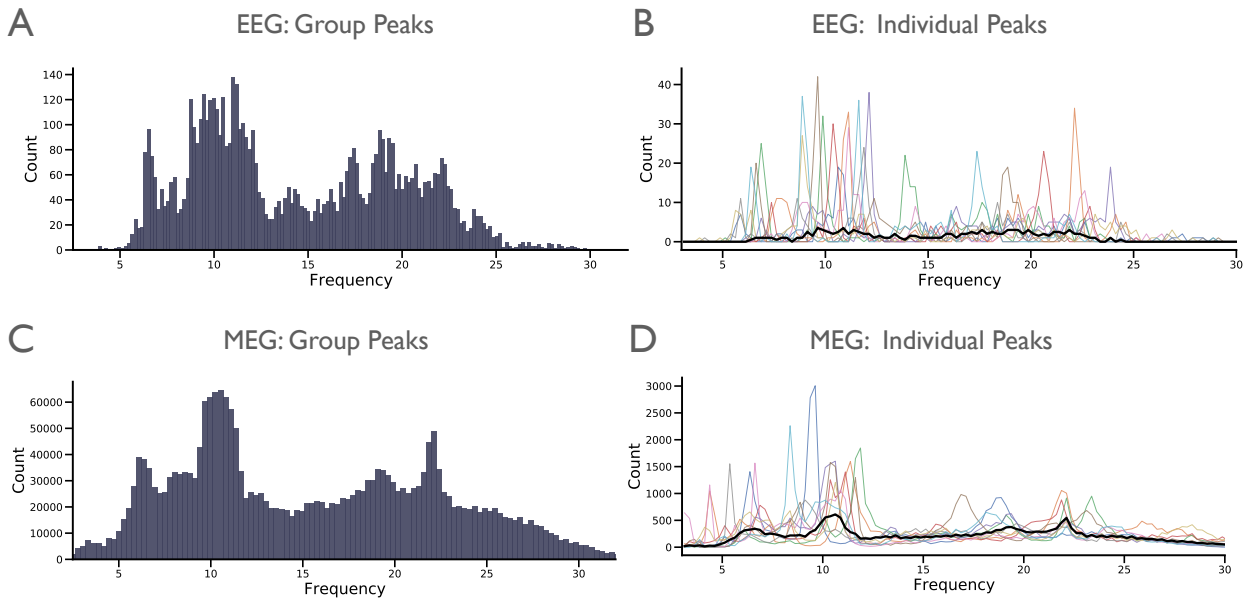

Figure 3.3 | Periodic activity in EEG and MEG data (**A**) The distribution of all center frequencies, across the group, in the EEG dataset. The distribution of peaks roughly captures canonical bands, though there is substantial heterogeneity. (**B**) Distributions of detected peaks for individual subjects. Each colored line is the count of peaks, per frequency, for an individual subject. For clarity, 10 individual subjects from the group are shown. The black line is the median number of peaks, per frequency, across all subjects. Notably, each subject shows idiosyncrasy in their distribution of peaks. (**C-D**) Same as A-B, but with the MEG dataset.

comparison, the correlation of aperiodic exponent between subjects was much lower (average correlation: 0.05).

As a replication of the EEG results, the same topographical pattern of aperiodic exponent was found (data not shown), and there was also a significant difference in subjects' aperiodic exponent between the rest and task states ($t=6.23$, $p=<1x10^{-5}$, cohens-d=0.80). This dataset did not have enough age variation to examine age correlations. When calculating average features across task blocks, we found a significant correlation of alpha power ($r=0.70$, $p=0.025$) with block number, and a trending ($r=-0.61$, $p=0.060$) relation of alpha center frequency. The correlation of aperiodic exponent across task blocks was not significant ($r=-0.50$, $p=0.138$).

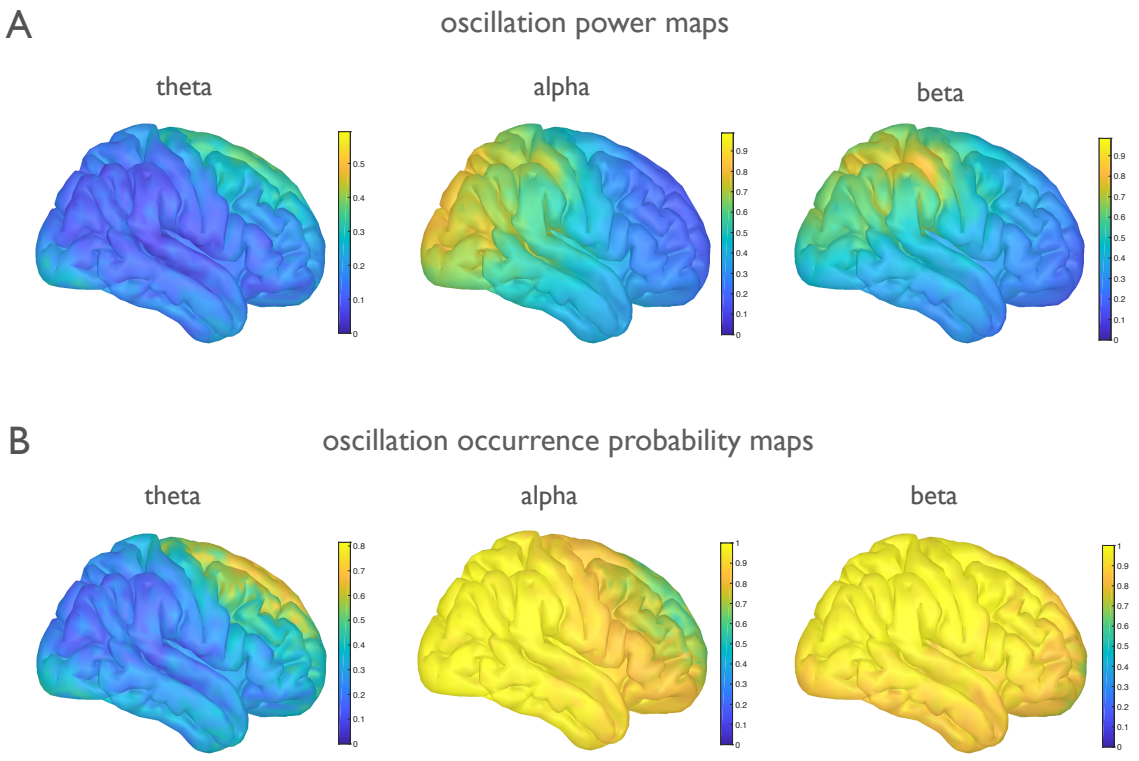

Figure 3.4 | Oscillation band power and occurrence. (**A**) The group level aperiodic-adjusted power, per band. For each participant, the oscillation power within the band was normalized between 0 and 1, and then averaged across all participants, such that a maximal relative power of 1 would indicate that all participants have the same location of maximal band-specific power. Note that alpha and beta have maximal values approaching 1, reflecting a high level of consistency in location of maximal power, whereas in theta the values are lower, reflecting more variability. (**B**) Oscillation occurrence, measured as the proportion of participants for whom an oscillation peak was fit, at each vertex, per band.

Across all analyzed datasets, when collapsed across participants and all cortical locations (channels or vertices), the distribution of center frequencies for all algorithm-extracted oscillations partially recapitulates canonical frequency bands, wherein the most common frequencies are centered in the theta, alpha, and beta ranges (EEG: **Fig. 3A,** MEG: **Fig 3C**). Notably, however, there are extracted oscillations across all frequencies, so while canonical bands do capture the modes of oscillatory activity, they are not an exhaustive description of

periodic activity in the human neocortex. When analyzed at the individual level, there is significant individual variability in detected peaks (EEG: **Fig. 3B,** MEG: **Fig 3D**). Interestingly, individual subjects appear to have narrow ranges of center frequencies within any given band, whereas the observed variability of peaks across whole band ranges is a group level phenomenon (black lines in **Fig. 3B** & **Fig. 3D**). As extracted peaks are broadly consistent with canonical bands, we post-hoc clustered peaks into theta (3-7 Hz), alpha (7-14 Hz), and beta (15-30 Hz) bands for subsequent analyses,

3.2 Topographical Results

Using source-reconstruction with the resting state MEG data, we quantified how spectral parameters varied across the cortex. When examined across the cortex, we find that the aperiodic-adjusted oscillation band power also recapitulates well-documented spatial patterns (Niso et al., 2016b), where theta power is concentrated at the frontal midline, alpha power is predominantly distributed over posterior and sensorimotor areas, and beta power is focused centrally, over the sensorimotor cortex (**Fig. 4A**). However, prior reports using canonical methods may be at least partially driven by aperiodic activity, because they do not separate or quantify if, or how often, oscillations are present over and above the aperiodic component. To address this, we quantified how often an oscillation was observed, for each band, across the cortex (**Fig. 4B**). These two metrics were then combined into an "oscillation score", which is a composite of the group-level oscillation occurrence probability weighted by the relative power of algorithmically identified parameters (**Fig. 5A**).

The oscillation score allows us to examination the variability of periodic activity across participants. For example, the oscillation scores approaching 1.0 in both alpha and beta indicate a very high degree of consistency in these bands (a maximum score of 1.0 tells us that every participant has an oscillation of maximum relative power in the same location). We find that alpha and beta are ubiquitous across the cortex, though their relative power is concentrated in specific regions (Fig. 4A). By contrast, theta is more variable, with max oscillation scores <0.4 indicating significant variability in whether theta is present, and in its relative power. Theta oscillations are only sometimes observed in frontal regions at rest and are almost entirely absent in visual regions.

The explicit parametrization of each feature allows us to separately examine how each parameter varies across the cortex. Note, for example, that the consistency of oscillation presence and relative power do not imply that these oscillations are consistent in their center frequency, because we also see significant variation of peak frequencies (Fig. 3A). Periodic power and oscillation occurrence vary systematically across the cortex (Fig. 4). There is also spatial heterogeneity of the aperiodic exponent such that highest exponent values are found in posterior regions, and the exponent gets gradually smaller (flatter) as it moves anteriorly (Fig. 5B). We calculated the correlation between the aperiodic exponent and age, per vertex, and found a pattern of correlations in the MEG data (Fig. 5D), that was broadly consistent with the pattern found in the EEG data (Fig 2B).

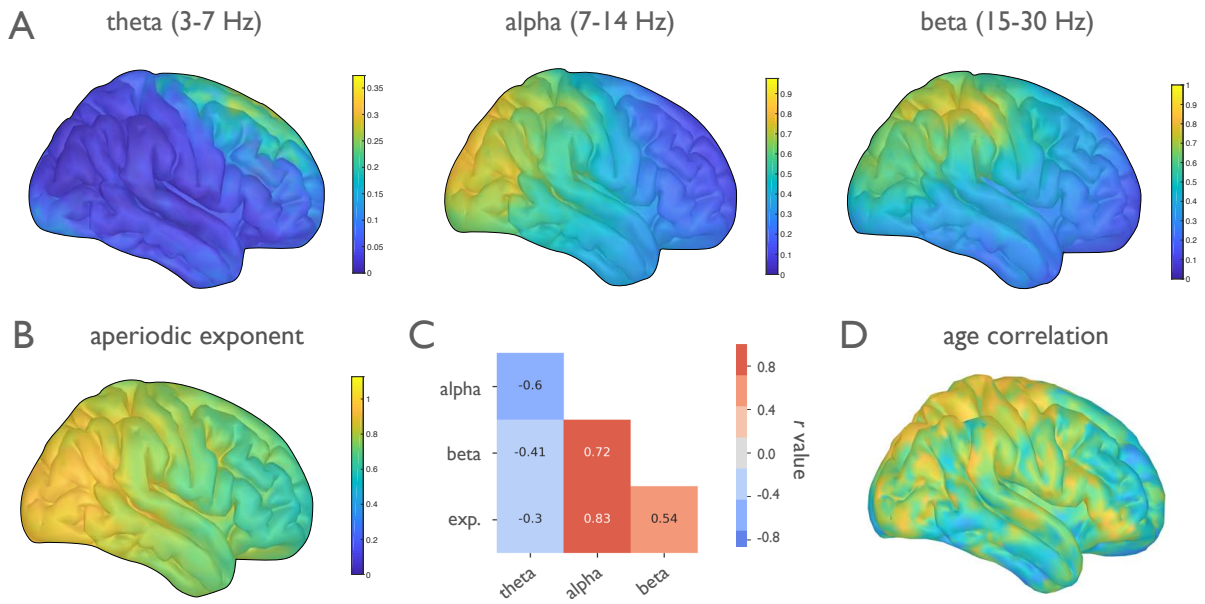

Figure 3.5 | Topographies of spectral features. (**A**) Oscillation topographies reflecting the oscillation score: the probability of observing an oscillation in the particular frequency band, weighted by relative band power, after adjusting for the aperiodic component (see **Methods**). These topographies quantify the known qualitative spatial distribution for canonical oscillation bands theta (3-7 Hz), alpha (7-14 Hz), and beta (15-30 Hz). (**B**) The topography of resting state aperiodic exponent fit values across the cortex. Group exponent—calculated as the average (mean) exponent value, per vertex, across all participants—shows that the aperiodic exponent is lower (flatter) for more anterior cortical regions. (**C**) Correlations between the oscillation topographies and the exponent topography show that theta is spatially anti-correlated with the other parameters. (**D**) Correlation of aperiodic exponent to age, computed across vertices.

We also examined relationships between parameters, calculated as correlations between the spatial topographies of oscillation scores per parameter (**Fig. 5C**). The strongest observed relationships were a negative correlation between theta and alpha ($r=-0.60$, $p<0.0001$) and a positive correlation between alpha and the aperiodic exponent ($r=0.83$, $p<0.0001$). Collectively, these analyses allow us to verify patterns of aperiodic-adjusted periodic activity, and quantify, for the first time, the consistency of occurrence of oscillations. In addition, the spatial topography of the aperiodic exponent is important to note when exploring topographies of presumed oscillations derived from narrowband analyses, given that the aperiodic component can drive observed spatial differences.

Discussion

In this work, we explored power spectrum parameterization as a method for measuring periodic and aperiodic activity, across the human cortex, exploring the variability of measured results both within and between subjects. These findings highlight the large degree of variability that may be missed in many analyses that use only fixed frequency band and group level analyses, and motivates the need to consider and measure both aperiodic and periodic activity.

In periodic activity, we find a significant variability of measured peaks. Notably, though the structure of the data at the group level is consistent with distinct oscillation bands, there is a high degree of variability within subjects. This replicates prior work on center frequency variability, systematically mapping this variability across all bands. Spectral parameterization is also able to indicate if there is evidence for the presence of oscillatory activity, and also provides information on a new feature of interest, which is the peak bandwidth. Oscillation bandwidth has not traditionally been measured, and as such there is scant prior work to validate against or compare to.

Importantly, we find significant individual variability of aperiodic activity, consistent with other reports (Demuru & Fraschini, 2020). The observed between subject variability is consistent with prior results that aperiodic activity varies between subjects, relating to factors such as subject age (W. He et al., 2019; Voytek et al., 2015) and clinical diagnoses (Molina et al., 2020; Robertson et al., 2019). We extend these findings by demonstrating that there is also within subject variability, including across cortical location, and between different tasks states. Variability of aperiodic activity between states is consistent with work showing that it varies across

states such as anesthesia (Colombo et al., 2019) and sleep (Lendner et al., 2020). Here we show this variability is present in more subtle state shifts, such as being task and rest, and even between eyes-open and eyes-closed resting state conditions.

This measured variability is another demonstration that aperiodic activity is a dynamic and potentially informative feature of neural activity. The dynamics of aperiodic activity may be a measure of interest, as the aperiodic exponent is a putative marker of excitatory / inhibitory balance (Gao et al., 2017). The observed variability and dynamics of aperiodic activity – between cortical regions, brain state, and across subjects – are an exciting avenue for future work, including work that further investigates the putative interpretations and functional roles of such activity.

Considering the variability of aperiodic activity is also important for methodological reasons. Measures proposed and interpreted as measuring oscillatory activity, but that do not consider aperiodic activity, are at risk of being confounded, and may actually relate to dynamic aperiodic activity, such as has been demonstrated for band ratio measures (Donoghue et al., 2020). These potential methodological problems are all the more salient in light of the variability of aperiodic activity, which increases both the importance and difficulty of adjudicating between periodic and aperiodic changes in the data. This variability is also a challenge for methods such as spectral whitening, or relative power, which attempt to control for aperiodic activity, under the assumption that it is stationary.

Recent investigations have examined oscillatory frequency bands across age, finding patterns of changes across bands (Hashemi et al., 2016; Vlahou et al., 2014), which are interpreted as changes in specific frequency bands. However, patterns of differences across

frequency bands are consistent with differences in aperiodic activity, which can exhibit as statistically significant differences in particular frequencies (Haller et al., 2018). Investigations which do not consider and measure aperiodic activity may be conflating changes in periodic and aperiodic activity, as has been demonstrated to be the case in band-by-band analyses of electrophysiological activity through development (W. He et al., 2019). Many of these known examples thus far reflect between subject comparisons, and these issues may also be exasperated by the dynamic nature of within subject aperiodic activity.

Using the MEG dataset, we were also able to explore spatial distributions of source projected data. Notably while these results broadly recapitulate expected patterns of activity (Demirtaş et al., 2019; Frauscher et al., 2018b), the explicit parameterizations reveal details that are not possible with traditional approaches. For example, we show that there are band-specific patterns of the detectability of oscillatory peaks, and can also explore the variability of each isolated spectral feature. In doing so, we are able to demonstrate topographies of aperiodic-adjusted periodic power, as well as a topographical gradient of the aperiodic exponent (Demirtaş et al., 2019).

We also find that some spectral parameters, such as alpha power, can vary systematically over time. This replicates prior work on this topic (Benwell et al., 2019). We are also able to demonstrate that this effect appears to be specific to alpha power, as we do not find clear evidence in our data of aperiodic parameters also varying over time. Such variability across time is important as it challenges the assumed stationarity of spectral features (when absent of task manipulations).

A key development of the current work is that it provides quantifications of spectral parameters across multiple, large, available datasets, of non-clinical participants. This serves to further demonstrate the scalability of the employed methods, and a proof-of-concept of mapping distributions and variability of these features. Future work could seek to analyze and further integrate available data, which could be extended to offer quantified norms of spectral parameters for large populations of subjects. This can then be used as a comparison group, investigating, for example, if data from groups of interest, such as particular disease states, deviate from the comparison group, and, if so, in which parameters.

There are some limitations to the current work, which also highlight additional opportunities for future investigations. For example, though we explored and noted individual differences in measured oscillations, for several analyses at the group level, we still had to apply group level oscillation bands. Future work should investigate approaches for detecting and potentially clustering detected oscillations within subjects, as well as methods for acknowledging individual variation in group level measures. All the analyses here also examined relatively long segments of data. Future work should seek to investigate and seek to improve the temporal resolution of methods that allow for separating and measuring aperiodic and periodic activity, such that their dynamics through time can be further explored.

Conclusion

Altogether, we find that there is significant within and between subject variability of periodic and aperiodic neural activity. This suggests potentially useful and informative variation, that may be productively investigated. It is also raises important methodological considerations – since multiple different overlapping features can all be shown to be dynamic, it illustrates and motivates the importance of careful adjudication of which features are changing in which ways, and what aspects of the data relate to covariates of interest, all of which can be done with spectral parameterization.

References

Baillet, S., Riera, J. J., Marin, G., Mangin, J. F., Aubert, J., & Garnero, L. (2001). Evaluation of inverse methods and head models for EEG source localization using a human skull phantom. *Physics in Medicine and Biology*, *46*(1), 77–96. https://doi.org/10.1088/0031-9155/46/1/306

Bell, A. J., & Sejnowski, T. J. (1995). An information-maximisation approach to blind separation and blind deconvolution. *Neural Computation*, 38. https://doi.org/10.1162/neco.1995.7.6.1129

Benwell, C. S. Y., London, R. E., Tagliabue, C. F., Veniero, D., Gross, J., Keitel, C., & Thut, G. (2019). Frequency and power of human alpha oscillations drift systematically with time-on-task. *NeuroImage*, *192*, 101–114. https://doi.org/10.1016/j.neuroimage.2019.02.067

Busch, N. A., Dubois, J., & VanRullen, R. (2009). The Phase of Ongoing EEG Oscillations Predicts Visual Perception. *Journal of Neuroscience*, *29*(24), 7869–7876. https://doi.org/10.1523/JNEUROSCI.0113-09.2009

Buzsáki, G., Anastassiou, C. A., & Koch, C. (2012). The origin of extracellular fields and currents—EEG, ECoG, LFP and spikes. *Nature Reviews Neuroscience*, *13*(6), 407–420. https://doi.org/10.1038/nrn3241

Buzsáki, G., & Draguhn, A. (2004). Neural oscillations in cortical networks. *Science*, *304*(5679), 1926–1929. https://doi.org/10.1126/science.1099745

Cole, S. R., Donoghue, T., Gao, R., & Voytek, B. (2019). NeuroDSP: A package for neural digital signal processing. *Journal of Open Source Software*, *4*(36), 1272. https://doi.org/10.21105/joss.01272

Colombo, M. A., Napolitani, M., Boly, M., Gosseries, O., Casarotto, S., Rosanova, M., Brichant, J.-F., Boveroux, P., Rex, S., Laureys, S., Massimini, M., Chieregato, A., & Sarasso, S. (2019). The spectral exponent of the resting EEG indexes the presence of consciousness during unresponsiveness induced by propofol, xenon, and ketamine. *NeuroImage*, *189*, 631–644. https://doi.org/10.1016/j.neuroimage.2019.01.024

Cox, R., Schapiro, A. C., & Stickgold, R. (2018). Variability and stability of large-scale cortical oscillation patterns. *Network Neuroscience*, *2*(4), 481–512. https://doi.org/10.1162/netn_a_00046

Del Pozo-Banos, M., Alonso, J. B., Ticay-Rivas, J. R., & Travieso, C. M. (2014). Electroencephalogram subject identification: A review. *Expert Systems with Applications*, *41*(15), 6537–6554. https://doi.org/10.1016/j.eswa.2014.05.013

Demirtas, M., Burt, J. B., Helmer, M., Ji, J. L., Adkinson, B. D., Glasser, M. F., Van Essen, D. C., Sotiropoulos, S. N., Anticevic, A., & Murray, J. D. (2018). *Hierarchical heterogeneity across human cortex shapes large-scale neural dynamics*. https://doi.org/10.1101/341966

Demirtaş, M., Burt, J. B., Helmer, M., Ji, J. L., Adkinson, B. D., Glasser, M. F., Van Essen, D. C., Sotiropoulos, S. N., Anticevic, A., & Murray, J. D. (2019). Hierarchical Heterogeneity across Human Cortex Shapes Large-Scale Neural Dynamics. *Neuron*, *101*(6), 1181-1194.e13. https://doi.org/10.1016/j.neuron.2019.01.017

Demuru, M., & Fraschini, M. (2020). EEG fingerprinting: Subject-specific signature based on the aperiodic component of power spectrum. *Computers in Biology and Medicine*, *120*, 103748. https://doi.org/10.1016/j.compbiomed.2020.103748

Donoghue, T., Dominguez, J., & Voytek, B. (2020). *Electrophysiological Frequency Band Ratio Measures Conflate Periodic and Aperiodic Neural Activity*. https://doi.org/10.1101/2020.01.11.900977

Espenhahn, S., de Berker, A. O., van Wijk, B. C. M., Rossiter, H. E., & Ward, N. S. (2017). Movement-related beta oscillations show high intra-individual reliability. *NeuroImage*, *147*, 175–185. https://doi.org/10.1016/j.neuroimage.2016.12.025

Fingelkurts, A. A., Fingelkurts, A. A., Ermolaev, V. A., & Kaplan, A. Ya. (2006). Stability, reliability and consistency of the compositions of brain oscillations. *International Journal of Psychophysiology*, *59*(2), 116–126. https://doi.org/10.1016/j.ijpsycho.2005.03.014

Fischl, B. (2012). FreeSurfer. *NeuroImage*, *62*(2), 774–781. https://doi.org/10.1016/j.neuroimage.2012.01.021

Fonov, V., Evans, A., McKinstry, R., Almli, C., & Collins, D. (2009). Unbiased nonlinear average age-appropriate brain templates from birth to adulthood. *NeuroImage*, *47*, S102. https://doi.org/10.1016/S1053-8119(09)70884-5

Fransson, P., Metsäranta, M., Blennow, M., Åden, U., Lagercrantz, H., & Vanhatalo, S. (2013). Early Development of Spatial Patterns of Power-Law Frequency Scaling in fMRI Resting-State and EEG Data in the Newborn Brain. *Cerebral Cortex*, *23*(3), 638–646. https://doi.org/10.1093/cercor/bhs047

Frauscher, B., von Ellenrieder, N., Zelmann, R., Doležalová, I., Minotti, L., Olivier, A., Hall, J., Hoffmann, D., Nguyen, D. K., Kahane, P., Dubeau, F., & Gotman, J. (2018a). Atlas of the normal intracranial electroencephalogram: Neurophysiological awake activity in different cortical areas. *Brain*, *141*(4), 1130–1144. https://doi.org/10.1093/brain/awy035

Frauscher, B., von Ellenrieder, N., Zelmann, R., Doležalová, I., Minotti, L., Olivier, A., Hall, J., Hoffmann, D., Nguyen, D. K., Kahane, P., Dubeau, F., & Gotman, J. (2018b). Atlas of the normal intracranial electroencephalogram: Neurophysiological awake activity in different cortical areas. *Brain*, *141*(4), 1130–1144. https://doi.org/10.1093/brain/awy035

Freeman, W. J., Holmes, M. D., Burke, B. C., & Vanhatalo, S. (2003). Spatial spectra of scalp EEG and EMG from awake humans. *Clinical Neurophysiology*, *114*(6), 1053–1068. https://doi.org/10.1016/S1388-2457(03)00045-2

Freeman, W. J., & Zhai, J. (2009). Simulated power spectral density (PSD) of background electrocorticogram (ECoG). *Cognitive Neurodynamics*, *3*(1), 97–103. https://doi.org/10.1007/s11571-008-9064-y

Fries, P. (2005). A mechanism for cognitive dynamics: Neuronal communication through neuronal coherence. *Trends in Cognitive Sciences*, *9*(10), 474–480. https://doi.org/10.1016/j.tics.2005.08.011

Gao, R., Peterson, E. J., & Voytek, B. (2017). Inferring synaptic excitation/inhibition balance from field potentials. *NeuroImage*, *158*, 70–78. https://doi.org/10.1016/j.neuroimage.2017.06.078

Gao, R., van den Brink, R. L., Pfeffer, T., & Voytek, B. (2020). *Neuronal timescales are functionally dynamic and shaped by cortical microarchitecture* [Preprint]. Neuroscience. https://doi.org/10.1101/2020.05.25.115378

Gramfort, A., Luessi, M., Larson, E., Engemann, D. A., Strohmeier, D., Brodbeck, C., Parkkonen, L., & Hämäläinen, M. S. (2014). MNE software for processing MEG and EEG data. *NeuroImage*, *86*, 446–460. https://doi.org/10.1016/j.neuroimage.2013.10.027

Grandy, T. H., Werkle-Bergner, M., Chicherio, C., Lövdén, M., Schmiedek, F., & Lindenberger, U. (2013). Individual alpha peak frequency is related to latent factors of general cognitive abilities. *NeuroImage*, *79*, 10–18. https://doi.org/10.1016/j.neuroimage.2013.04.059

Gross, J., Baillet, S., Barnes, G. R., Henson, R. N., Hillebrand, A., Jensen, O., Jerbi, K., Litvak, V., Maess, B., Oostenveld, R., Parkkonen, L., Taylor, J. R., van Wassenhove, V., Wibral, M., & Schoffelen, J.-M. (2013). Good practice for conducting and reporting MEG research. *NeuroImage*, *65*, 349–363. https://doi.org/10.1016/j.neuroimage.2012.10.001

Haegens, S., Cousijn, H., Wallis, G., Harrison, P. J., & Nobre, A. C. (2014). Inter- and intra-individual variability in alpha peak frequency. *NeuroImage*, *92*, 46–55. https://doi.org/10.1016/j.neuroimage.2014.01.049

Haller, M., Donoghue, T., Peterson, E., Varma, P., Sebastian, P., Gao, R., Noto, T., Knight, R. T., Shestyuk, A., & Voytek, B. (2018). Parameterizing neural power spectra. *BioRxiv*. https://doi.org/10.1101/299859

Hashemi, A., Pino, L. J., Moffat, G., Mathewson, K. J., Aimone, C., Bennett, P. J., Schmidt, L. A., & Sekuler, A. B. (2016). Characterizing Population EEG Dynamics throughout Adulthood. *ENeuro*, *3*(6). https://doi.org/10.1523/ENEURO.0275-16.2016

He, B. J. (2014). Scale-free brain activity: Past, present, and future. *Trends in Cognitive Sciences*, *18*(9), 480–487. https://doi.org/10.1016/j.tics.2014.04.003

He, W., Donoghue, T., Sowman, P. F., Seymour, R. A., Brock, J., Crain, S., Voytek, B., & Hillebrand, A. (2019). Co-Increasing Neuronal Noise and Beta Power in the Developing Brain. *BioRxiv*, 49. https://doi.org/10.1101/839258

Huang, M. X., Mosher, J. C., & Leahy, R. M. (1999). A sensor-weighted overlapping-sphere head model and exhaustive head model comparison for MEG. *Physics in Medicine and Biology*, *44*(2), 423–440. https://doi.org/10.1088/0031-9155/44/2/010

Izhikevich, L., Gao, R., Peterson, E., & Voytek, B. (2018). Measuring the average power of neural oscillations. *BioRxiv*. https://doi.org/10.1101/441626

Langer, N., Ho, E. J., Alexander, L. M., Xu, H. Y., Jozanovic, R. K., Henin, S., Petroni, A., Cohen, S., Marcelle, E. T., Parra, L. C., Milham, M. P., & Kelly, S. P. (2017). A resource for assessing information processing in the developing brain using EEG and eye tracking. *Scientific Data*, *4*, 170040. https://doi.org/10.1038/sdata.2017.40

Lendner, J. D., Helfrich, R. F., Mander, B. A., Romundstad, L., Lin, J. J., Walker, M. P., Larsson, P. G., & Knight, R. T. (2020). An electrophysiological marker of arousal level in humans. *ELife*, *9*, e55092. https://doi.org/10.7554/eLife.55092

Lindsley, D. B. (1938). Electrical Potentials of the Brain in Children and Adults. *The Journal of General Psychology*, *19*(2), 285–306. https://doi.org/10.1080/00221309.1938.9711205

Martín-Buro, M. C., Garcés, P., & Maestú, F. (2016). Test-retest reliability of resting-state magnetoencephalography power in sensor and source space: Reliability of Resting-State MEG Power. *Human Brain Mapping*, *37*(1), 179–190. https://doi.org/10.1002/hbm.23027

McEvoy, L. K., Smith, M. E., & Gevins, A. (2000). Test-retest reliability of cognitive EEG. *Clinical Neurophysiology*, *111*(3), 457–463. https://doi.org/10.1016/S1388-2457(99)00258-8

Molina, J. L., Voytek, B., Thomas, M. L., Joshi, Y. B., Bhakta, S. G., Talledo, J. A., Swerdlow, N. R., & Light, G. A. (2020). Memantine effects on EEG measures of putative excitatory/inhibitory balance in schizophrenia. *Biological Psychiatry: Cognitive Neuroscience and Neuroimaging*, S2451902220300471. https://doi.org/10.1016/j.bpsc.2020.02.004

Näpflin, M., Wildi, M., & Sarnthein, J. (2007). Test–retest reliability of resting EEG spectra validates a statistical signature of persons. *Clinical Neurophysiology*, *118*(11), 2519–2524. https://doi.org/10.1016/j.clinph.2007.07.022

Niso, G., Rogers, C., Moreau, J. T., Chen, L.-Y., Madjar, C., Das, S., Bock, E., Tadel, F., Evans, A. C., Jolicoeur, P., & Baillet, S. (2016a). OMEGA: The Open MEG Archive. *NeuroImage*, *124*, 1182–1187. https://doi.org/10.1016/j.neuroimage.2015.04.028

Niso, G., Rogers, C., Moreau, J. T., Chen, L.-Y., Madjar, C., Das, S., Bock, E., Tadel, F., Evans, A. C., Jolicoeur, P., & Baillet, S. (2016b). OMEGA: The Open MEG Archive. *NeuroImage*, *124*, 1182–1187. https://doi.org/10.1016/j.neuroimage.2015.04.028

Nolte, G., & Curio, G. (1999). The effect of artifact rejection by signal-space projection on source localization accuracy in MEG measurements. *IEEE Transactions on Biomedical Engineering*, *46*(4), 400–408. https://doi.org/10.1109/10.752937

Podvalny, E., Noy, N., Harel, M., Bickel, S., Chechik, G., Schroeder, C. E., Mehta, A. D., Tsodyks, M., & Malach, R. (2015). A unifying principle underlying the extracellular field potential spectral responses in the human cortex. *Journal of Neurophysiology*, *114*(1), 505–519. https://doi.org/10.1152/jn.00943.2014

Pritchard, W. S. (1992). The Brain in Fractal Time: 1/F-Like Power Spectrum Scaling of the Human Electroencephalogram. *International Journal of Neuroscience*, *66*(1–2), 119–129. https://doi.org/10.3109/00207459208999796

Robertson, M. M., Furlong, S., Voytek, B., Donoghue, T., Boettiger, C. A., & Sheridan, M. A. (2019). EEG Power Spectral Slope differs by ADHD status and stimulant medication exposure in early childhood. *Journal of Neurophysiology*. https://doi.org/10.1152/jn.00388.2019

Surwillo, W. W. (1961). Frequency of the "Alpha" rhythm, reaction time and age. *Nature*, *191*(4790), 823–824. https://doi.org/10.1038/191823a0

Tadel, F., Baillet, S., Mosher, J. C., Pantazis, D., & Leahy, R. M. (2011a). Brainstorm: A User-Friendly Application for MEG/EEG Analysis. *Computational Intelligence and Neuroscience*, *2011*, 1–13. https://doi.org/10.1155/2011/879716

Tadel, F., Baillet, S., Mosher, J. C., Pantazis, D., & Leahy, R. M. (2011b). Brainstorm: A User-Friendly Application for MEG/EEG Analysis. *Computational Intelligence and Neuroscience*, *2011*, 1–13. https://doi.org/10.1155/2011/879716

Tan, H.-R. M., Gross, J., & Uhlhaas, P. J. (2015). MEG—measured auditory steady-state oscillations show high test–retest reliability: A sensor and source-space analysis. *NeuroImage*, *122*, 417–426. https://doi.org/10.1016/j.neuroimage.2015.07.055

Van Essen, D. C., Smith, S. M., Barch, D. M., Behrens, T. E. J., Yacoub, E., & Ugurbil, K. (2013). The WU-Minn Human Connectome Project: An overview. *NeuroImage*, *80*, 62–79. https://doi.org/10.1016/j.neuroimage.2013.05.041

Van Essen, D. C., Ugurbil, K., Auerbach, E., Barch, D., Behrens, T. E. J., Bucholz, R., Chang, A., Chen, L., Corbetta, M., Curtiss, S. W., Della Penna, S., Feinberg, D., Glasser, M. F., Harel, N., Heath, A. C., Larson-Prior, L., Marcus, D., Michalareas, G., Moeller, S., … Yacoub, E. (2012). The Human Connectome Project: A data acquisition perspective. *NeuroImage*, *62*(4), 2222–2231. https://doi.org/10.1016/j.neuroimage.2012.02.018

VanRullen, R. (2016). Perceptual Cycles. *Trends in Cognitive Sciences*, *20*(10), 723–735. https://doi.org/10.1016/j.tics.2016.07.006

Varela, F. J., Lachaux, J.-P., Rodriguez, E., & Martinerie, J. (2001). The brainweb: Phase synchronization and large-scale integration. *Nature Reviews Neuroscience*, *2*(4), 229–239. https://doi.org/10.1038/35067550

Vlahou, E. L., Thurm, F., Kolassa, I.-T., & Schlee, W. (2014). Resting-state slow wave power, healthy aging and cognitive performance. *Scientific Reports*, *4*(1). https://doi.org/10.1038/srep05101

Voytek, B., & Knight, R. T. (2015). Dynamic Network Communication as a Unifying Neural Basis for Cognition, Development, Aging, and Disease. *Biological Psychiatry*, *77*(12), 1089–1097. https://doi.org/10.1016/j.biopsych.2015.04.016

Voytek, B., Kramer, M. A., Case, J., Lepage, K. Q., Tempesta, Z. R., Knight, R. T., & Gazzaley, A. (2015). Age-Related Changes in 1/f Neural Electrophysiological Noise. *Journal of Neuroscience*, *35*(38), 13257–13265. https://doi.org/10.1523/JNEUROSCI.2332-14.2015

Wang, X.-J. (2010). Neurophysiological and Computational Principles of Cortical Rhythms in Cognition. *Physiological Reviews*, *90*(3), 1195–1268. https://doi.org/10.1152/physrev.00035.2008

Welch, P. (1967). The use of fast Fourier transform for the estimation of power spectra: A method based on time averaging over short, modified periodograms. *IEEE Transactions on Audio and Electroacoustics*, *15*(2), 70–73. https://doi.org/10.1109/TAU.1967.1161901

Conclusion

In this dissertation, we have examined methods of investigation for neural field data, and how they relate to the different components that comprise this data, in particular relating to both periodic (oscillatory) and aperiodic activity. Through this work, we have noted and investigated potential pitfalls with methods that do not explicitly consider and measure both components of the data, as well as the benefits and novel findings of doing so.

An overarching theme of this work is that how conceptualize the data we analyze is of the utmost importance – whether that be through explicit deliberation, or implicitly through the application of methods that embody particular assumptions. The methods and practices we employ are contextualized through a history of practice and the contingencies of the times in which they were developed. We can and should acknowledge this work, it's history, and the large body of knowledge and practices it has propelled, while also being deliberate and consistently vigilant in evaluating and considering the methods we employ and the conceptualizations of the data that they embody.

Through this work, I have also come to value and appreciate the power and utility of using and developing open-source software in science. In particular, there is great power and utility in developing openly available software tools while employing best practices from the field of software development. This allows for developing methods that can be rigorously tested, through the use of formal code tests as well as with the use of systematic simulation tests, and also easily shared, both in terms of portability of the code, and through the development of thorough code and module documentation. The transparency, shareability, and accessibility of

employing open-source practices has undeniably been a key factor in the success that we have had in developing and deploying new methods, and in them being adopted by others.

This dissertation is focused primarily on the task of measuring and describing neural field data. This is but a small piece in the context of the broader task of interpreting and understanding the physiological generators, functional roles, and correlates of such activity. There is a large body of existing work on these topics, and I hope future work and the development of the methods here can aid in continuing to investigate, and ultimately, interpret and understand patterns of brain activity, and how they relate to the functional organization of brain activity. Notably, though much of this work started with the goal of better isolating and measuring oscillatory activity, I now find myself particularly excited by the somewhat lesser known, but clearly dynamic and interesting, signal component of aperiodic activity, which is now the topic of an increasing amount of work.

Altogether, and in conclusion, here we propose that explicit parameterization of spectral features of interest, embodied in a new method to parameterize neural power spectra into constituent components of aperiodic and periodic activity, is a well-motivated and productive method for continuing to investigate and attempt to understand the properties and workings of the brain, as seen through the lens of neural field data.